

EHD1 ATPase, catalyses membrane fission via a novel mechanism

A Thesis

Submitted in partial fulfilment of the requirements

Of the degree of

Doctor of Philosophy

By

Manish Singh Kushwah

20123176



Indian Institute of Science Education and Research, Pune.

2016

Acknowledgements

I would like to express my deepest gratitude to my Ph.D. supervisor Dr. Thomas Pucadyil for his support, guidance, willingness to work on the bench side by side to carry out experiments and criticism which has helped immensely in taking this work forward. Thomas has been always available to discuss experiments, concepts which was of great help in understanding and taking project ahead. His expertise and vast knowledge of field brought lot of motivation and excitement to the work. This work couldn't have reached to this stage without him. He has been an inspiration and set up a high standard in terms of practice of research.

I would also like to thank my previous and current lab-mates Sachin, Srishti, Raunaq, Sukrut and Devika. I started in lab with working alongside Sachin. He was always around to help-out during experiments, and his questionnaire about work was an interesting way to learn and work in the lab. Working with Srishti was always lot of fun. She brought lot of rigor to the work and was always around for the smallest project we undertook together. She has been an excellent lab-mate and an amazing friend who has been candid to criticise and discuss during the toughest time I faced during Ph.D. It's been really great experience having known and working with her. Raunaq has been a great, towering friend who has been around in good and bad times alike. We have spent amazing moments in and outside the lab. I have enjoyed his scepticism and enthusiasm for science. He has been the friend who I could depend upon, talk about my problems and joys and share drinks, get drunk with and take care of each other. It's been nice to have Sukrut as a lab-mate, whom I could always count on. I have received great help and support at the time of need. Devika has been interesting person to hang around with. She has always been helpful and has been really great support during time of need.

I have had great friends Aniruddh Sastry, Jay Prakash Shukla, Ravi Devani, Mahesh Chand, Chaitanya Mungi at IISER. They have always helped in scientific and non-scientific discussion which made my stay here an enjoyable experience. I have always enjoyed Aniruddh's company. We have discussed on scientific and non-scientific issues and it's always been interesting to hear his take and I have resorted to him for professional and personal doubts. His take has always shown a different way to look at things and has helped me taking decision at multiple times. Also we have enjoyed outings and drinks together, which again has made my stay here enjoyable and pleasant.

Jay-prakash (JP) has been a friend who I could relate to at multiple occasion and he has been a great friend and been always there in fun and serious times alike. Chaitanya has been an enjoyable person to be around and has a peculiar point of view which has been refreshing to listen to. We have also shared long rides and memorable times. Ravi has been a great friend with whom I have enjoyed several outings with. He has always come across calm and enjoyable person. Mahesh has always been a friend who can help you get over your problems with a hearty smile.

I would also like to thank Dr, Nagaraj Balasubramanian with whom I have had lot of discussion on scientific and non-scientific aspects. I would also like to thank Dr. Sudha Rajamani for several great discussions (on scientific and non-scientific topics). She has given multiple suggestion which have helped during PhD and during my thesis writing and I couldn't thank her enough for that.

My family has been greatest support during this venture, despite their reservation and little to no information in terms of what I was doing (with my life at the first place). They put their trust in me and I couldn't have done it without that.

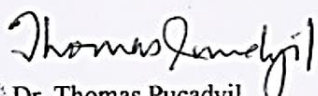
At last I would like to thank IISER, Pune and bio-department which has provided all the facilities and an environment where science could be practiced and discussed in a conducive manner.

Declaration

This thesis is a presentation of my original research work. Wherever contributions of others are involved, every effort is made to indicate this clearly, with due reference to the literature, and acknowledgement of collaborative research and discussions. The work was done under the guidance of Dr. Thomas Pucadyil, at the Indian Institute of Science Education and Research, Pune.

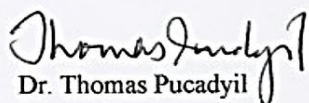
Manish Singh Kushwah

In my capacity as supervisor of the candidate's thesis, I certify that the above statements are true to the best of my knowledge.


Dr. Thomas Pucadyil

CERTIFICATE

Certified that the work incorporated in the thesis entitled "EHD1 ATPase, catalyses membrane fission via a novel mechanism" submitted by "Manish Singh Kushwah" was carried out by the candidate, under my supervision. The work presented here or any part of it has not been included in any other thesis submitted previously for the award of any degree or diploma from any other University or institution.


Dr. Thomas Pucadyil

December 23, 2016

Date:

Table of Contents

Table of Figures.....	9
Synopsis.....	10
1. Introduction.....	13
1.1 Vesicular transport and requirement of protein assisted membrane fission.....	13
1.2 Endocytic recycling and role of endocytic recycling compartment (ERC).....	14
1.3 EHD1 mediated regulation of endocytic recycling at ERC compartment.....	14
1.3.1 EHD1 discovery and effect on receptor recycling from ERC.....	14
1.3.2 Effect of EHD1 function on cellular processes.....	16
1.3.3 EHD1 mediated regulation of embryonic development.....	17
1.4 EHD protein domain architecture and structure	18
1.5. Understanding EHD1 function in recycling of receptors from ERC.....	19
2. Materials and methods	
2.1 Cloning, protein expression and purification.....	22
2. 2. Liposome preparation.....	23
2. 3. Lipid co-sedimentation assay, ATPase activity, estimation of Km.....	23
2. 4. PEGylation of Glass Coverslips.....	24
2. 5. Supported Membrane Tubes preparation (SMrT).....	25
2. 6. Tube scission assay and binding of fluorescent proteins to SMrT templates.....	25
2. 7. Fluorescence microscopy.....	26
2.8 Image analysis, Coefficient of Variation calculation, tube radius calculation and estimation of fission probability.....	26
2.9 FAT Blot assay.....	27
2.10 Dynamin and EHD1 assembly on SMrT templates.....	27

2.11 Formation of mEGFP encapsulated SMrT templates and EHD1 assembly.....28

3. Characterization of EHD1 mediated membrane fission

3.1. Introduction.....30

3.1.1 Necessity to reconstitute EHD1 function *in vitro*.....30

3.2 Results.....32

3.2.1 EHD1 expression and purification.....32

3.2.2 Biochemical characterization of EHD1.....32

3.2.3 Reconstitution of EHD1 function.....35

3.2.4. ATP binding imparts membrane deformation capability to EHD1.....35

3.2.5. EHD1 catalyses membrane fission in ATP hydrolysis dependent and
is sensitive to tube dimension.....36

3.2.6. EHD1 mediated fission is affected by the presence of non-bilayer lipids.41

3.3 Discussion.....43

4. Determinants of EHD1 Mediated Fission

4.1 Introduction.....49

4.1.1. Membrane binding regions of EHD proteins.....49

4.2. Results.....52

4.2.1 Helical loop plays an important role in EHD1 membrane binding and
fission.....52

4.2.2 Role of N-terminal region in EHD1 function.....54

4.3 Discussion.....60

5. Mechanism of EHD1 mediated membrane fission.

5.1 Introduction.....66

5.1.1. Protein catalysts for membrane fission.....66

5.1.2. Dynamin, a self-sufficient membrane fission catalyst.....67

5.1.3. Understanding mechanism of EHD1 mediated fission.....	67
5.2. Results.....	67
5.2.1. EHD1 assembly leads to expansion of tube dimension.....	67
5.2.2. EHD1 assembly mediated tube expansion leads to constriction in the adjacent region.....	69
5.3. Discussion.....	73
6. References.....	76

Table of figures

Figure 1-4-1. Structure of EHD proteins in close and open conformation	20
Figure 3-2-1. Recombinant EHD1 purification and biochemical characterization.....	34
Figure 3-2-2. ATP binding leads to oligomerization and imparts membrane deformation capability to EHD1.....	37
Figure 3-2-3. EHD1 catalyses membrane fission in ATP hydrolysis dependent manner and is sensitive to tube dimensions.....	39
Figure 3-2-4. EHD1 membrane deformation is tube dimension independent.....	40
Figure 3-2-5. EHD1 mediated fission is affected by the presence of non-bilayer lipids in membrane.....	42
Figure 4-1-1. EHD2 contains two membrane binding regions.....	50
Figure 4-2-1. Effect of EHD1 membrane binding mutant K328A on EHD1 membrane binding and function.....	53
Figure 4-2-2. EHD1-F322A mutant significantly affects membrane binding and fission activity.....	55
Figure 4-2-3. N-terminal unstructured region is required for EHD1 membrane binding and fission activity.....	57
Figure 4-2-4. EHD1 (Δ 2-9) is defective in membrane deformation capability.....	58
Figure 4-2-5. N-terminus GST or GFP fusion of EHD1 renders the protein inactive.....	59
Figure 5-1-1. Membrane fission via non leaky, hemi-fission intermediate.....	66
Figure 5-2-1. Dynamin and EHD1 deform the membrane to similar extent.....	68
Figure 5-2-2. EHD1 assembly leads to formation bulge like intermediate.....	70
Figure 5-2-3. EHD1 assembly increases lumen dimension of SMrT template.....	71
Figure 5-2-4. Pathway to EHD1 catalysed membrane fission.....	72

Synopsis

Eukaryotic cells are compartmentalized into functionally specialized organelles, such as the endosomal system, endoplasmic reticulum, and the Golgi network. These organelles maintain their own unique protein and lipid composition ensuring their identity as well as ability to perform distinct functions. Maintenance of the organellar identity is regulated by transporting lipids and proteins using vesicles as transport carriers between organelles via vesicular transport pathways. Formation of vesicles at the donor compartment via fission process and fusion to the acceptor compartment is necessary to continue vesicular transport.

Vesicle generation via membrane fission is a thermodynamically unfavourable process and requires specialized protein machinery (membrane fission catalysts; MFCs) to catalyze fission process. Till date, dynamin, a large multi-domain GTPase, is the best characterized MFC and catalyzes fission at plasma membrane and trans-Golgi network. It has been the best source of insights into protein catalysed membrane fission. However, dynamin knockdown does not perturb vesicular transport from intracellular organelles, indicating that multiple MFCs must exist to catalyze fission at various organelles.

Discovering the identities of novel MFCs has been difficult due to lack of high-throughput assays to detect membrane fission. Our lab has developed a tubular template system (Supported Membrane Tubes; SMrT) which allows easy and reliable detection of membrane fission. In this study, we have utilized the SMrT template to characterize a putative fission catalyst Eps15 homology domain protein 1 (EHD1). EHD1 is required for the exit of a large variety of receptors from endocytic recycling compartment (regulates receptor recycling to plasma membrane) and has been proposed to function as membrane fission catalyst. We have characterized bacterially expressed EHD1 and studied its ability to catalyze membrane fission.

Chapter 1 introduces vesicular transport and the requirement of protein machinery for membrane fission and fusion process. Regulation of recycling pathway by endocytic recycling compartment and EHD1's role in receptor recycling and functioning of various cellular processes and embryonic development and proposed function of EHD1 as membrane fission catalyst, is also introduced here.

Chapter 2 describes methods and materials used in the following chapters

Chapter 3 discusses the purification of bacterially expressed EHD1. We characterized EHD1 membrane binding and ATPase activity. Further, the chapter discusses the role of ATP

binding on EHD1 oligomerization on SMrT templates and membrane deformation. We show that EHD1 can catalyze membrane fission in ATP hydrolysis-dependent manner and is sensitive to tube dimensions. Further, we have discussed the role of different lipids on EHD1's ability to catalyze membrane fission.

Chapter 4 explores the effect of mutations in EHD1 on membrane binding and fission. We find that the protein regions proposed to be involved in membrane binding based upon EHD2 (EHD paralog) structure, are conserved in EHD1 and is required for binding. Additionally, we find that N-terminus of EHD1 is required for EHD1 assembly mediated membrane deformation and N-terminus fusion of GST or GFP renders the protein inactive.

In **chapter 5**, we explore the mechanism of EHD1 catalysed membrane fission. We find that EHD1 catalysed fission via a different mechanism than that is known for dynamin. Dynamin binding and oligomerization on membranes leads to constriction formation on SMrT template and fission occur in the constricted region in GTP-hydrolysis-dependent manner. Whereas EHD1 upon assembly leads to expansion of SMrT templates and due the membrane expansion, adjacent region undergoes constriction formation. In other words, dynamin assembly directly leads to constriction of SMrT template, whereas constriction in the case of EHD1 assembly is generated because of an indirect effect of tube dimension expansion in the adjacent region.

Chapter. 1

Introduction.

1. Introduction

1.1 Vesicular transport and requirement of protein assisted membrane fission.

The eukaryotic cell is a highly compartmentalized system, consisting of organelles with distinct protein and lipid composition defining their identity. This organellar identity is maintained by vesicular transport of proteins and lipids. The vesicle-like carriers are characteristic of the vesicular transport and are generated at the donor compartment via the process of membrane fission and ultimately fuse with the acceptor membrane via the process of membrane fusion. Both membrane fission and fusion process are essential for the information transfer from one compartment to the other.

Membrane fusion and fission both are energetically intensive processes and require assistance from protein machinery (Chernomordik and Kozlov, 2005; Kozlovsky and Kozlov, 2003; Kozlovsky et al., 2002; Mattila et al., 2015). The identity of protein(s) required for fusion and the mechanism of how membrane fusion occurs is well understood owing to the well-established *in vivo* and *in-vitro* assays (Jahn et al., 2003; Sudhof and Rothman, 2009). Membrane fission, like fusion, is an energetically unfavourable process and requires proteins machinery to catalyze the process. However, protein catalysed fission has remained less well studied for the following reasons; a) unlike fusion, which appears to use conservative sets of proteins to catalyze fusion at various compartments, fission is proposed to be catalysed by distinct, compartment-specific proteins (see below). b) Existing assays to detect fission are tedious (pulling a membrane tube from membrane reservoir source such as giant unilamellar vesicles (GUVs) or supported membrane with excess reservoir (SUPER) templates (Morlot and Roux, 2013; Pucadyil and Schmid, 2008). These assays also plagued with indirect read-out e.g, electron microscopy based detection of generation of small diameter vesicle from large liposomes upon addition of protein of interest is used as the proxy for membrane fission (Pucadyil and Schmid, 2009).

Dynamin, a large multi-domain GTPase is the only protein shown to catalyze fission in an *in-vitro* system and has been sole the source of protein catalysed membrane fission (Bashkirov et al., 2008; Dar et al., 2015; Pucadyil and Schmid, 2008; Roux et al., 2006). However, dynamin is involved in catalyzing fission at the plasma membrane, and trans-Golgi network (Schmid and Frolov, 2011) and perturbation of its function does not affect vesicular

transport between other membrane compartments (Cai et al., 2012), outlining the presence of yet unidentified proteins fission catalysts in cells.

1.2 Endocytic recycling and role of endocytic recycling compartment (ERC)

Endocytosis-mediated internalization of receptors helps in the various cell processes such as nutrient uptake, cell signaling and synaptic vesicle recycling. Receptor recycling pathways replenish the receptor pools depleted by the endocytic processes. It occurs via fast and slow recycling pathways (Maxfield and McGraw, 2004). The fast recycling occurs from sorting endosomes (SE), which are peripheral structures and receive receptors internalized via different endocytic pathways and also function as a sorting station. SEs separates recycling receptors from receptor destined for degradation, recycling receptors following slow recycling (predominant pathway) transit to endocytic recycling compartment (ERC) (Grant and Donaldson, 2009; Maxfield and McGraw, 2004).

ERC is a long-lived, perinuclear compartment which regulates recycling of receptors to the plasma membrane (Hopkins et al., 1994; Maxfield and McGraw, 2004). It has Rab11 (a small GTPase) and MICAL-L1 (molecules interacting with CasL-like protein1) as marker proteins and require microtubules to maintain the compartment architecture (Caplan et al., 2002; Sharma et al., 2009; Xie et al., 2016). As mentioned earlier, ERC receives receptors from SEs, which are then returned to the plasma membrane. In this manner, ERC functions as a transit station for a fairly large variety of receptor, reflecting its general role in receptor recycling (Grant and Caplan, 2008; Maxfield and McGraw, 2004; Xie et al., 2016). Also, ERC is also involved in proteins via retrograde and anterograde transport (van IJzendoorn, 2006; Taguchi, 2013), reflecting its importance in intracellular transport.

The exit of the receptors from ERC is severely affected in the absence of EHD1, a member of C-terminal EH domain containing protein (EHDs).

1.3 EHD1 mediated regulation of endocytic recycling at ERC.

C-terminal EHD proteins have four paralogs in mammals and one ortholog in *Drosophila melanogaster* and *Caenorhabditis elegans*. Mammalian paralogs share high sequence similarity (70-86%), localize to different compartments and are proposed to be involved in the transport from the respective compartment (Daumke et al., 2007; Grant and Caplan, 2008). Similarly, the invertebrate orthologues are involved in intracellular vesicular transport.

1.3.1 EHD1 discovery and effect on receptor recycling from ERC.

EHD1 function was first discovered in a mutagenesis screen in *C. elegans* aimed at identifying novel regulators of endocytic transport. Genetic loci which affected the endocytosis were termed as receptor-mediated endocytosis (rme) and one such protein, RME-1, localized to the basolateral endosome pool in the intestinal epithelial cell. Its depletion affected basolateral uptake of fluid phase markers (BSA and GFP) and led to intracellular accumulation in the form of large vacuoles without affecting endocytic uptake or bulk membrane transport from the apical surface in the intestinal epithelial cells. RME-1 mutants also showed severe defect on endocytosis of yolk protein (YP170) in oocytes. This defect was due to the accumulation of the cognate receptor in an enlarged compartment (vacuoles) resulting in decreased plasma membrane pool. Intracellular receptor accumulation phenotype in the absence of EHD1 was akin to the phenotype earlier observed upon pharmacological inhibition receptor recycling in mammalian cells, strengthening the hypothesis that RME-1 is involved in the exit of recycling receptors from endosomes than it being directly involved in receptor endocytosis (Grant et al., 2001).

RME-1's role in receptor recycling was further supported by study addressing the function of the mouse orthologue of RME-1 (mRME-1, subsequently termed as Eps15 homology domain protein 1 (EHD1) in mammalian cells (Lin et al., 2001). Fairly well characterized endocytic uptake and itinerary of receptors to degradative and recycling pathways made mammalian cells an ideal system to study the roles of proteins involved in vesicular transport. Receptors destined for degradation are separated at the sorting endosomes and are transported to lysosomes, whereas recycling receptors (e.g. transferrin) are sorted to ERC (Lin et al., 2001; Maxfield and McGraw, 2004; Yamashiro et al., 1984). EHD1 co-localized with recycling receptor (transferrin) to ERC (Lin et al., 2001).

Effects of EHD1 depletion/function perturbation on the transport of receptors following degradative (e.g. EGFR) and recycling (e.g. transferrin, Tf) pathways were studied using the pulse-chase method. At a steady state (incubation for 15-20 min) Tf predominantly localizes to ERC (Yamashiro et al., 1984). EHD1 knock-down or functional perturbation (via over-expression of dominant negative mutant (EHD1 G429R)) showed receptor accumulation at ERC at the end of 30 min whereas control cells showed barely any presence of Tf. This evidence along with the previous studies strengthened the EHD1 role in receptor exit from ERC (Lin et al., 2001). EHD1 since has been established as a general regulator of recycling of

receptors such as MHC-1, CFTR, β 1-integrin, LDLR, CD59, EGFR, GLUT4, AMPA, L1/NgCAM and TrkA receptor (Cai et al., 2011, 2012; Grant and Caplan, 2008; Hao et al., 2002; Jović et al., 2007; Lasiecka et al., 2010; Park et al., 2004; Picciano et al., 2003). All these receptors show accumulation at ERC upon EHD1 depletion. Additionally, EHD1 depletion also has structural effect on ERC and leads to its extensive tubulation and enlargement. (Cai et al., 2013; Lee et al., 2015)

1.3.2 Effect of EHD1 function on cellular processes

Perturbation of recycling process in the absence of EHD1 not only decreases the receptor pool at the plasma membrane but also adversely affects various processes in neuronal and non-neuronal cells alike and manifests deleteriously effects during the embryonic development. For example, β 1-integrin, which is required for the polarized cell migration, is transported from trailing to the leading edge of a migrating cell. During migration, integrin is disassembled from focal adhesions at the trailing edge and transported to the ERC. It's transport to the plasma membrane to the leading edge is regulated by EHD1. EHD1 null mouse embryonic fibroblasts (MEFs) show extensive intracellular accumulation of β 1-integrin, decreased filopodial extension and delayed dynamics of focal adhesions (increased lifetime) leading to considerable slowing down of cell migration (Jović et al., 2007). Macrophage and muscle development are also affected in case of EHD1 knockdown. Macrophage development, proliferation, and functional specification are specified by signaling from colony stimulating factor-1 (CSF-1)-CSF-1R interaction. CSF-1R traverses through ERC, and its numbers on the plasma membrane are reduced in the case of EHD1 knockdown (Cypher et al., 2016).

In neuronal cells, EHD1 function inhibition perturbs various aspects of neuronal development and function. For example, over-expression of EHD1 dominant negative mutant (G429R) in hippocampal neurons affects delivery and subsequent insertion of AMPA receptor to post-synaptic membranes during signal induced memory consolidation. Increased AMPA receptor density is essential for the establishment of long-term potentiation (LTP; the hallmark of synaptic plasticity) in neurons (a process which is marked by increased signal processing capacity of post-synaptic membranes and is a required step for of synaptic plasticity). AMPA receptors pool is localized at ERC (marked by co-localization with transferrin) and is delivered to the post-synaptic membrane upon stimulation. In the case of EHD1 knockdown, AMPA gets accumulated to ERC (Park et al., 2004).

During the neuron development, EHD1 regulated recycling is instrumental for growth cone migration, adhesion, and maturation. The growth cone is a highly specialized motile structure positioned at the distal end of the axon extended from the cell body to make connections with rest of neurons. Growth cone adhesion and migration in space are essential for axonal growth and formation of proper connections between neurons (Kalil and Dent, 2005; Tanaka and Sabry, 1995). Neural cell adhesion molecule L1 (NgCAM/L1) in such cell adhesion molecule is required for growth cone adhesion and migration (Kamiguchi and Lemmon, 1997). NgCAM/L1 is endocytosed from the cell body and transported to Tf and EHD1 positive compartment. EHD1 mutation leads to abrupt transport of NgCAM to the growth cone (Lasiecka et al., 2010; Yap et al., 2010).

EHD1 absence also affects neurite formation in the cultured neurons as well as in spinal cord cells post injury. Neurite formation is a signal dependent process involving activation using nerve growth factor/TrkA receptor interaction. TrkA receptor is transported from ERC to the plasma membrane upon stimulation (by NGF), a process which is perturbed in the absence of EHD1 (Kobayashi and Fukuda, 2013; Wu et al., 2016).

Recently cells with EHD1 knockdown are shown to be arrested at the cytokinesis step of cell division which involves separation of nascent daughter cells by formation of an ingressing furrow requires membrane deposition via exocytotic and recycling pathways. In the absence of EHD1 and its interacting partner MICAL-L1, cells are arrested at the cytokinetic step and show multinucleated phenotype (Reinecke et al., 2015).

1.3.3 EHD1 mediated regulation of embryonic development

The wide range of effects of EHD1 regulated vesicular transport becomes evident in EHD1 knockout mouse models. EHD1 knockout mouse manifests genotype dependent partial to complete embryonic lethality. In the case of partial lethality, surviving littermates showed lower muscle mass, micro-ophthalmia, and male sterility. Decreased muscle mass was caused by the inability of myocytes to fuse and form fully grown muscle. Defective spermatogenesis due to defective vesicular transport at the step of maturation of spermatozoa led to male sterility (Demonbreun et al., 2015; Doherty et al., 2008; Mate et al., 2012; Posey et al., 2011, 2014; Rainey et al., 2010).

In the case of more severe, complete lethality of EHD1 null embryos, it was observed that absence of EHD1 caused severe developmental defects as early as 9.5 dpc (days post coitum) and led to abrupt somitogenesis (somites formation), and neural tube closure defect.

Neural tube closure defect occurred because of aberrant sonic hedgehog signalling (SHH) generated due to defect in primary cilium formation. The primary cilium is hub of SHH signaling in neural epithelium cells. The formation of cilium necessitates the transport of regulator protein smoothened (smo) from recycling endosomes to cilium body, a process which is perturbed in EHD1 null background (Bhattacharyya et al., 2016; Lu et al., 2015).

Although diverse examples of EHD1 functional perturbation appear disparate and unrelated, EHD1 mediated regulation of vesicular transport from ERC has been proposed to be the main reason for the perturbation of the cellular processes.

1.4 EHD structure and domain architecture:

EHD paralogs are high sequence similarity (70-83%) similar to each other in mammals (Daumke et al., 2007; Hoernke et al., 2017; Melo et al., 2017). Domain architecture and structure of EHD2 and 4 shows similar domain architecture and orientation indicating the conservation of protein structure among four paralogs. EHD proteins possess dynamin-like G-domain flanked by two helical domains and C-terminal EH domain which is connected to the rest of the protein via a flexible linker. Despite being similar to dynamin, EHD's G-domain binds and hydrolyses ATP. The crystallographic unit of EHD proteins is a dimer and dimerization occurs via unique, conserved and largely hydrophobic dimerization interface present in the G-domain. In the structure of the dimer, EH domains of the cognate monomer are present on the G-domain of the adjacent monomer in a criss-cross fashion. EH domains bind to NPF motifs, and the binding site of the domain is occupied by GPF motif present in the linker domain (Daumke et al., 2007) (Fig. 1-4-1).

EHD proteins are shown to tubulate liposomes containing sufficient negative charge (Daumke et al., 2007; Melo et al., 2017; Pant et al., 2009). This function has been attributed to the oligomerization property of EHD proteins. Based upon similarity to dimerization interface used by other proteins (such as BDLP), it is proposed that EHD proteins oligomerize using an interface formed by G-domain and helical domains. Dimeric units interact using this surface to form an oligomer and EH domains support oligomer formation by interacting with NPF motif of the unstructured loop of G domain in the adjacent dimeric unit (Daumke et al., 2007).

EHD proteins are present in closed and open conformation. EHD2 bound to AMP-PNP (non-hydrolysable ATP analog), and Δ N-EHD4 bound ATP _{γ} S represents a closed and open conformation, respectively. These conformations differ mainly in the orientation of the helical domain on the G-domain in the crystallographic dimeric unit. As mentioned earlier, AMP-PNP

bound EHD proteins have G and helical domain aligned parallel to the crystallographic axis where the membrane binding helical loop is separated by a short distance (~ 30 Å). However, open conformation of ATP $_{\gamma}$ S-bound Δ N-EHD4 shows $\sim 50^\circ$ rotation of helical domain away G-domain resulting into the separation of the helical loops by 130 Å (Fig. 1-4-1). This rotation reorients membrane binding helical loop leading to an exposition of new membrane binding residues in the protein. EHD proteins contain two membrane binding sites, N-terminus unstructured region and helical loop present at the tip of the protein. N-terminus region is unstructured and binds to the hydrophobic pocket in G domain while the protein is in solution. However, it assumes an intermediate helical structure when EHD interacts with the membrane. In the open conformation the disordered KPFxxxNPF loops occupies the hydrophobic pocket in G-domain and opens up a new oligomerization interface involving disordered NPF motif and region of the helical domain. The reoriented helical domains display membrane binding residues, such that the residues on either monomer are parallel and facing each other (Hoernke et al., 2017; Melo et al., 2017).

1. 5. Understanding EHD1 function in the recycling of receptors from ERC.

The diverse effects of EHD1 on cellular processes via regulation of recycling from ERC compartment outline the importance EHD1 in cellular physiology, leading to the search for EHD1 function at ERC. Based on the presence of dynamin-like G-domain, membrane tubulation property and membrane stimulated nucleotide hydrolysis (ATPase) activity, EHD proteins are categorized as dynamin superfamily members (Daumke et al., 2007; Lee et al., 2005; Pant et al., 2009). Based upon the similarity to dynamin, EHD1 has been postulated to work like dynamin to catalyze membrane fission (Daumke et al., 2007; Grant and Caplan, 2008; Grant and Donaldson, 2009).

In a microscopy-based assay utilizing SMrT template as a model membrane system (Dar et al., 2015) EHD1 has been identified as a potential membrane fission catalyst (Sukrut Kamerkar). In the following study, we have performed biochemical characterization of recombinant EHD1 and have established that EHD1 catalyzes membrane fission and does so by a novel mechanism.

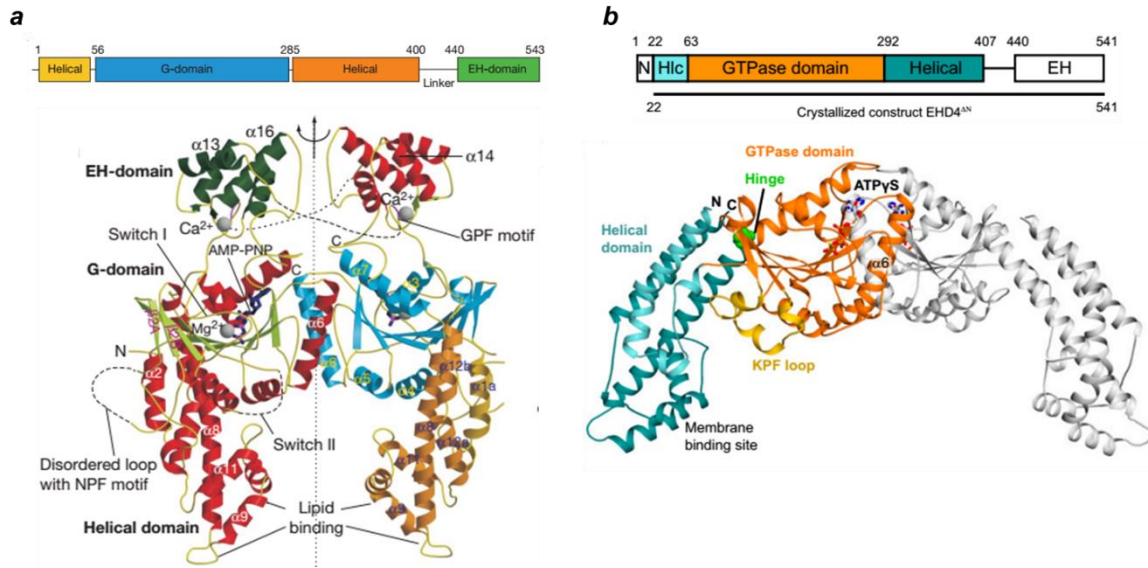


Figure 1-4-1. The structure of EHD proteins in close and open conformation. (a) Top panel. Domain architecture of EHD2. Lower panel. The structure of EHD2 dimer in the presence of AMP-PNP. The right monomer is coloured as shown in the domain. The structure shows the position of a different domain. Note helical domain is positioned just below the G-domain and the membrane binding sites in the helical loop are close to each other (Daumke et al., 2007). (b) Top panel: Domain architecture of EHD4 (similar to EHD2). Lower panel: Structure of EHD4 dimer bound to ATP γ S. Similar to a, one monomer is coloured in the same manner as the domain to denote the relative position of the protein in the dimer. Note the hinge and localization of helical domain away from each other and orientation of membrane binding sites (Melo et al., 2017).

CHAPTER 2.

Materials and Methods

2.1 Cloning, protein expression, and purification

Human EHD1 was amplified from cDNA (GE, Dharmacon; BC104799) was cloned pET15b vector downstream to the 6xHis-thrombin cleavage site, (His-EHD1; EHD1) and between the 6xHis-TEV site and strep sequence (His-EHD1-Strep; EHD1-strep). N-terminus fusion mEGFP-EHD1 was generated by cloning the GFP between 6xHis and N-terminus of EHD1 in WT 6xHis-EHD1. GST-fused EHD1 was generated by cloning EHD1 downstream to GST sequence in pGEX4T-1 vector. EHD1 EHD1(Δ 2-9), EHD1 K328A and EHD1 F322A were generated via site-directed mutagenesis to delete/mutate respective sequence in EHD1 clone. All the clones were confirmed using DNA sequencing.

Proteins were expressed in BL21(DE3) in auto-induction medium (Formedium, UK) at 18 °C for 24 hours, harvested and frozen at -80 °C before use. For purification of EHD1, GFP-EHD1, EHD1 mutants (EHD1 EHD1(Δ 2-9), K328A and F322A), frozen bacterial pellets were resuspended in lysis buffer (20 mM HEPES (pH 7.4), 300 mM KCl, and 20 mM Imidazole, supplemented with 1 mM PMSF and 2 mM 2-Mercaptoethanol) and lysed using sonication in ice-water mix. The lysate was spun at 18,500 g to remove debris and supernatant was incubated with pre-equilibrated HisPur Cobalt Resin (Thermo Scientific) for an hour at 4 °C (batch purification). Beads were then collected in the PD-10 column and washed with 100 ml of cold lysis buffer. Proteins were eluted in 20 mM HEPES (pH 7.4), 300 mM KCl, and 200 mM Imidazole.

For GST-EHD1 purification bacterial pellets were resuspended in GST-lysis buffer (20 mM HEPES (pH 7.4) 300 mM KCl supplemented with one mM DTT) and processed as his-EHD1 purification. The supernatant was incubated with GST-beads (GE Lifesciences) for an hour at 4 °C, collected in PD10 column and washed with 100 ml ice-cold GST-lysis buffer. Protein was eluted with 50 mM Tris (pH 8.0), 300 mM KCl, 15 mM reduced glutathione.

EHD1-strep was purified in a similar manner as EHD1, and the elution of the HisPur beads was loaded onto StrepTrap column (GE Lifesciences) and washed with 70 ml of lysis buffer. EHD1 was eluted with 20 mM HEPES (pH 7.4), 300 mM KCl and 2.5 mM Desthiobiotin.

Purified proteins were dialyzed against storage buffer (20 mM HEPES (pH 7.4), 300 mM KCl, 10% v/v glycerol, 1mM EDTA and one mM DTT) overnight at 4 °C, flash frozen in liquid N₂ and stored at -80 °C until use.

For fluorescently label the proteins, purified proteins were dialyzed overnight against HKS (20 mM HEPES (pH 7.4), 150 mM KCl) supplemented with 1mM EDTA and spun down 100,000g to remove aggregates. EHD1 was incubated with thiol reactive BODIPY® FL Iodoacetamide (Molecular probes, D6003) in 1:10 protein: dye molar excess ratio for one hr at room temperature and the reaction was stopped by addition of 1 mM DTT. Free dye was removed by dialyzing the protein again in HKS supplemented with 1 mM DTT and 1 mM EDTA overnight 4⁰C and judged by the absence of free dye band close to dye front on SDS-PAGE.

2.2 Liposome preparation

Liposomes of varying DOPS/DOPA content were made using the combination of DOPC, DOPS, and DOPA (Avanti Polar Lipids). For each lipid composition, required amount of each lipid was aliquoted in cleaned glass tubes to the final concentration of 1mM. Lipids were dried by rotary evaporation and followed by drying in vacuum at 50 ⁰C for half an hour. Required volume of HKS was added post-drying and lipids were hydrated at 50 ⁰C water-bath for half an hour with intermittent vortexing. Liposomes were extruded to 100 nm size using extrusion apparatus (Avanti Polar lipids).

2.3 Lipid co-sedimentation assay, ATPase activity, estimation of Km.

Liposome-cosedimentation assay was used to as described by Lee et al, 2015, with few modifications. Briefly, EHD1 was dialyzed overnight against HKS (20 mM HEPES (pH 7.4), 150 mM KCl, supplemented with 1mM DTT and 1mM EDTA) at 4 ⁰C and spun at 100,000 g for 20 minutes at 4 ⁰C. The supernatant was collected, and concentration was estimated using absorption at 280 nm. For all binding assay, 1 μ M EHD1 was incubated with 100 fold excess of liposomes of different PS mol % in reaction buffer in a final volume of 100 μ l reaction volume (supplemented with 1 mM MgCl₂ and 1 mM DTT) in Beckman TLA100.3 ultracentrifuge tubes for 20 minutes at RT. The reaction was spun at 100,000 g for 30 minutes at 20 ⁰C. The supernatant was collected, and 5x laemilli buffer was added to final 1x concentration. Pellet was resuspended in 100 μ l of 1x laemilli buffer, and 20 μ l of supernatant and pellet for each lipid composition was run on SDS-PAGE and stained with coomassie to estimate relative proportion of EHD1 in supernatant and pellet. Estimation of percent bound protein in each condition was done as described in (Lee et al., 2015).

To estimate basal and stimulated ATPase activity, two vials containing EHD1(2x) and ATP: Mg²⁺ (basal) (2x) or with 100 μ M liposomes (2x) solution were prepared and incubated

at 37 °C for 5 min. A 10µl aliquot from each vial was taken and added to a well containing 5 µl of 0.5 M EDTA (0 min reading). Rest of the solution were mixed to attain a final concentration of 1 µM EHD1, 1mM ATP and 1 mM Mg²⁺ and 100 µM liposomes (1x) and incubated at 37 °C. 20 µl aliquots were taken at a definite time interval or at 10 min (end-point assay) and added to 5 µl of 0.5 M EDTA solution to stop the reaction.

Estimation of ATPase activity was done by detecting the release of inorganic phosphate for each time point by malachite green assay adapted from (Baykov et al., 1988) with few modifications. Briefly, 400 µl of malachite green (Sigma, 229105) solution (in 3N H₂SO₄) was mixed with 100 µl of 7.5% Ammonium molybdate (Sigma, 244252) solution and 8 µl of 11% Tween-20 solution. 50 µl of reconstituted solution was added to each well, incubated for 10 minutes at RT and plate was read at 630 nm. The phosphate standard 0-200 µM was used to convert OD@ 630 to phosphate released. Pi released was plotted against the time to estimate the ATPase activity of EHD1 under various conditions.

To estimate basal and lipid stimulated k_m , EHD1 (1 µM) was incubated with varying concentration of ATP was in the absence (basal) or presence (lipid stimulated) of 100 fold excess of 100 mol% PS liposomes. The ATPase activity was estimated as described above and plotted against the ATP concentration and fit to Michaelis-Menten equation using GraphPad Prism (6.0) to calculate K_m .

2.4 PEGylation of Glass Coverslips

Glass coverslips were passivated by covalent attachment of polyethylene glycol (PEG) as described in Dar et al., 2015. Briefly, glass coverslips were cleaned with 3 N NaOH for 5 min and rinsed with water. Clean coverslips were treated with piranha solution (conc. H₂SO₄: 30% H₂O₂ = 3:2 v/v) for 1 hr at room temperature, rinsed with water and dried on a heat block set at 90°C. Dried coverslips were silanized with neat 3-glycidyloxypropyltrimethoxysilane (Sigma) for 5 hrs under vacuum. Silanized coverslips were rinsed with acetone, air-dried and placed in a glass beaker containing PEG400 (Sigma) or molten PEG8000 (USB) maintained at 90°C for 48-60 hrs. Coverslips were rinsed extensively with water and stored dry in a closed container. Coverslips were sequentially cleaned with 1% SDS, water, methanol and water in between experiments and could be used 4-5 times without significant loss in surface passivation.

2.5 Supported Membrane Tubes preparation (SMrT)

SMrT templates were prepared as described in (Dar et al., 2015). Briefly, Lipid stocks

(Avanti Polar Lipids) were aliquoted into glass vials in required proportions, diluted to a final concentration of 1 mM total lipid in chloroform and stored at -80°C . p-Texas Red-DHPE isomer was separated from a mixed isomer stock of Texas Red DHPE (Invitrogen) using thin layer chromatography on silica gel plates (Sigma) against 100% methanol as described earlier (Jung et al., 2009).

Lipid stocks were brought to room temperature before use. A small aliquot ($\sim 1\text{-}5$ nmol total lipid) was spread on a freshly cleaned PEGylated coverslip and kept under high vacuum for 5 min to remove all traces of chloroform. A ~ 35 μl flow cell (Biopetechs) was assembled by placing a 0.1 mm silicone spacer between the PEGylated coverslip and an ITO-coated slide. The flow cell was filled with filtered and degassed PBS left undisturbed for 10 min at room temperature. For experiments involving fluorescently-labeled dynamin, PEG8000-coated glass coverslips were used and the hydration buffer contained 1% (w/v) BSA (Sigma).

Supported membrane tubes (SMrT) were created by extrusion of the large vesicles, formed during hydration, to narrow membrane tubes by flowing excess PBS at high (~ 30 mm/s particle velocity inside the chamber) flow rates. SMrT templates were judged ready for experiments when the entire membrane reservoir was extruded into tubes that remained pinned at discrete sites to the surface.

2.6 Tube scission assay and binding of fluorescent proteins to SMrT templates

SMrT templates were first equilibrated in filtered and degassed HKS (20 mM HEPES (pH 7.4), 150 mM KCl) containing an oxygen scavenger cocktail of 0.2 mg/ml glucose oxidase (Sigma, G-2133), 0.035 mg/ml catalase (Sigma, C-40), 4.5 mg/ml glucose (Sigma) and 1 mM DTT and 1 mM MgCl_2 . EHD1, previously dialyzed overnight against pre-chilled HKS (containing 1 mM DTT and 1 mM EDTA) and spun at 100,000g for 20 min to remove aggregates, was reconstituted in HKS to a final concentration of 1 μM with oxygen scavenger cocktail, 1 mM MgCl_2 .

EHD1 (1 μM) solution in oxygen scavenger cocktail was flowed onto SMrT templates in absence or presence of $\text{ATP}_{\gamma}\text{S}$ or ADP at 25/37 oC at a low flow rate of ~ 1 mm/sec to minimize focus drifts, and the movie was collected via stream acquisition using Metamorph software.

EHD1 catalyzed membrane fission in the presence of ATP, and the bulk fission kinetics was analyzed by estimating the time-of-cut for all events occurring in a single field. For each field data were ordered in an ascending fashion and subtracted by the time of the first cut. This operation normalized the difference in the time of arrival of EHD1 across different experiments into the field of view. Data for three fields were pooled and arranged in ascending order and

plotted as cumulative frequency. The rate of fission was calculated using linear part of the plot for the conditions.

To see EHD1 distribution on SMrT templates, BODIPY-conjugated proteins were mixed with unlabeled protein (0.5+0.5 μM) to a final concentration of 1 μM and added to the SMrT templates in absence or presence of various nucleotides (ATP γS , ADP or ATP) and incubated for 10 minutes at 25 $^{\circ}\text{C}$, washed with 200 μl of HKS (pH 7.4) and imaged for both membrane and protein channel (Texas Red and FITC channel) respectively.

2.7 Fluorescence microscopy

Fluorescence imaging was carried out on an Olympus IX71 inverted microscope equipped with a 100X, 1.4 NA oil-immersion objective. Fluorescent probes were excited with a stable LED light source (Thor Labs), and fluorescence emission was collected through filters (Semrock) with excitation/emission wavelength bandpasses of $482 \pm 35 \text{ nm}/536 \pm 40 \text{ nm}$ for Alexa488 and $562 \pm 40 \text{ nm}/624 \pm 40 \text{ nm}$ for Texas Red probes simultaneously on two Evolve 512 EMCCD cameras (Photometrics). Image acquisition was controlled by Metamorph software (Molecular Devices).

All the movies were collected at 100 ms exposure at 1x (10 Mhz gain) 100 gain settings.

2.8 Image analysis, Coefficient of Variation (COV) calculation, tube radius calculation and estimation of fission probability

Image analysis of fluorescence micrographs and time-lapse movies were carried out using Fiji (version 1.47) (Schindelin et al., 2012) and nonlinear regression analyses were carried out using Graphpad Prism (version 6.0).

To calculate the tube radius from the tube fluorescence, we utilized supported bilayer formed near the source during SMrT template preparation as an in-situ calibration standard (Pucadyil and Holkar, 2016). Fluorescence of a diffraction-limited, membrane-bound objects is proportional to the net membrane surface area (Kunding et al., 2008). For each experiment, fluorescence micrographs of the SLB and tubes were acquired. To generate standard the integrated fluorescence intensity of ROIs of various sizes on SLB was estimated and the integrated intensity was plotted against corresponding area (μm^2) and data fitting to a linear curve provided calibration constant K1. Next, the integrated fluorescence intensity of ROIs of a defined length (l) placed on tubes was collected and converted to net membrane area using K1. From the area, calculated radius tube r was estimated using $r = \text{area}/(2\pi l)$. Plotting the

estimated tube radius (r) against the corresponding maximum pixel intensity in ROIs placed on tubes to get calibration constant K_2 . To calculate the radius of a given tube, ROI is placed to acquire maximum intensity. Maximum intensity is then divided by K_2 to obtain the radius.

The probability of fission was calculated by dividing tubes which underwent cut to the total number of tubes in a radius range. Whether a tube is cut or not was defined by estimating the tube radius for all the tubes in a field followed by seeing whether a tube of given radius has undergone cut at the end of the movie (~7 min).

To calculate COV, 200-pixel long line (single pixel width) was placed on the tube and mean, and standard deviation (SD) was calculated using Fiji. To estimate the COV, over the time course of the reaction, mean and SD was calculated manually by placing a 200-pixel long line on each membrane tube and estimating mean and SD for the entire time course. COV was calculated for each time point by dividing SD with corresponding mean value.

2.9 FAT Blot assay.

Lipid stocks of DOPC, DOPS, PI4P and PI (4,5) P2 were reconstituted in ChCl_3 to the final concentration of 1 mM. 1 nM of each of the lipid was spotted onto the nitrocellulose membranes and blocked by incubating the membrane with 3% fatty-acid free BSA prepared in HKS (20 mM HEPES-KOH, pH 7.4, 150 mM KCL) (Blocking) for 1hr at RT. EHD1-strep (1 μM) was added to the mix and incubated at RT for 3 hours followed by the excess washing with HKS. Blot was immersed in 1 $\mu\text{g/ml}$ of Streptavidin-A-488 conjugate prepared in HKS and incubated for an hour with gentle shaking followed by an extensive wash with HKS. The images were captured using green filters on LAS-4000 (GE).

Quantitation of the enrichment of EHD1 binding to lipid was done by placing ROI on the signal. Background intensity was subtracted from fluorescence intensity for each lipid. To obtain the relative binding of EHD1 to the lipids, all the intensities were normalized to the lipids with the highest intensity for each experiment.

2.10 Dynamin and EHD1 assembly on SMrT templates.

SMrT templates containing PS, (DOPC: DOPS: *pTxRed*; 59:40:1) were made as described earlier. To perform assembly of Dyn and EHD1, SMrT templates were first equilibrated in filtered and degassed HKS (20 mM HEPES (pH 7.4), 150 mM KCl) containing an oxygen scavenger cocktail of 0.2 mg/ml glucose oxidase (Sigma, G-2133), 0.035 mg/ml catalase (Sigma, C-40), 4.5 mg/ml glucose (Sigma) and 1 mM DTT and 1 mM MgCl_2 .

Dynamin-1 and EHD1 were previously dialyzed overnight against pre-chilled HKS (containing 1 mM DTT and 1 mM EDTA) and spun at 100,000g for 20 min to remove aggregates and reconstituted in HKS to the final concentration of 0.5 and 1 μ M, respectively, with oxygen scavenger cocktail, 1 mM MgCl₂. Dyn-1 and EHD1+ATP γ S (1 mM) were flowed into the chamber at 25 °C at a low flow rate of ~1 mm/s and 100 msec time lapse was captured.

2.11 Formation of mEGFP encapsulated SMrT templates and EHD1 assembly.

GFP encapsulated SMrT templates were made by using lipid mix containing 5 mol% DGS-NTA lipid in addition to 40 mol% PS (DOPC:DOPS:DGS-NTA:pTxRed; 54:40:5:1). Lipid mix was added to PEG-8000 coverslips and dried. The coverslip was assembled in the chamber and hydrated with 5 μ M mEGFP in oxygen scavenger cocktail for 10 min. Afterward SMrT templates were made by passing degassed HKS. At this time GFP is bound to both inner and outer leaflet of the tube. To selectively remove the GFP from an outer leaflet, 1 ml of 100 mM EDTA, reconstituted in HKS buffer was flowed at low flow rate and subsequently excess of HKS (~5 ml) was passed to remove the EDTA. After the procedure tubes were scanned for the uniform fluorescence of membrane and GFP. The field with maximum number of tubes containing uniform GFP intensity was selected for the reaction. EHD1 assembly reaction was carried out as mentioned in 3.2.1. For the analysis of change in GFP fluorescence, single pixel line at the region of the interest, intensity was obtained and normalized to the intensity value of the first frame.

For the analysis of before and after EHD1 assembly, line was placed on the tube in each case and membrane and GFP intensity was collected. The Intensity was normalized to the mean value for each condition and plotted in Prism.

Chapter. 3

Characterization of EHD1 mediated membrane fission

3.1. Introduction:

3.1.1 Necessity to reconstitute EHD1 function in-vitro.

Accumulation of receptor at ERC and tubular expansion of the compartment in the absence of EHD1 (achieved either by knocking down EHD1 or over-expressing dominant negative mutant), EHD1 has been proposed to carry out scission of membrane tubules present at the ERC. Till date, tubular to vesicular redistribution of recycling receptors (Tf) or ERC markers (MICAL-L1) been used as the proxy to arrive at conditions which affect EHD1 function (Cai et al., 2011, 2012, 2013; Jovic et al., 2009). However, these qualitative assays are not necessarily indicative of EHD1 mediated fission and additionally, are plagued by numerous limitations such as:

- 1) Spatio-temporal resolution: As membrane fission necessitates bilayers to be nearby (~5 nm; the dimension of a bilayer), spotting and tracking of such a diffraction-limited precursor of the fission reaction become a daunting task due to the sheer 3D volume of the cell.
- 2) Biochemical Complexity: Cells contain plethora of proteins that regulate vesicular transport from a given organelle. Cell-based assays can only provide the information relating to the involvement of a given protein in fission. Such assays, however, cannot reveal whether a given protein independently catalyzes fission or is mere an accessory molecule in the membrane fission machinery.

Recently, EHD1's ability to catalyze fission was tested using a semisynthetic approach. HeLa cells were semi-permeabilised to remove cytosol and peripherally bound membrane proteins. Under these conditions, MICAL-L1 coated membrane tubes (ERC) were used as the membrane substrate and recombinantly expressed GST-EHD1 was added to these cells in the presence of ATP. Subsequently, the disappearance of MICAL-L1 coated tubes in the presence of GST-EHD1 and ATP was used to provide the evidence that EHD1 can catalyze membrane fission. The rationale is that in the absence of EHD1, ERC assumes an extensively tubulated and enlarged state and an extensive increase in tubular localization of MICAL-L1, an ERC marker, reflects this change in ERC morphology (Cai et al., 2013; Lee et al., 2015). The study is a significant advancement in the field of EHD1 mediated fission and provides first qualitative evidence of EHD1 being capable of catalyzing membrane fission. However, it leaves several questions unanswered. a) The disappearance of MICAL-L1 coated tube is observed at the end of 30 minutes making it an end point assay, precluding the observation of fission reaction, and on the kinetics of EHD1 mediated fission. This becomes important as ERC controls transport

of a large variety of receptors from the ERC which necessitates a fast acting fission machinery to maintain the flow of traffic. b) PS (phosphatidylserine), PI4P (phosphatidyl inositol-4-phosphate), PI4,5P₂ (phosphatidyl-inositol 4,5 bisphosphate), PA (phosphatidic acid) and lysolipids are present on ERC (Cai et al., 2012; Giridharan et al., 2013; Jovic et al., 2009). The semi-synthetic approach does not allow evaluation of various lipids in EHD1 recruitment/function. c) Importance of ATP binding and hydrolysis in EHD1 recruitment/function. ATP binding is shown to be important for membrane localization of EHD1 *in vivo* (Lin et al., 2001), however, *in vitro* studies indicate that EHD1 can bind membrane in absence of nucleotide (Lee et al., 2015). These contradictory reports raise the question of the precise role of ATP binding in EHD1 function. d) Lack of localization of EHD1 to the site of fission discourages the direct correlation between EHD1 and membrane fission. Previously, studies addressing membrane fission function of a given protein (such as dynamin1 or dynamin-related protein 1; Drp1) find that dynamin1 co-localization to clathrin punctae or Drp1 co-localization at the tubular mitochondria precedes disappearance of clathrin punctae (an indication of the release of clathrin bud) and fission of mitochondria respectively. This provides a strong support for dynamin and Drp1's involvement in membrane fission (Friedman et al., 2011; Meinecke et al., 2013).

We have taken an *in vitro* reconstitution approach to address whether EHD1 can catalyze membrane fission. Our interest studying EHD1's capability to catalyze fission is also motivated by following reasons:

- a) Unlike the rest of the GTP binding members of the dynamin superfamily, EHD proteins are only known ATP binding proteins in the dynamin superfamily. Also, they are the only known ATP binding, peripheral membrane proteins with the ability to oligomerize and tubulate membranes (Daumke et al., 2007; Lee et al., 2005; Pant et al., 2009) making EHDs an interesting candidate membrane fission catalyst.
- b) EHD proteins only share structural similarity to the G-domain of dynamin and the role of the rest of the domains in the context of protein function is yet undetermined, leaving an opportunity to probe and understand whether these proteins behave in a similar way as dynamin or have evolved to function differently.
- c) If EHD1 indeed functions as a fission catalyst, it opens up avenues to test the function of other EHD family members. Despite the very high sequence similarity (~70-80%) among the 4 (EHD1-4) paralogs in mammals (Daumke et al., 2007), EHD proteins localize to separate endosomal compartments and are required to maintain the directional vesicular transport.

The high sequence similarity among the EHDs could indicate the similarity in their function despite difference their localization.

To address whether EHD1 can indeed catalyze membrane fission, we took the in-vitro reconstitution approach. We use a set of assays including, protein-liposome binding and ATPase activity to arrive at the suitable membrane composition in order to re-constitute EHD1 function on SMrT template system which is developed in our lab and has been shown to report fission capability of well-known fission catalyst dynamin (Dar et al., 2015).

3.2 Results:

3.2.1 EHD1 expression and purification.

EHD1 has been shown to interact with its partner proteins such as Syndapin2 (SDP2) via the EH domain-NPF motif interaction. Immunoprecipitation with GST-SDP2 and GST-NPF pulls down EHD1 in cells (Braun et al., 2005). We tried using a similar strategy to pull down EHD1 from bacteria using GST-SDP2 and GST-NPF as bait but faced several issues; a) the binding of EHD1 to the bait was very little which we could not dissociate from the GST-NPF. b) Use of full-length SDP2 led to pulling down of several other proteins, precluding a homogenous preparation of EHD1 (data not shown).

We next resorted to recombinantly expressed EHD1 in bacteria and purification using affinity chromatography methods. We initially followed expression protocol using IPTG induction for EHD2 (Daumke et al., 2007). To obtain better yields, we replaced the LB media to the terrific broth. Under both conditions, we obtained good yields, but the purified protein was prone to precipitation after purification and showed variable yields (data not shown).

We finally resorted to express the protein in auto-induction medium for 24 hours, harvested the bacterial culture and purified the protein (see Methods). We could purify recombinant EHD1 to a high purity and obtained reproducible yields with low precipitation of the purified protein (Fig. 3-2-1 a).

3.2.2 Biochemical characterization of EHD1.

To reconstitute EHD1 function, we assayed the recombinantly expressed and purified EHD1 for lipid specificity and ATPase activity. To test the lipid specificity of EHD1, we looked at EHD1 binding to PS, PA, PI4P, PI(4,5)P₂ using a FAT blot assay (Munnik and Wierchowicka, 2013). These lipids were chosen based on the EHD1 co-localization or

binding to membranes enriched in these lipids (Blume et al., 2007; Giridharan et al., 2013; Lee et al., 2015; Naslavsky et al., 2007; Sharma et al., 2009b). We spotted lipids (1 nM) on a nitrocellulose membrane strip, incubated EHD1-strep (1 μ M) and probed with Alexa488-streptavidin. We found that EHD1 showed similar binding to PS, and PI (4,5)P₂, and relatively lesser binding to PI4P and very little binding to PA (Fig. 3-2-1 b.). The binding to PS is consistent with the recent report of PS being enriched at the ERC (Lee et al., 2015).

We chose PS for further characterization for the following reason, a) PS appears to be required for the recruitment EHD1 to ERC in-vivo, and its depletion leads to diffused localization of EHD1. The change in EHD1 distribution recapitulates EHD1 knockdown phenotype, namely receptor accumulation and enlargement of ERC (Lee et al., 2015); b) Increasing PS fraction at the expense of PC in a liposome-binding assay provides an easy system to understand EHD1 membrane binding characteristics in response to increasing membrane charge.

To study the EHD1 binding response with increasing membrane charge, we carried out the liposome-co-sedimentation assay of EHD1 using liposomes with increasing PS content. We incubated EHD1 (1 μ M) with a 100-fold excess of liposomes with increasing PS content (20, 40, 60, 80 and 100 mol% PS) and pelleted down the liposomes using an ultra-centrifuge spin (see methods). Quantitation of the enrichment of EHD1 in the pellet in comparison to the total protein indicated that EHD1 showed a sigmoidal increase in the binding with increasing PS content. We fitted the binding response to “one site - specific binding with hill slope” which gave us half-maximal binding to be ~40 mol% PS (Fig. 3-2-1 c-d).

To access whether membrane binding has any effect on the protein function (especially on ATPase activity), we estimated EHD1 ATPase activity under the conditions of liposome co-sedimentation assay (see methods). EHD1 showed a basal ATPase activity of ~1 μ M Pi.min⁻¹. μ M⁻¹ and did not show an increase in the presence of PC or 20 mol% PS-containing liposomes. On increasing the PS content in the liposomes, ATPase activity showed a sharp increase (membrane stimulated ATPase activity) and reached as high as ~8.5 μ M Pi.min⁻¹. μ M⁻¹ with 40 mol% PS liposomes. ATPase activity showed saturation upon an additional increase in PS. The rise in ATPase activity closely matches EHD1 membrane binding, indicating the membrane binding leads to direct activation of ATPase activity (Fig. 3-2-1 d-e).

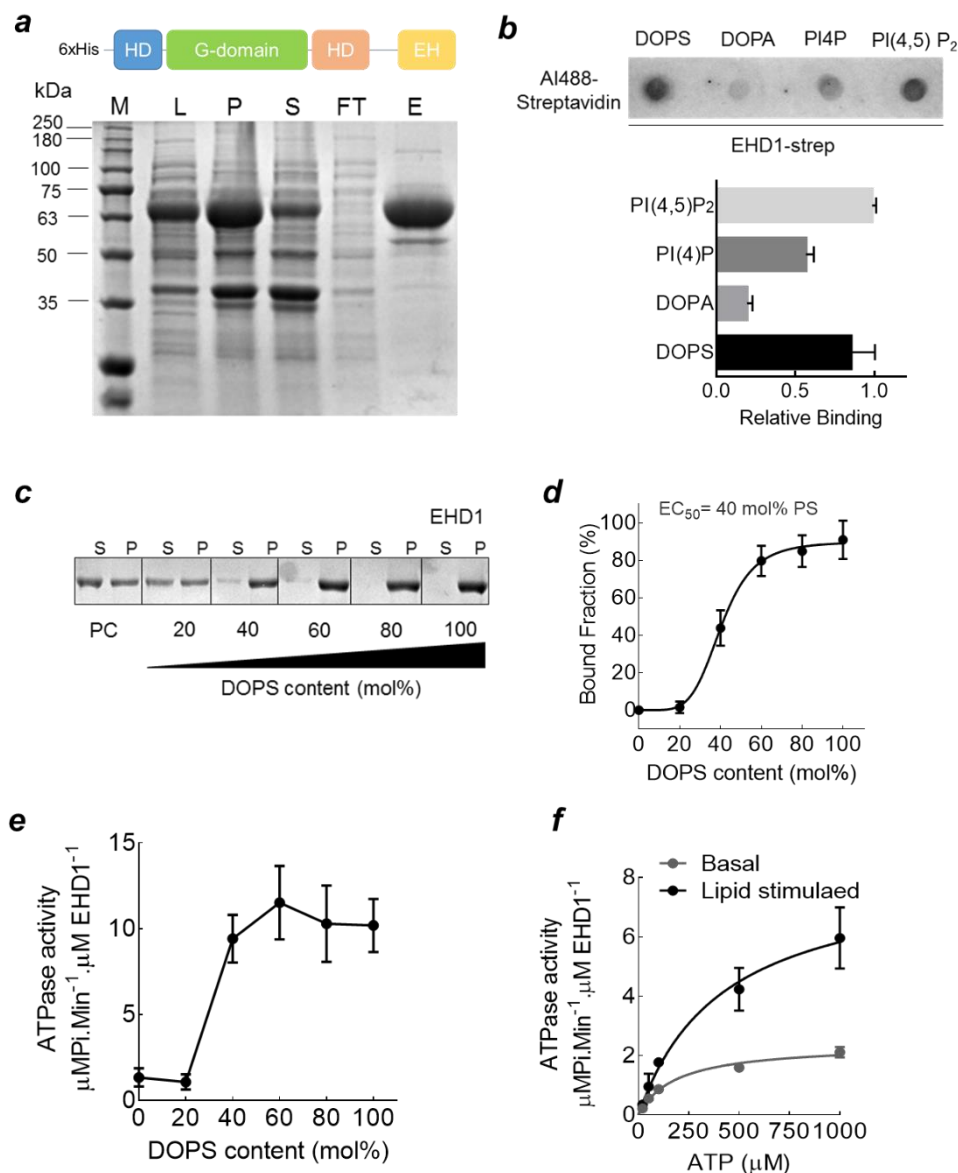


Figure 3-2-1. Recombinant EHD1 purification and biochemical characterization. (a) Purification of recombinant EHD1 using immobilized metal affinity chromatography. M=marker, L=lysate, P=pellet, S=Supernatant, FT= Flow-through and E=Elution. (b) FAT blot result of recombinant EHD1-Strep. Top panel, a representative image of FAT blot of recombinant EHD1 probed with Alexa-488 Streptavidin. Lower panel graph shows the relative binding of EHD1 to individual lipid (Data is pooled from 3 independent experiment). (c) Representative gel images of the liposome-cosedimentation assay of EHD1. The supernatant (S) and pellet (P) for EHD1 and liposomes with increasing PS content (d) Quantitation of the enrichment of EHD1 in pellet for (c). Data represents mean \pm SD for 3 experiments. All the value are fit to “One site-specific binding with hill slope” using GraphPad Prism 6. (e) EHD1 ATPase activity with liposomes containing increasing PS content. (f) Estimation of ATP affinity of EHD1 and effect of the membrane on ATP affinity of EHD1.

Together, the membrane binding and ATPase assay helped us narrow down the membrane composition which could be used to reconstitute EHD1 function. We find that

EHD1 shows half maximal binding and saturation of stimulated ATPase activity at 40 mol% PS. Based on these criteria, we chose 40 mol% PS-containing membranes to reconstitute EHD1 function.

As we observed stimulation of ATPase activity in the presence of membranes, we tested whether the stimulation is due to EHD1's increase in apparent affinity for ATP in the presence of membranes. To this end, we measured the EHD1's affinity to ATP in absence and presence of liposomes (100 mol% PS) (see methods). Recombinant EHD1 displayed about 2.5 fold ($\sim 420 \mu\text{M}$) higher affinity to ATP in presence of liposomes (100%PS) as opposed to the absence of liposomes ($\sim 180 \mu\text{M}$) (Fig. 3-2-1 f).

3.2.3 Reconstitution of EHD1 function.

EHD proteins are the sole ATP binding members of dynamin superfamily (Daumke et al., 2007; Lee et al., 2005). To study whether EHD1 can deform the membrane and catalyze fission, we used Supported *membrane tubes* (SMrT) template assay which was devised in our lab and was shown to be a well suited to report membrane deformation and fission capability of dynamin (Dar et al., 2015). Additionally, EHD1 localizes to tubular membrane templates *in vivo* (Cai et al., 2011, 2012, 2013; Caplan et al., 2002; Jovic et al., 2009; Sharma et al., 2009), making SMrT templates are suitable to test EHD1 function. We tested EHD1 binding to SMrT templates and effect of the ATP-binding on EHD1 membrane binding.

3.2.4 ATP binding imparts membrane deformation capability to EHD1.

As mentioned earlier, we used 40 mol% PS (40-PS) containing SMrT templates to study EHD1 function. SMrT Templates (40 mol% PS) were stable for hours and showed a mean tube radius $11 \pm 3 \text{ nm}$ (Fig. 3-2-2 c) (see methods to tube radius calculation). PS distributed uniformly across the length of the SMrT template as judged by the uniform GFP fluorescence of mEGFP fused to PS specific probe LactC2 (Yeung et al., 2008) (Fig.3-2-2 b). EHD1 ($1 \mu\text{M}$) was added to these SMrT templates in absence or presence of nucleotides (ADP or ATP γ S) at room temperature. The addition of EHD1 alone or with ADP (1 mM) did not cause any membrane remodelling of SMrT templates. Whereas, EHD1 addition in the presence of ATP γ S (1 mM; slowly hydrolysable ATP analog, represents ATP-bound state) led to the formation of regular, alternative high and low membrane intensity regions (Fig. 3-2-2 d). As the fluorescence of diffraction-limited object is proportional to the area, low-intensity regions on tube reflect the formation of constriction upon membrane deformation by ATP-bound EHD1.

The effect of ATP binding also reflected in protein binding and distribution on SMrT templates. Addition of BODIPY labelled EHD1 (0.5 μ M labelled+ 0.5 μ M unlabelled; final concentration 1 μ M) like mEGFP-LactC2, displayed rather uniform binding across the length of the SMrT template (Fig.3-2-2 e; BODIPY EHD1). ATP γ S bound EHD1 on the other hand, showed punctate localization on SMrT templates and as shown earlier, caused constriction of membrane tube (Fig. 3-2-2 f; BODIPY-EHD1+ATP γ S).

Kymograph of BODIPY-EHD1 binding to SMrT template showed that EHD1 bound uniformly across the length of tube which increases in intensity over time. ATP bound EHD1 on the other hand, bound as distinct punctae at the earliest stages and each punctae further grew in intensity (Fig.3-2-1 e-f; compare BODIPY EHD1 and BODIPY-EHD1+ATP γ S kymograph). The distinct differences in the manner in which EHD1 bound SMrT templates in absence and presence of ATP indicate that ATP binding brings about conformational changes and makes EHD1 oligomerization and membrane remodeling competent (see discussion).

3.2.5 EHD1 catalyzes membrane fission in an ATP hydrolysis-dependent manner and is sensitive to tube dimension.

Further, we probed the role of ATP hydrolysis in EHD1 function and added EHD1 (1 μ M) with ATP on 40 mol% PS SMrT templates. We carried out this reaction at 37 °C as EHD1 shows 2 fold higher stimulated ATPase activity at 37 °C when compared to 25 °C (Fig. 3-2-3 a). The addition of EHD1+ATP led to constrictions (similar to EHD1+ATP γ S) on templates followed by multiple cuts in the field of observation (Fig. 3-2-3 b). As we did not see this phenotype with ADP and only at long incubations with ATP γ S (slowly hydrolysable analog), we propose that EHD1 requires ATP hydrolysis to catalyze membrane fission. Remarkably, we observed that a number of tubes remained intact at the end of the fission reaction (Fig. 3-2-2 c). We observed that the tubes remained intact had higher initial tube fluorescence intensity. As the fluorescence for limited diffraction object depends upon the area, high and low-intensity tubes represented the large and small diameter of the tube, respectively.

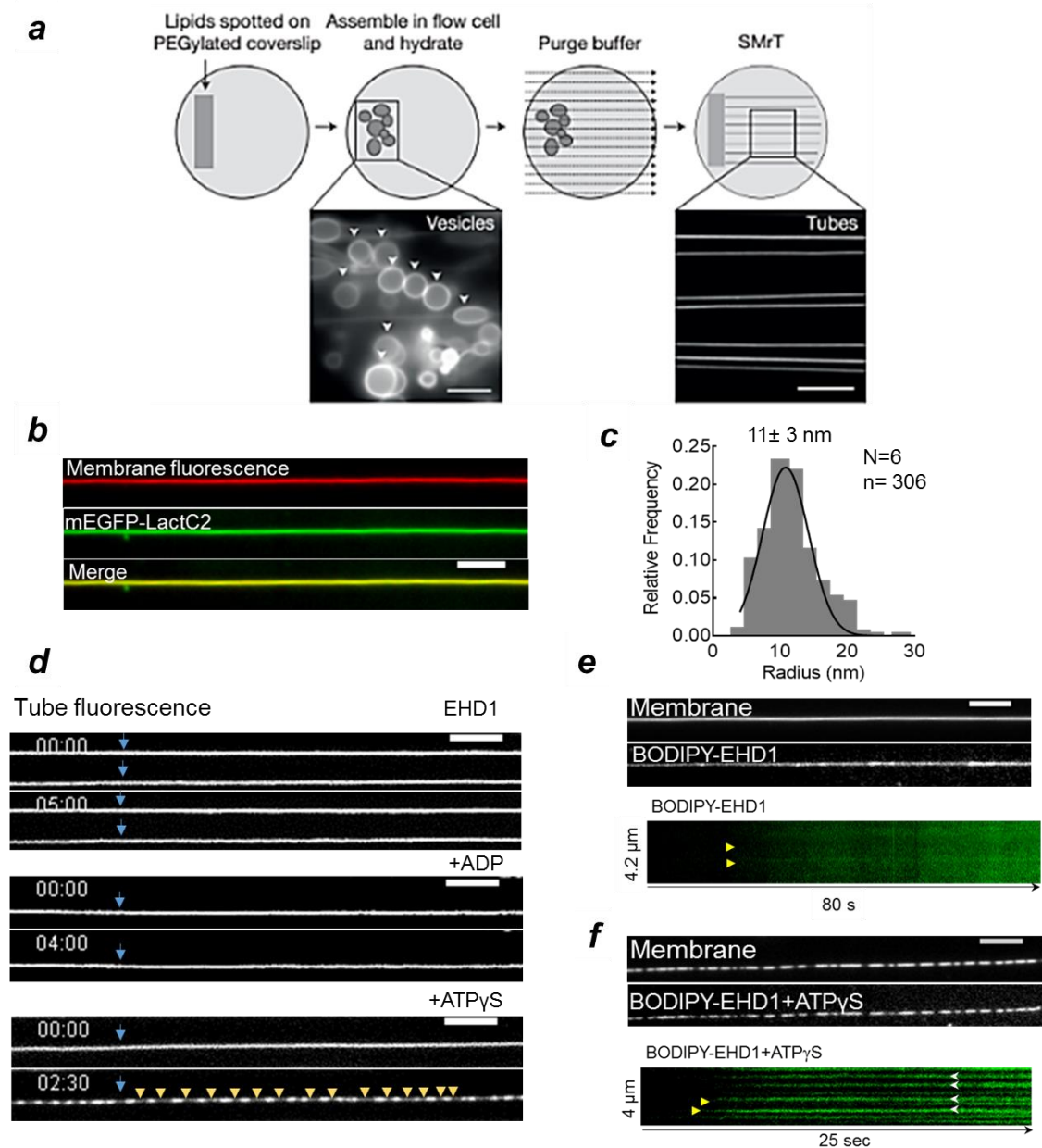


Figure 3-2-2. ATP binding leads to oligomerization and imparts membrane deformation capability to EHD1. (a) Schematic representation of SMrT template preparation (Dar et al., 2015). Scale bars, 10 μm . (b) DOPS distribution on tubular SMrT templates using PS specific mEGFP -LactC2. (c) Radius distribution of 40-PS SMrT templates on PEG400 coverslips. (d) Effect nucleotide binding on SMrT templates morphology. ATP bound EHD1 (+ATP γ S) leads constrictions of the SMrT templates. Blue arrow indicate membrane tube. (e-f) Effect of ATP binding on EHD1 distribution. EHD1 shows uniform distribution (BODIPY-EHD1). Kymograph (in green; BODIPY-EHD1) of EHD1 binding indicates the uniform binding of the protein to the SMrT template (e) (yellow arrowhead initiation of EHD1 binding). ATP bound EHD1 shows punctate distribution on SMrT template (BODIPY-EHD1+ATP γ S) on SMrT template. Kymograph (in green; BODIPY-EHD1+ATP γ) reflects nucleated binding of the protein (yellow arrowheads indicate the start of binding, white arrowhead indicate scaffold). Scale bars, 5 μm

To confirm whether the fission depends upon initial tube radius, we estimated the tube radius (see methods) and measured the fission probability for all the tubes in the field. Strikingly, we found that EHD1 mediated fission showed sharp dependence on initial tube radius. Tubes below 10 nm radius always underwent fission (fission probability=1) whereas for a tube with radii between 10-20 nm, the fission probability became fractional and tubes radius higher than 20 nm did not undergo fission at all (Fig. 3-2-3 d). Estimation of cumulative EHD1 fission rate on tubes which underwent fission (fission compliant) showed that EHD1 catalyzes fission at $1.7 \text{ cut}\cdot\text{sec}^{-1}$. To further characterize EHD1 mediated fission, we made kymographs of the effect of the addition of EHD1+ATP on SMrT templates and estimated fission time (time difference between cut and appearance of membrane deformation on the tube; Fig. 3-2-3 f-g). We find that EHD1 takes on an average 42 sec to catalyze fission. Based on the k_{cat} of EHD1 stimulated ATPase activity ($8.5 \mu\text{MPi}\cdot\text{min}^{-1}\cdot\mu\text{M EHD1}^{-1}$) (0.14 sec^{-1}), we found that EHD1 subunit hydrolyze ~ 6 ATP molecules to catalyze membrane fission.

To understand the basis of the tube dimension sensitivity of EHD1 mediated fission, we looked at the capability of EHD1 to deform fission compliant and fission resistive tubes. Comparison of the kymograph of the EHD1 assembly indicated that fission compliant tubes underwent fission (Fig.3-2-4 b; fission event). However, EHD1 assembly on resistive tube displayed a peculiar phenotype, where EHD1 assembly first led to deformation, which over time started disappearing (Fig.3-2-4 b; abortive event) and the tube intensity returned to near uniformity (Fig. 3-2-4 b; compare kymograph for fission and abortive event). To understand the reason behind the abortive event on thicker tubes, we quantitated the extent of membrane deformation by EHD1 on fission compliant and resistive tubes.

To estimate EHD1 mediated membrane deformation, we utilized “coefficient of variation (COV)” as a measure of non-uniformity of the membrane tube upon deformation. EHD1 assembly (oligomerization) mediated membrane deformation leads to the striated appearance of the tube owing to the formation of high and low tube fluorescence intensity. This change leads to increase in the standard deviation (SD) of the tube fluorescence intensity whereas the mean tube fluorescence remains largely unchanged. The change can be represented by COV analysis. COV is the ratio of standard deviation (SD; σ) to the mean for a given data set.

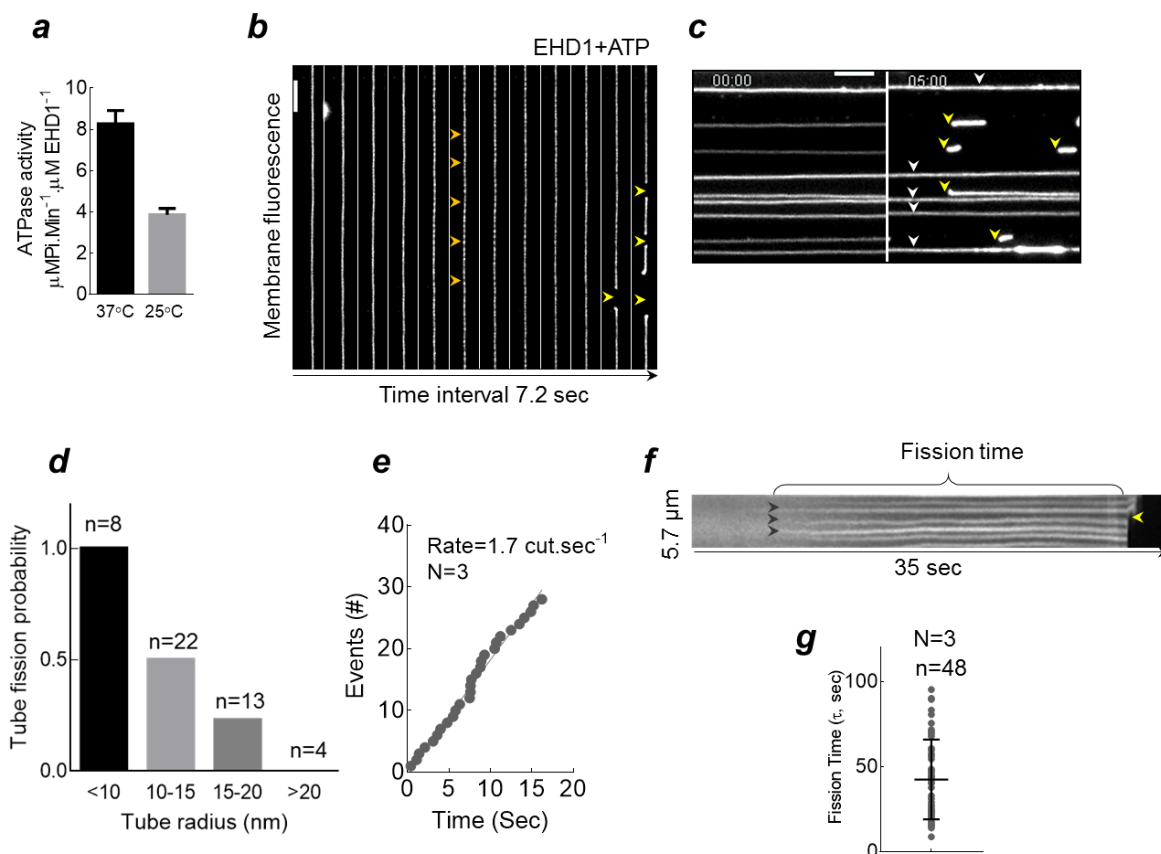


Figure 3-2-3. EHD1 catalyzes membrane fission in ATP hydrolysis-dependent manner and is sensitive to tube dimensions. (a) EHD1 stimulated ATPase activity at 25 °C and 37 °C. (Data pooled from 3 independent experiments). (b) Representative image of a time-lapse movie of EHD1+ATP addition to 40-PS SMrT templates at 37 °C. EHD1+ATP caused striation formation (orange arrowhead) followed by cut (yellow arrowheads). (c) The micrograph is depicting the variability of fission by EHD1+ATP at 37 °C. (d) The probability of EHD1 mediated fission as a function of the radius of membrane tubes. (Data is pooled from 3 independent experiments) (e) Cumulative fission rate for EHD1 (Data pooled from 3 experiments). (f) Kymograph of EHD1 fission reaction. Time difference between the start of deformation (black arrowhead) to the fission (yellow arrowhead) is defined as fission time. (g) Fission time of EHD1 mediated fission at 37 °C on 40 mol% PS SMrT templates. N, the number of independent experiments, n, number of events analyzed. Scale bars, 5 μm .

Hence change COV value over the course of fission reaction reflects protein assembly induced membrane deformation. Estimation of COV during the fission reaction on SMrT templates indicated that over time the COV increases from ~ 0.1 to 0.4 (Fig. 3-2-4 c). Comparison of change in COV on thin (fission compliant) and thick tube (fission resistive) displayed that rise in COV is essentially same for both thin and thick tube and reaches maximum value ~ 0.4 (Fig. 3-2-4 d-e). At this point the thin tubes underwent fission, whereas thick tube start showing decrease in COV value which was reflected by the dissipation of striations on thick tubes. This effect could arise due to the limitation in extent of EHD1 scaffold mediated deformation (see discussion).

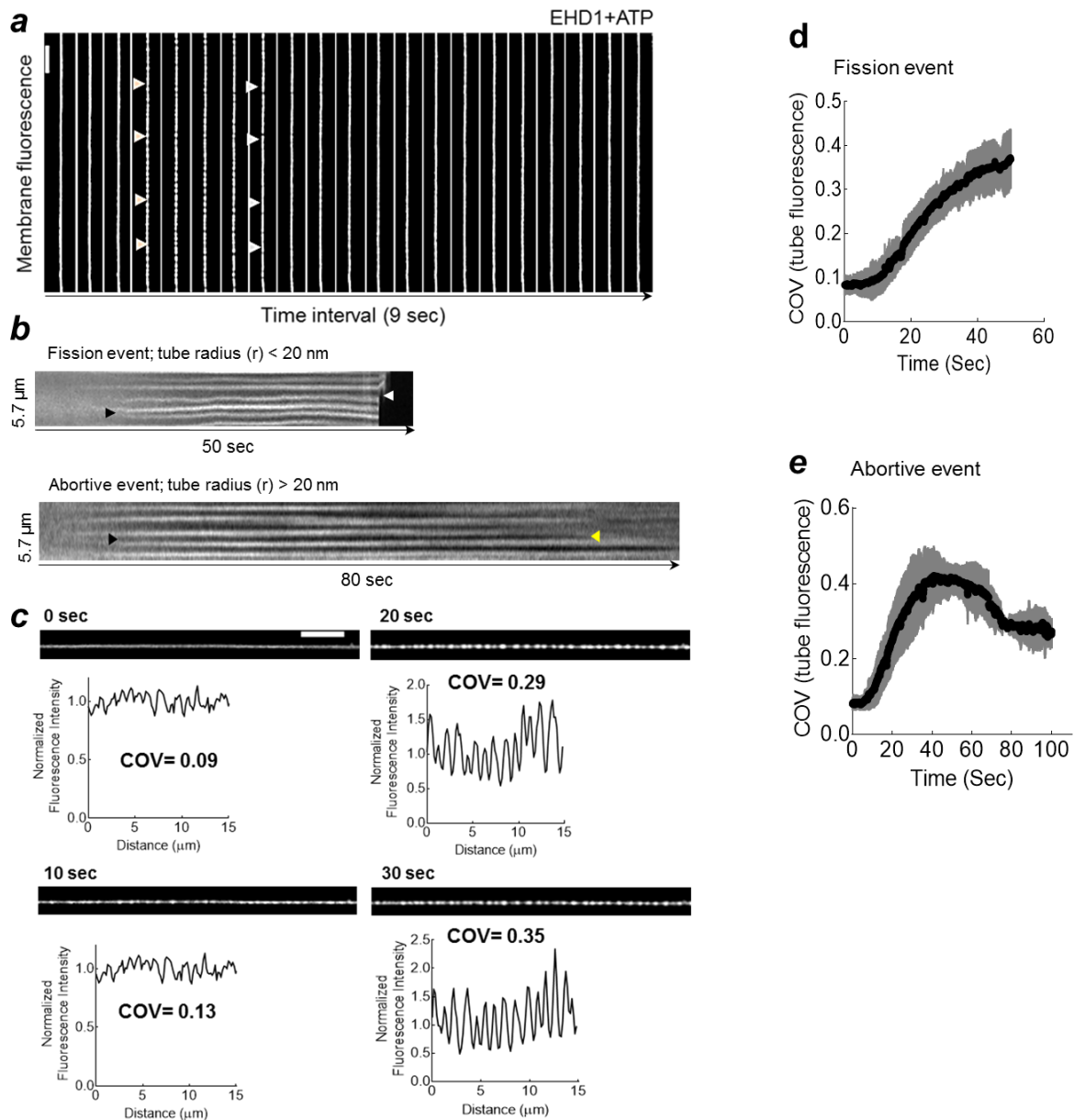


Figure 3-2-4. EHD1 mediated membrane deformation is tube dimension independent. (a) Representative image panel is showing the topological transformation on membrane tubes which do not undergo membrane fission. Note the formation of striations (orange arrowheads) which later dissipate (white arrowheads) (b) Estimation of EHD1+ATP mediated membrane deformation on 40-PS SMrT templates using Coefficient of Variance (COV). Panel 0-30 sec depicts time points during EHD1 mediated deformation accompanied with a graph depicting the tube fluorescence intensity at given time and corresponding COV value. The increase in COV indicates increased membrane remodeling (see text). (c-d) Change in COV values for tubes which undergo fission (d) and tubes which remain intact (e). Note that in both cases COV values reach ~ 0.4 at which thin tubes undergo fission whereas thick one remain intact and striations dissipate leading to the lowering of COV values. Scale Bar, 5 μm .

3.2.6 EHD1 mediated fission is affected by the presence of non-bilayer lipids.

Previous studies have indicated the ERC is enriched in lysolipid species and that the depletion of these species leads to the accumulation of receptors (Cai et al., 2012). As EHD1 regulates the recycling of the receptor and having shown that EHD1 can catalyze fission in an *in vitro*, we set out to define the look at the effects of the presence of lysolipids on EHD1 function.

We looked at the liposome binding and stimulated ATPase activity of EHD1 in the presence of liposomes containing 5-30 mol% LPA (PC-LPA liposomes) and found that EHD1 neither showed membrane binding nor stimulated ATPase activity under these conditions (data not shown).

To test whether the presence of lysolipids affects EHD1 mediated fission, we added 5 mol% LPA along with 40% PS (PS-LPA: 40-5) in our lipid mix and made SMrT templates. Estimation of fission rates at 37 °C on these SMrT templates indicated that EHD1 fission rates were increased by ~3 fold (1.7 cuts/sec; N=3 vs. 6 cuts/sec, N=3, for PS and PS: LPA SMrT templates, respectively) (Fig. 3-2-5 a-b). This suggests that LPA which has single phospholipid chain and assumes an inverted cone shape in a bilayer made of cylindrically shaped lipids (Chernomordik et al., 1993; Fuller and Rand, 2001; Kooijman et al., 2005) (e.g. PC and PS) increases rates of EHD1 mediated fission. Based on this observation, we hypothesized that presence of conical shaped lipid (e.g. PA) should in principal decrease EHD1 mediated fission rates. To test this hypothesis, we chose phosphatidic acid. Phosphatidic acid is enriched at ERC and specifically recognized by EHD1 interacting proteins MICAL-L1 and SDP2 (Giridharan et al., 2013; Xie et al., 2014). However, it's not clear whether EHD1 can recognize PA. To test whether EHD1 can bind PA, we performed the liposome-cosedimentation assay with 100 nm extruded liposomes, containing 0-50 mol% PA, to test for EHD1 binding. EHD1 showed extensive binding to PA liposomes (Fig. 3-2-5 c). PA recruited more protein than PS at a lesser mole fraction (EC50 is 40 and 20 mol% for PS and PA, respectively, (Fig. 3-2-5 c), however, with increasing surface charge EHD1 binding to PA liposomes increased in a seemingly linear fashion when compared to PS (sigmoidal response). PA-stimulated binding also led to robust stimulation of ATPase activity (Fig. 3-2-5 d).

-

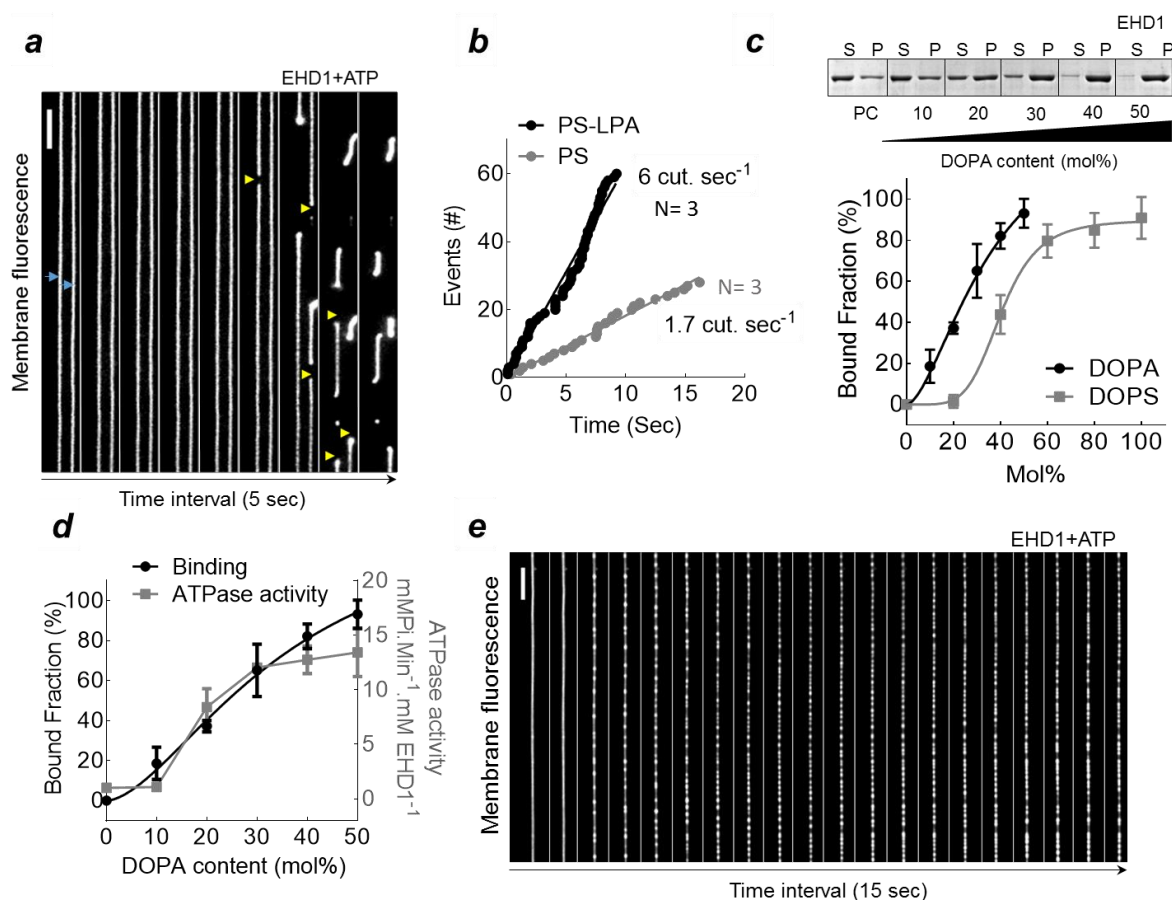


Figure 3-2-5. EHD1 mediated fission is affected by the presence of non-bilayer lipids in the membrane. (a) The panel shows a representative image of fission of PS-LPA (40-5) SMrT templates. Blue arrow indicate the membrane tube (b) Comparison of cumulative fission rate on 40-PS and PS-LPA (40-5) SMrT templates (Data is pooled from 3 independent experiments for each condition) (c) Top panel, representative gel for EHD1 liposomes-cosedimentation assay with PC-PA liposomes. The bottom panel represents a comparison of EHD1 membrane binding to PC-PA or PC-PS liposomes. Mean \pm SD of fraction bound protein is presented for each condition (Data is pooled from 5 and 3 independent experiments for PC-PS and PC-PA liposome respectively). The panel shows a representative image of the addition of EHD1 in the presence of ATP on 20 mol% PA SMrT templates. SMrT template undergoes striation formation, but striations do not resolve into fission. (d) EHD1 membrane binding and ATPase activity on PA liposomes. (e) Representative image of membrane deformation on 20 mol% PA membrane tube upon EHD1+ATP addition. Note the absence of fission on SMrT template. Scale bar, 5 μ m.

We made SMrT templates containing 20 mol% PA (20-PA) and performed EHD1 mediated fission. We found that 20-PA SMrT templates underwent similar transformations as PS containing SMrT templates. However, we saw few peculiar differences; a) although constrictions were formed and progressed as seen on PS SMrT templates, very few, if at all, underwent fission (Fig. 3-2-5 e), b) striations on PA templates showed considerable lateral movement on the SMrT templates. Estimation of COV of the membrane deformation indicated

that the EHD1 mediated deformation led to increase in COV which was similar to what seen for PS (data not shown), although we did not see fission. Strikingly, unlike the EHD1 on the thicker tube, we did not see the dissipation of striations on the SMrT templates. Taken together, we found that presence of inverted cone lipids, increased EHD1 mediated fission whereas the presence of cone-shaped lipids inhibited EHD1 mediated fission (see discussion).

3.3 Discussion

We recombinantly expressed and purified EHD1 and using the combinatorial approach of membrane binding and ATPase activity estimation arrived at a membrane composition to reconstitute EHD1 function. Our results unequivocally establish that EHD1 can catalyze membrane fission on a tubular membrane containing sufficient negative charge.

Purified EHD1 shows similar binding to PS (consistent with the recent report (Lee et al., 2015) and phosphoinositides. Although PIPs have higher negative charge than PS, EHD1's relatively similar binding to PS and PIP2 and better binding than PI4P indicates that the binding does not solely depend upon charge. Nevertheless, lack of specific binding to one of the lipids tested also rules out lipid-specificity of EHD1. Taken together, FAT blot data indicates that EHD1 binds similarly to PS and PIP2 and relatively better than PI4P but does not point towards a lipid-specific binding.

EHD1 binding to liposomes with increasing PS contents indicates that membrane binding is nucleotide independent and requires a negative charge. More importantly, membrane binding leads to stimulation of ATPase activity, indicating membrane binding regulates EHD1 function (ATPase activity) and under optimal condition, membrane binding can lead to ~8 fold stimulation of ATPase activity.

Although we observed nucleotide-independent membrane binding of EHD1, we find a striking effect of ATP binding on SMrT templates. Using fluorescently labeled EHD1 (BODIPY-EHD1), we find that EHD1 binds uniformly to the tube and binding does not affect the tube morphology. However, in the presence of ATP, EHD1 shows non-uniform discrete punctate organization on SMrT templates. Interestingly, under these conditions, EHD1 leads to the formation of constrictions on membrane tubes. Earlier, dynamin which has a tendency to oligomerize has been shown to bind SMrT templates in non-uniform, punctate manner on SMrT templates and each of these puncta represents dynamin scaffold which constricts the underlying tube (Dar et al., 2015). Similarly, we speculate that non-uniform, punctate distribution of EHD1 is the reflection scaffold-like organization of EHD1.

We observed that EHD1 binding to membrane tube is strikingly different in absence and presence of ATP. EHD1 binds uniformly to the tube in the absence of ATP, whereas ATP-bound EHD1 binds the tube in a punctate manner. The change in EHD1 distribution on SMrT templates upon ATP binding is a reflection of ATP binding triggered conformational change leading to EHD1 oligomerization. Our observation supports an earlier report that ATP binding is required for EHD1 oligomerization (Lee et al., 2005). However, our findings of nucleotide binding independent membrane binding of EHD1 is inconsistent with cytosolic localization (no membrane binding) of ATP binding defective EHD1 mutant (EHD1 T72A/G65A) (Caplan et al., 2002; Lee et al., 2005; Lin et al., 2001). We speculate that *in vivo* cytosolic localization of EHD1 ATP-binding mutants could be due to the combination of decreased membrane affinity of apo-EHD1 (due to the absence of protein-protein interaction) and reduced interaction with interacting partners such as Syndapin 2 (SDP2) (Braun et al., 2005).

Observation of membrane stimulated ATPase could be explained by ATP-dependent oligomerization. Earlier dynamin oligomerization has been shown to stimulate GTPase activity in the presence of membranes (Warnock et al., 1996) indicating that the similar mechanism could be responsible for EHD1's stimulated ATPase activity.

ATP bound EHD1 oligomer also contain the ability to deform membranes and constrict SMrT templates. EHD1 oligomerization-dependent constriction of SMrT templates in ATP-bound form highlights that ATP binding causes EHD1 oligomerization and EHD1 oligomers are capable of deforming membrane. EHD1's dependence on ATP binding to cause membrane deformation is strikingly different than dynamin, which can bind catalyze membrane deformation in the absence of GTP and only requires GTP for membrane fission (Bashkirov et al., 2008; Dar et al., 2015; Pucadyil and Schmid, 2008).

EHD1 in addition to deforming and constricting SMrT templates catalyzed fission of SMrT templates in the presence of ATP. The addition of EHD1 with ADP or ATP_γS did not cause fission of SMrT templates under the typical time scales of the experiment, ruling out the possibility of EHD1 catalyzing fission in either ATP or ADP-bound form. Based on these observations, EHD1 mediated fission requires ATP hydrolysis. We find that EHD1 showed bulk fission rate of 1.7 cuts.sec⁻¹ and took ~42 s to catalyze membrane fission. Based on the stimulation of ATPase activity and the fission time, we found that EHD1 would require hydrolysis of 6 ATP molecules on an average to catalyze fission. This makes EHD1 an efficient fission machinery in comparison to dynamin (which requires hydrolysis of 18 GTP molecules

for a fission event (Dar et al., 2015). Although it is essential to note that dynamin under identical condition shows multiple cuts on the SMrT template, emphasizing on the extensive processivity of dynamin.

In our SMrT template fission assay, we find that EHD1 mediated fission is highly sensitive to tube dimension and critically depends upon initial tube radius. Tubes thinner or equal to 10 nm radius always undergo fission, whereas tubes between 10-15 nm and 15-20 nm display 0.5 and 0.3 fission probability, respectively. Tubes with initial radius more than 20 nm do not undergo fission. EHD1 curvature dependent membrane fission is similar to the earlier reports of dynamin's characteristic of membrane curvature dependent membrane fission (Bashkirov et al., 2008; Dar et al., 2015). The most probable reason of dimension dependent fission could be due to the inability of EHD1 to bind membrane tubes of the higher radius. However, we see that EHD1 can constrict on tubes of all ranges of radius tested. To quantitate whether EHD1 remodels thin and thick tube to the similar extent we utilized coefficient of variation (COV).

COV is a ratio of standard deviation (SD) to the mean and reflects the uniformity or non-uniformity of the data around the mean value. As mentioned the rise in COV value in fission reaction reflects membrane deformation. High COV values also depict large differences between high and low-intensity fluorescence states. Use of COV also has following advantages: a) As both SD and mean are expressed in same units, COV becomes a dimensionless quantity and can be used to compare across different experimental conditions and between different proteins; b) COV is not affected by changes in the mean as the standard deviation is a derived parameter which depends upon mean itself; c) As COV is determined by computing mean and SD over long area (150-200 pixel long line along the tube axis), it reflects a global changes across the length of the tube upon protein binding and membrane deformation.

Quantitation of COV values on tubes indicated that EHD1 mediated deformation is independent of tube radius as it remodels both thin (fission compliant) and fission resistive tubes to the same extent (0.4 COV). Strikingly, thin tubes upon reaching the maximum value of COV undergo fission, whereas thick tubes start showing dissipation of striations leading to decrease in COV values. The similar extent of membrane deformation with more or less same time reflects that EHD1 can bind, assemble and deform a tube of the different radius in a similar manner. This attribute differs from dynamin which shows uniform distribution on thicker tubes (22 nm) (Dar et al., 2015). Despite the EHD1 assembly and deformation on thick tubes, the

inability of EHD1 to catalyze fission indicates EHD1 scaffold cannot bring down the bilayers close enough to catalyze fission on thicker (>20 nm) tubes (also see chapter 5).

Membrane tubules are in the ranges from 50-200 nm in ERC (Caplan et al., 2002; Xie et al., 2016). EHD1 sensitivity to tube dimension indicates that *in vivo* the tube dimension must be brought in the range of 20 nm for EHD1 to act. MICAL-L1, Syndapin2 (SDP2) interact and recruit EHD1 to ERC in cells. These proteins are also capable of remodeling membranes. Interestingly, Syndapin2 has been shown to tubulate liposomes into a diameter of 20-50 nm (Tanaka-Takiguchi et al., 2013). SDP2 alone or in complex with other proteins may work upstream of EHD1 to bring down the tubule diameter to aide EHD1 recruitment and function *in vivo*.

ERC has been shown to contain phosphatidic acid (PA), phosphatidylserine (PS) and cholesterol, and lysolipids (Cai et al., 2012; Gagescu et al., 2000; Giridharan et al., 2013; Lee et al., 2015; Mukherjee et al., 1998). PA content at ERC membrane tubule is essential for the ERC function as it interacts with SDP2 which in turn recruits EHD1. Relatively enriched cholesterol content recruits calcium-dependent phospholipase A2 α (cPLA2 α) which in turn generate lysolipids. Lysolipids are inverted cone-shaped lipids, and their depletion leads to receptor recycling defect (Cai et al., 2012).

We find that the addition of 5 mol% LPA to 40 mol % PS SMrT templates leads to ~3 fold increase in EHD1 fission rates. As membrane tubes containing 5 mol% LPA (in addition to 40 % PS) were not susceptible to breakage, either upon incubation for longer time, or upon incubation with EHD1 alone, the instability of tubes was ruled out as the determining factor of increased rate of fission. Observation of increase in the EHD1 mediated fission rate in presence of LPA (inverted cone shaped lipid), led us to postulate that the presence conical shaped lipid should cause decrease in EHD1 mediated membrane fission.

Liposome cosedimentation assays indicated that EHD1 showed equivalent binding to PA containing liposomes at half the lipid content. EHD1 bound PA liposomes containing as low as 10 mol% PA, and the binding showed an almost linear increase with increasing PA content on the liposome, reaching ~100% binding at 50 mol% PA. This was surprising for two reasons a) EHD1 showed very weak binding to PA in our FAT blot assay; b) LPA which contains similar head group and charge did not show binding in liposome binding assay. Further testing EHD1 mediated fission on 20 mol% PA containing SMrT templates showed that EHD1 mediated fission was highly suppressed. The absence of fission was quite surprising

because membrane binding and ATPase activity of EHD1 on 20 mol% PA liposomes was similar to 40 mol% PS liposomes. We attribute the differential activity EHD1 on PA vs. PS membranes to the shape these lipids adopt in membranes. PS is cylindrical lipid and make bilayers whereas, PA and LPA are non-bilayer lipids which assume cone and inverted cone shape, respectively (Kooijman et al., 2005). Increase in the EHD1 membrane binding on PA liposomes in comparison to PS liposomes might be due to the conical shape of PA. It is possible that having conical shaped lipid on the membrane increases EHD1 binding. This is further supported by the fact that both PS and PA contains -1 negative charge at physiological pH (Kooijman et al., 2009). However, suppression of EHD1 mediated fission 20 mol% PA SMrT templates indicate that the conical shape of the lipid might somehow inhibits membrane fission. We conclude that EHD1 mediated fission is severely affected by the presence non-bilayer lipids. Conical lipid inhibits fission, whereas the presence of inverted cone lipids accentuates EHD1 mediated membrane fission (see discussion of chapter 5).

We have established that EHD1 can catalyze membrane fission and it is only second protein molecule known to do so. This opens up new avenues to study the role of other EHD paralogs. EHD1-4 share high sequence similarity (70-83%) but are localized to different compartments. EHD1 and 3 are present at ERC, EHD2 is present at the plasma membrane, and EHD4 localizes to early endosomes (Blume et al., 2007; Daumke et al., 2007; Sharma et al., 2008). It becomes interesting to study that despite the conserved membrane binding regions, how different EHDs are localized to the different compartment and whether they all catalyze membrane fission.

Chapter. 4

Determinants of EHD1 Mediated Fission

4.1 Introduction

4.1.1. Membrane binding regions of EHD proteins

EHD proteins are a relatively new addition to the repertoire of the proteins involved in intracellular transport. The first evidence implicating EHD1 in endocytic recycling was obtained from a study of RNA expression patterns in *C.elegans* (Grant et al., 2001; Mintz et al., 1999). Subsequent studies in mammalian cells addressed the localization and function of EHD1-4 paralogs, establishing their function in endocytic and intracellular transport (Cai et al., 2013; Caplan et al., 2002; Galperin et al., 2002; Guilherme et al., 2004; Lin et al., 2001; Naslavsky, 2006; Shah et al., 2014; Sharma et al., 2008; Yap et al., 2010).

The insight in EHD protein domain organization and function was elucidated by EHD2 structure (Daumke et al., 2007). EHD2 structure sheds light on the composition of different domains, their relative organization in the crystal structure, and the fact that EHD2 exists as a dimer which together constitutes a curved membrane binding region. Based on high amino acid sequence identity this study proposes that EHD paralogs ought to have a similar domain organization, structure and employ similar membrane binding regions. A recent study suggests that EHD2 (and by extension EHD family) contains two membrane binding regions (Shah et al., 2014) a helical loop present at the tip of the helical domain, and an unstructured N-terminus region (Fig. 4-1-1 a-b). The helical loop assumes a loop-helix structure and shows no similarity to any known membrane binding domain. The region contains hydrophobic residues (F322) and a polybasic stretch of charged residues (K324, 327 and 328) (Fig. 4-1-1 b). Mutation of phenylalanine to alanine or charge reversal of lysine residues 327 and 328 leads to the cytosolic localization in cells and reduced binding in an *in-vitro* liposome binding assay (Fig. 4-1-1 b) (Daumke et al., 2007). These findings were further corroborated by studying the membrane insertion of above mentioned residues using site-directed spin labeling of residues and electron paramagnetic resonance (EPR) spectroscopy (Shah et al., 2014).

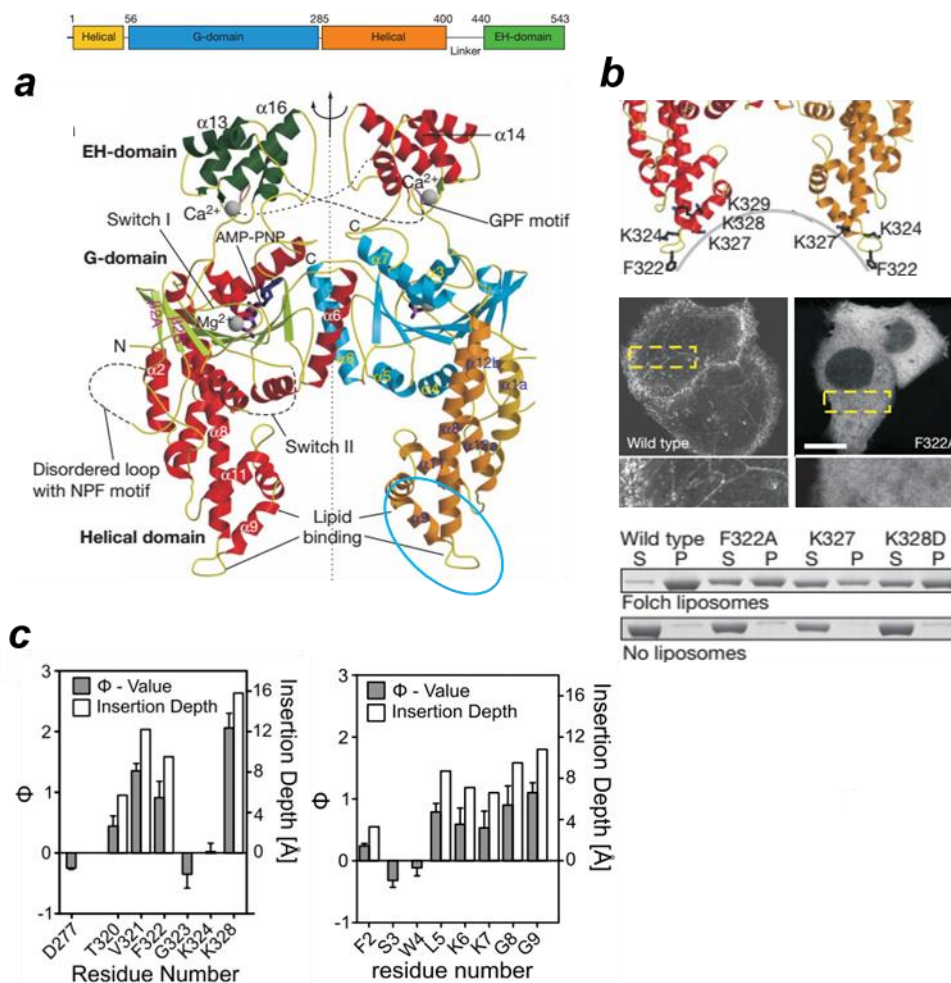


Figure 4-1-1. Membrane binding regions of EHD2. (a) The top panel shows the domain organization of EHD2. The bottom panel shows a ribbon-type representation of crystal structure of EHD2 dimer (PDB=2QPT) (Daumke et al., 2007). The structure shows relative organization of protein domains in EHD2. Membrane binding loop in the center of the middle helical domain of one of the monomers is encircled in blue. Membrane binding region is adjacent to G domain, and EH domain sits atop G-domain. (b) The hydrophobic and positively charged residues of the EHD2 dimer (top). A stark difference is seen between wild-type and F322A mutant localization (middle) (Daumke et al., 2007). Liposome co-sedimentation assay of wild type and mutant EHD2 (bottom). Band in S and P represents the relative enrichment of protein in supernatant and pellet respectively. (c) Membrane insertion of residues present in membrane binding regions middle helical domain (left) and N-terminus (right) (Shah et al., 2014).

EPR based detection of protein-membrane interaction relies on detecting the interaction of a spin labeled amino acid residue with the membrane containing paramagnetic quenchers. The specific residue of the protein of interest is first converted to cysteine which is then conjugated with paramagnetic spin label (1-oxyl-2,2,5,5-tetramethylpyrroline-3-methyl) methanethiosulfonate (MTSL) to generate spin labeled group R1 (Shah et al., 2014). N-O* group in R1 contains an unpaired electron which upon application of magnetic field aligns

parallel or antiparallel to the direction of magnetic field. The unpaired electron shifts from the ground state to the excited state (parallel to anti-parallel) upon the absorbance of a specific frequency followed by slow relaxation resulting in a molecule specific spectra (Klug and Feix, 2008). This spectrum is dependent on side chain movement (Altenbach et al., 2005) and spectra of membrane-interacting side chains show ordering of R1 spectra owing to the confined movement of the side chain (Altenbach et al., 1994). Additionally, R1 spectra are sensitive to the interaction with other paramagnetic species. This property is exploited to gain information about membrane interaction of the particular position. To know whether a R1 group is interacting with the membrane, R1 protein is added to the membrane, and its spectra is collected in the presence of membrane (O_2) and water soluble (Ni-EDDA) paramagnetic species. (Klug and Feix, 2008). Both O_2 and Ni-EDDA have short relaxation time (hence facilitate faster R1 relaxation) and interact with R1 via dipole-dipole interactions. This interaction decreases with the increasing distance between interacting species. This provides a distance specific accessibility (Π) of R1 to O_2 or Ni-EDDA (Altenbach et al., 1994; Páli et al., 1992). The logarithm of the ratio of accessibility of O_2 to Ni-EDDA provides an important parameter known as depth parameter (Φ) (Altenbach et al., 1994). Positive values of Φ reflect R1 membrane insertion whereas negative values reflect water soluble R1 group (Altenbach et al., 1994, 2005; Páli et al., 1992).

Using EPR based detection; it was revealed that a few residues of the helical loop including F322 and K328 showed positive Φ values and greater insertion depth into the membrane establishing their role in EHD2 membrane binding. This study also revealed previously unknown membrane binding region which is present at the N-terminus unstructured region of EHD2. The depth analysis indicated that residue 2 and 4-9 displayed positive Φ values and deep insertion into the membranes (Fig. 4-1-1 c). This region was proposed to assume an intermediate, ordered helix-like structure upon membrane binding, indicating membrane interaction. However deletion of the 1-19 residue had a small effect on EHD2 membrane localization and on EHD2 mediated membrane tubulation (Shah et al., 2014).

As EHD proteins share high sequence identity, EHD proteins are proposed to use same regions for membrane binding. However the evidence for the same is still lacking. Having established EHD1 function as membrane fission catalyst, we probed whether membrane binding regions are conserved in EHD1 and how do they affect EHD1 function. To achieve this, we generated mutants of hydrophobic and charged residue in helical membrane binding

region and N-terminus deletion construct by removing the 2-9 residue of the N-terminus and studied their role in EHD1 function.

4.2. Results

4.2.1 Helical loop plays an important role in EHD1 membrane binding and fission.

Residues in the EHD membrane binding loop, phenylalanine at 322 position and three lysines (K324, 327 and 328) are conserved across mammalian EHDs (Fig. 4-2-1 a). F322 and K328 which were shown to insert deeply into the membrane in EHD2 were mutated to alanine to study the contribution of hydrophobic and electrostatic interactions in EHD1 membrane binding. We first tested the effect of K328A on EHD1 function.

EHD1-K328A (Fig. 4-2-1 b) showed similar membrane binding trend as WT-EHD1 with increasing PS content in the liposome co-sedimentation assay (Fig. 4-2-1 c-d). And like wild type, K328A also showed stimulation of ATPase activity upon membrane binding. Intriguingly, the trend of stimulated ATPase activity of K328A was different than what we observed for wild type. Unlike EHD1 WT which showed saturation of ATPase activity at 40 mol% PS, K328A shows continued increase in ATPase activity with increasing membrane binding (Fig. 4-2-1 e). K328A stimulated ATPase activity was similar to wild type till 40 mol%-PS liposomes, but further increase in PS content led to a linear increase in ATPase activity and reached saturation at 80-PS liposomes (Fig. 4-2-1 f). Due to this linear increase, the resultant ATPase activity of K328A was ~2-5 higher than wild type with 100 mol% PS liposomes (Fig. 4-2-1 f). As the membrane binding of K328A did not appear different than WT, we did not pursue K328A effect on EHD1 fission.

We next tested the effect of F322A mutant on the EHD1 binding. (Fig. 4-2-2 a). F322A exhibited drastically reduced membrane binding when compared to WT with almost no binding to 40-PS liposomes. This defect in membrane binding could partially be rescued by increasing PS content, and we observed a linear increase in binding with increasing PS content on liposomes. F322A showed ~50 % membrane binding at a highest negative charge (100% PS; Fig. 4-2-2 b-c). This defect in membrane binding also reflected in ATPase activity as we did not see any stimulation of ATPase activity at 40-PS liposomes. However, a further increase in PS content led to unexpected, sharp increase in ATPase activity. F322A exhibited ATPase activity similar to WT on 60-PS liposomes despite the significantly lower membrane binding and reached ~2 and 2.5 fold higher ATPase activity on 80-PS and 100-PS liposomes

respectively (Fig. 4-2-2 e) (see discussion). When compared to K328A, F322A showed a dramatic defect on EHD1 membrane binding.

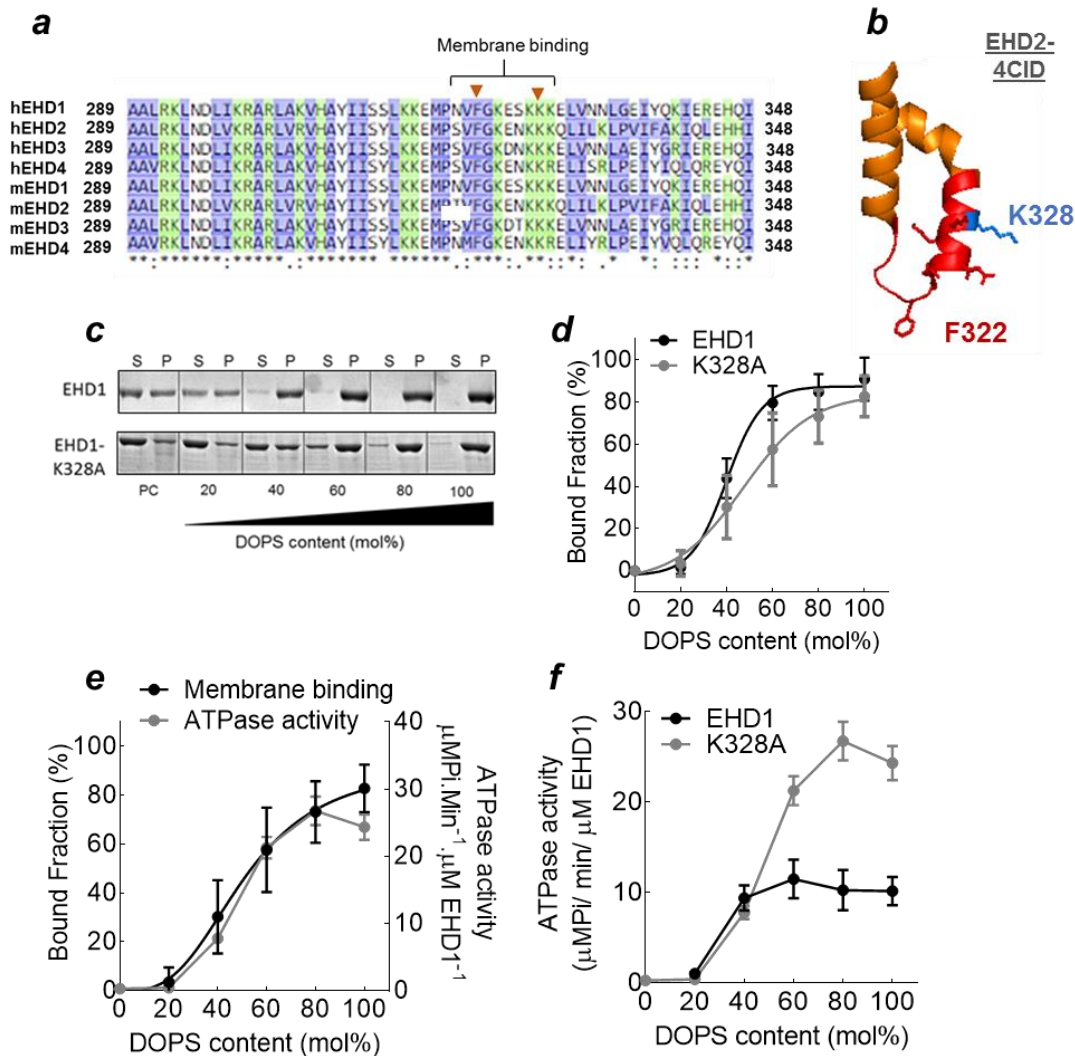


Figure 4-2-1. Effect of K328A on EHD1 membrane binding and function. (a) Conservation of helical loop region among EHD paralogs from *Homo sapiens* (h) and *Mus musculus* (m). Membrane binding region based on EHD2 structure (Daumke et al., 2007) is denoted by the bracket. Brown arrow-heads indicate the mutation of conserved residues used in the study. (b) Ribbon diagram of membrane binding loop of EHD2 depicting side chains of conserved phenyl alanine and lysine residues. Residue in blue indicates the K328 which is mutated to alanine. (c) Liposome-cosedimentation assay of the wild type and K328A mutant. (d) Quantitation of the enrichment of EHD1 in the pellet with increasing PS content. Data represents mean \pm SD for 3 independent experiments. (e) Comparison of stimulated ATPase activity of K328A with wild type EHD1. Note the steady rise of stimulated ATPase activity with increasing membrane binding. Data represents mean \pm SD for 3 independent experiments. (f) Comparison of stimulated ATPase activity of WT-EHD1 and K328A mutant. Note the difference in stimulated ATPase activity of WT and K328A mutant. Data represents mean \pm SD for 3 and 2 independent experiments for WT and K328 respectively.

Effect of the drastically reduced binding of F322A also reflected in fission assay as we did not see the occurrence of fission events upon addition of 1 μ M EHD1-F322A in the constant presence of ATP to 40-PS SMrT templates. Increasing the negative charge to 80 mol% on SMrT templates could partially rescue the fission defect, but cumulative fission rates on 80 mol% SMrT templates remained \sim 1 cut/sec indicating the crucial role of F322 in membrane binding of EHD1 and fission. These observations indicated that hydrophobic interactions via helical loop play an indispensable role in EHD1 membrane binding (see discussion).

4.2.2 Role of N-terminal region in EHD1 function

Having demonstrated a crucial role of conserved membrane binding loop in EHD1 membrane binding and fission, we next focused on the function of membrane binding region present at the unstructured N-terminus region (Shah et al., 2014). We created EHD1(Δ 2-9) mutant (Fig. 4-2-3 a) and screened for its effects on EHD1 function. Comparison of EHD1(Δ 2-9) binding to WT-EHD1 indicated that EHD1(Δ 2-9) showed a shallow increase in membrane-bound fraction with increasing PS content in liposomes and showed significantly lower binding than wild type even at all PS contents tested (Fig. 4-2-3 b-c).

Surprisingly, defect in membrane binding barely affected the stimulated ATPase activity of EHD1(Δ 2-9) mutant. We observed stimulated ATPase activity similar to wild type at 40-PS liposomes for EHD1(Δ 2-9), which further increased in the presence of liposome containing higher PS content and was almost two-fold higher than wild type under identical conditions (Fig. 4-2-3 d-e). We tested EHD1(Δ 2-9)'s ability to catalyze fission on 40-PS SMrT templates. Upon addition of EHD1(Δ 2-9) in the presence of ATP to SMrT templates at 37 $^{\circ}$ C, we found that membrane tubes showed striated appearance similar to wild type, but we did not observe any fission event (Fig. 4-2-3 f). This observation is quite striking as the mutant was capable of deforming the membrane and led to the formation of striations (Fig. 4-2-3 f).

To understand the reason behind the inability of EHD1(Δ 2-9) to catalyze membrane fission, we looked at the transformations the membrane tube underwent during the fission reaction in the presence of wild type and EHD1(Δ 2-9). During a fission reaction, EHD1 assembly induces membrane deformation leading to striated appearance of the membrane tube from a more uniform tube appearance at the start of the reaction. We used “coefficient of variation (COV)” as a measure of membrane deformation.

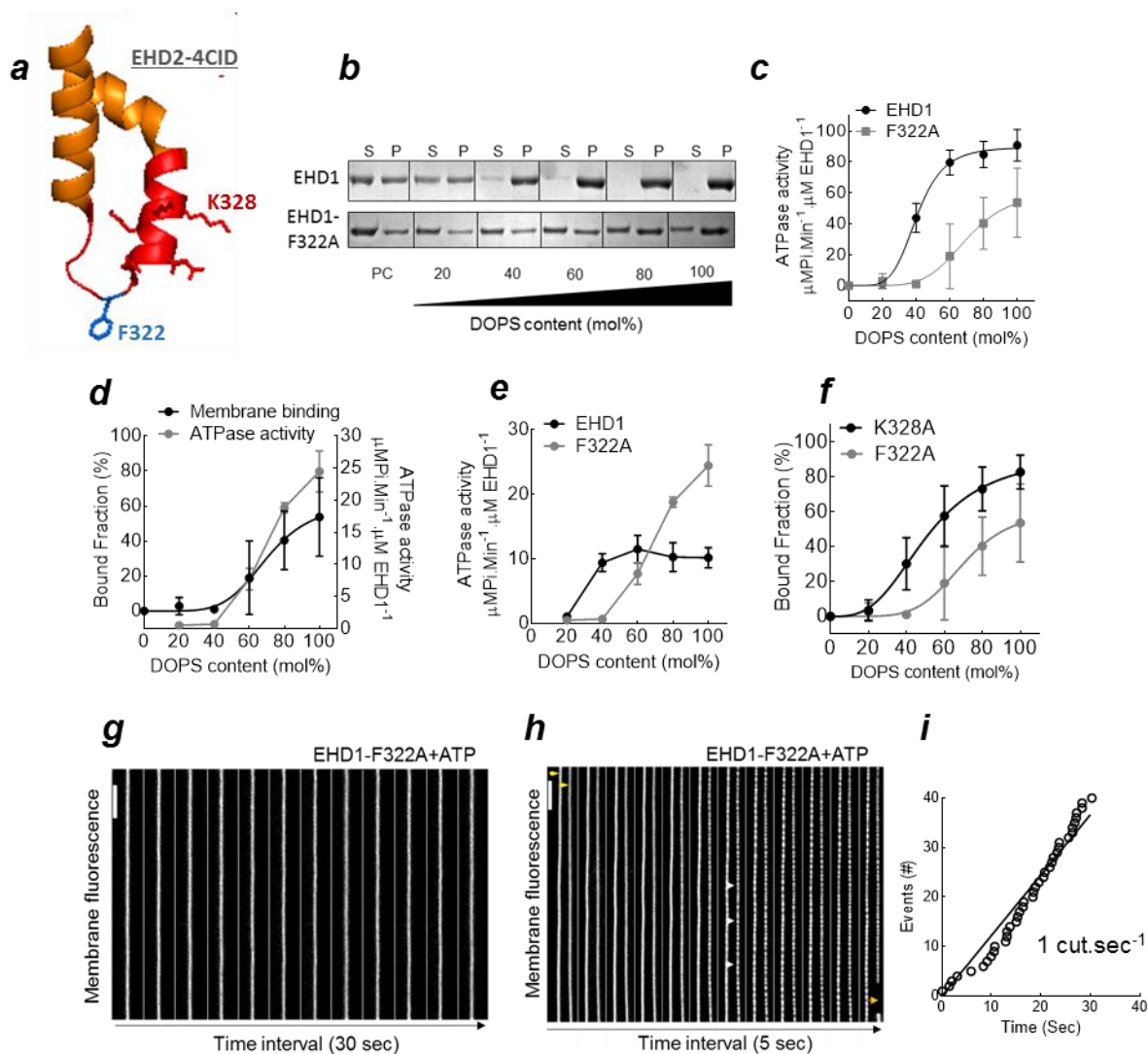


Figure 4-2-2. EHD1-F322A mutant significantly affects membrane binding and fission activity. (a) Ribbon diagram of membrane binding loop of EHD2 depicting conserved lysine and phenyl alanine. Residue in blue indicates the F322 which is mutated to alanine. (b) Liposome-cosedimentation assay of the wild type and F322A mutant. (c) Quantitation of the enrichment of EHD1 in the pellet with increasing PS content. (Data represents mean \pm SD for 3 independent experiments). (d) Stimulated ATPase activity response of F322A as the function of membrane binding. (e) Comparison of stimulated ATPase activity of WT-EHD1 and F322A mutant. (Data represents mean \pm SD for 3 independent experiments). (f) The difference in membrane binding of K328A and F322A. (g-h) EHD1 addition in the presence of ATP at 37 °C to SMrT templates containing 40 and 80 mol% PS, respectively. The addition of F322A does not cause any changes on tube topology on 40-PS SMrT template even after incubation for long periods (g). F322A shows membrane deformation (white arrow heads) and fission (orange arrow) on 80-PS SMrT templates (h). Scale Bar=5 μm (i) Cumulative fission rate of EHD1-F322A on 80-PS SMrT templates. Data is pooled from three independent experiments. Scale Bar, 5 μm

Estimation of the COV on 40-PS membrane tubes across the course of the fission reaction for WT and EHD1(Δ 2-9) showed stark differences. EHD1 assembly induced membrane deformation, as reflected by a stark increase in COV values (0.06 to 0.4) (Fig. 4-2-4 a-b). EHD1(Δ 2-9) assembly, on the other hand, did not deform membranes significantly and could not bring about large changes in COV values even on long incubation (Fig. 4-2-4 c-d). Plotting the COV against the time course of reaction indicated that EHD1 WT was able to change the COV values from minimum (\sim 0.05) to very high values (\sim 0.35) in a very short time and showed a sigmoidal response but EHD1(Δ 2-9) was defective in creating pronounced membrane deformation and even long incubation it could not increase the COV beyond 0.2 (Fig. 4-2-4 e-f). This reflects the inability of EHD1(Δ 2-9) mutant to cause pronounced membrane deformation upon protein assembly, a step which is required to catalyze membrane fission (see discussion).

As we discovered the essential role of the N-terminus on EHD1 mediated membrane fission, we focussed on understanding the effect of having a large protein fused to N-terminus of EHD1. Most of the studies on EHD1 use an N-terminally tagged construct of EHD1, for example- intracellular localization of EHD1 was seen using N-terminus GFP fusion of EHD1 (Cai et al., 2011, 2012; Caplan et al., 2002; Park et al., 2004) and GST-EHD1 was used in assays for reconstitution EHD1 function (Cai et al., 2013). We proposed that as the N-terminus region is involved in EHD1 mediated efficient membrane deformation, having a big fusion protein would affect the protein function. To test our hypothesis, we generated GST and GFP fusion of EHD1 (Fig. 4-2-5 a) and tested them for membrane binding and stimulated ATPase activity. We found that GST-EHD1, like EHD1(Δ 2-9), showed drastically reduced binding to PS liposomes (Fig. 4-2-5 b-c). GST-EHD1 binding was quite similar to EHD1(Δ 2-9) binding (Fig. 4-2-5 d). But unlike EHD1(Δ 2-9), GST-EHD1 showed high ATPase activity even in the presence of PC or 20-PS liposomes, a condition at which we have seen minimal ATPase activity for wild type or any other mutants we tested. This ATPase activity was almost similar to maximally stimulated ATPase activity of WT and did not show further increase as PS content on liposomes was increased (Fig. 4-2-5 e). This indicated that GST-EHD1 is incapable of showing stimulated ATPase activity.

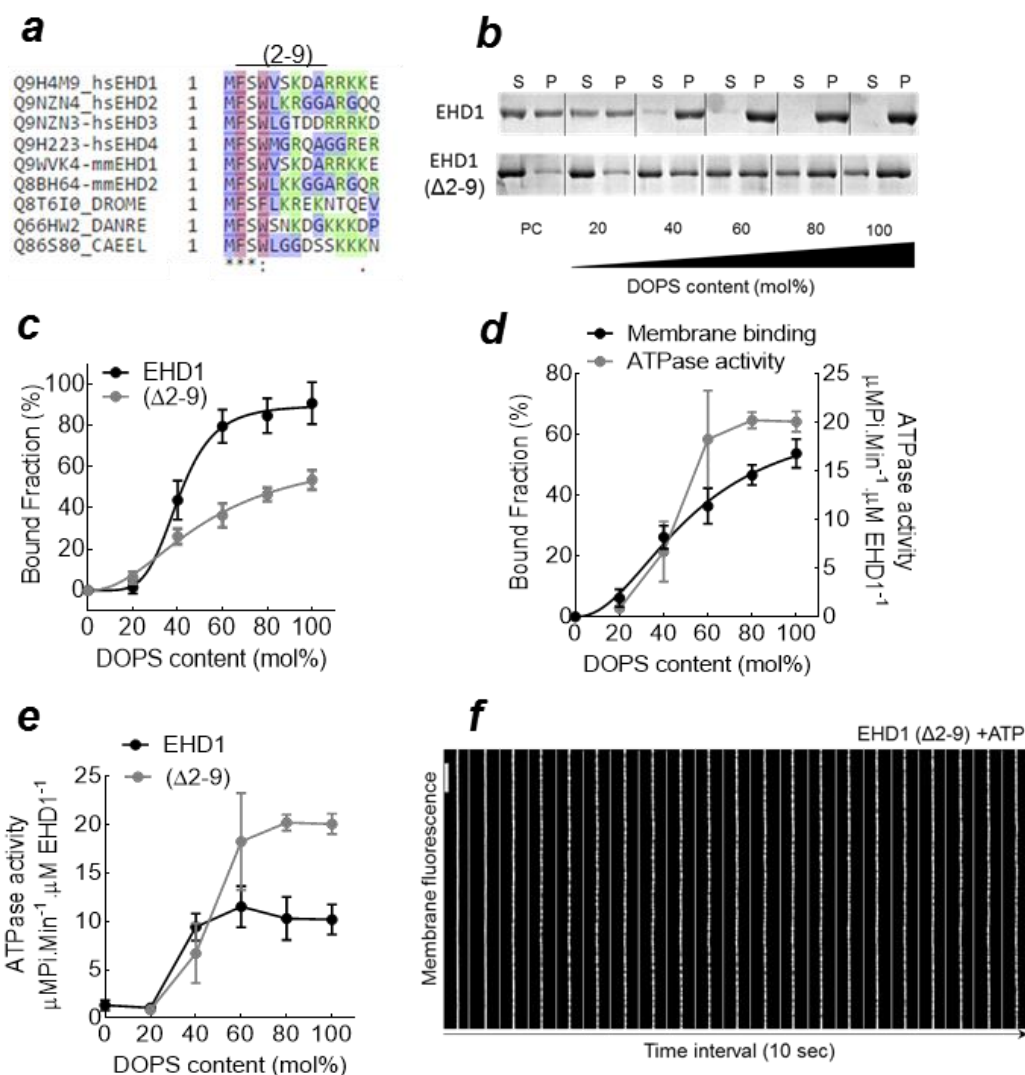


Figure 4-2-3. The N-terminal unstructured region is required for EHD1 membrane binding and fission activity. (a) Multiple alignments of N-terminus region (1-9) amongst different EHD1 homologs across species. Membrane-interacting region (2-9) is shown by a black line and is deleted in EHD1 ($\Delta 2-9$) mutant. (b) Representative gel for liposome cosedimentation assay of the wild type and EHD1 ($\Delta 2-9$) mutant. (c) Quantitation of the enrichment of EHD1 in the pellet with increasing PS content. Data represents mean \pm SD for 3 independent experiments. (d) Stimulated ATPase activity of ($\Delta 2-9$) in response to membrane binding. (e) Comparison of stimulated ATPase activity of WT-EHD1 and ($\Delta 2-9$) mutant. Note the ATPase activity of ($\Delta 2-9$) is similar to wild type at 40-PS. Data represents mean \pm SD for 3 independent experiments. (f) The difference in ATPase activity of wild type and ($\Delta 2-9$) mutant. (f) Image panel shows the effect of the addition of EHD1($\Delta 2-9$) in the presence of ATP at 37 °C to 40-PS SMrT templates. The addition of ($\Delta 2-9$) causes membrane deformation leading to the striated appearance of the membrane tube but does not cause fission of the membrane tubes. Note that striations are maintained over the course of the reaction. Scale Bar, 5 μ m

The addition of GST-EHD1 with ATP to 40-PS containing membrane tubes did not show the emergence of striations or fission of membrane tubes (Fig. 4-2-5 f). The inability of

fission was not specific to presence of GST per se, as addition of GFP-EHD1 with ATP was also unable to deform and cut the

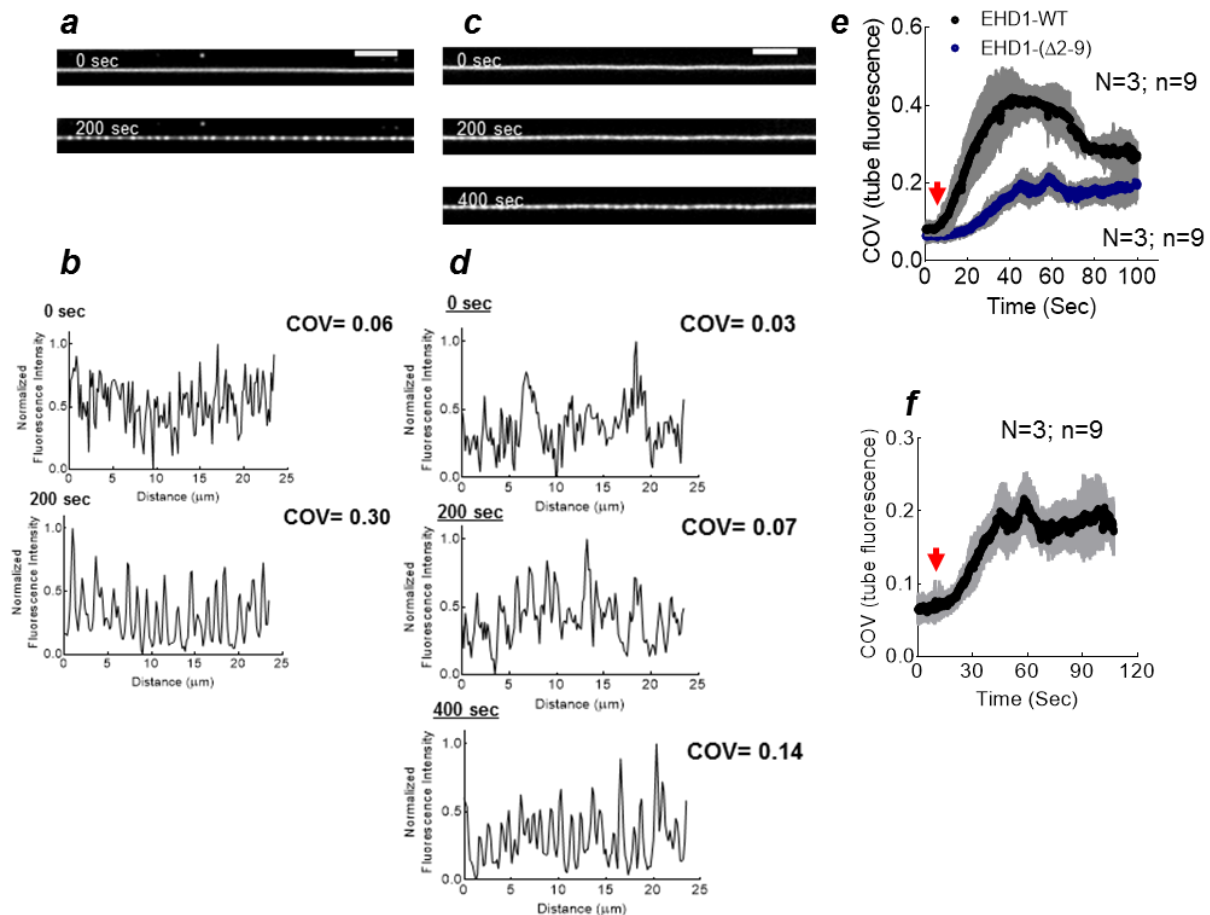


Figure 4-2-4. EHD1 ($\Delta 2-9$) is defective in membrane deformation. (a) Representative image of 40-PS SMrT templates upon addition of EHD1 in the presence of ATP. 0 and 200 sec depict the changes in membrane tube topology in the presence of WT-EHD1. (b) Distribution in membrane tube intensity shown in (a) at 0 and 200 sec. Tube intensities are normalized to the highest intensity of the data set and represented as a fraction. COV values indicate the dispersal of the intensities at 0 (0.06) and 200 sec (0.3). (c) Representative image of 40-PS SMrT templates upon addition of EHD1($\Delta 2-9$) in the presence of ATP. 0, 200 and 400 sec depict the changes in membrane tube topology in the presence of EHD1 ($\Delta 2-9$). (d) Distribution of membrane tube fluorescence shown in (c) at 0, 200 and 400 sec. Note the difference on redistribution of tube intensity in comparison to wild type. At 200 sec, EHD1($\Delta 2-9$) shows little redistribution in tube intensity (marginal increase in COV values 0.03 to 0.07) and longer incubation till 400 sec, shows relatively better-resolved intensity re-distribution (COV value 0.14). (e) The plot of COV of tube fluorescence over the time course of the reaction by EHD1 and ($\Delta 2-9$). Note the significant increase in COV of SMrT templates in the presence of EHD1 while COV of membrane tube in the presence of ($\Delta 2-9$) show an unusually shallow increase. Red arrow indicates the commencement of formation of striations on membrane tube. Note the increase in the maximal value of COV for EHD1 and ($\Delta 2-9$). N indicates the number of experiments and n represents the number of membrane tubes analyzed (f) Plot represents the COV increase of membrane tube in the presence of ($\Delta 2-9$) and ATP. Note that extended incubation of the protein cannot rescue the defect in a change in COV values. Scale bar, 5 μ m.

membrane tubes (Fig. 4-2-5 g). We used GFP-EHD1 and fluorescently labelled GST-EHD1 to investigate whether these constructs have bound SMrT templates. We found that both GST and GFP-EHD1 show uniform distribution of the protein across the SMrT templates even in the presence of ATP (Fig. 4-2-5 h-i). This distribution was similar to EHD1 in the absence of nucleotide and was quite unlike the distribution of ATP bound EHD1 (chapter 2), indicating their ability to assemble into scaffolds (see discussion).

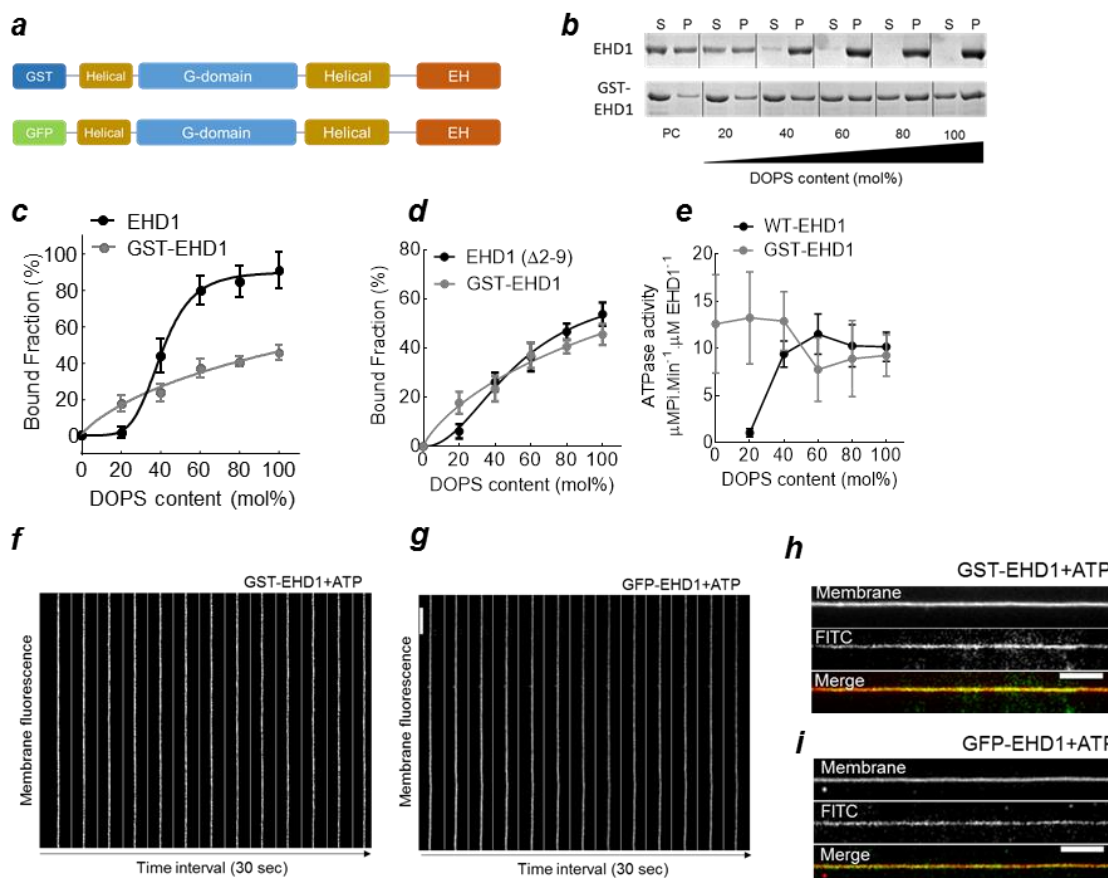


Figure 4-2-5. N-terminus GST or GFP fusion of EHD1 renders the protein inactive. (a) Domain architecture of GST and GFP-EHD1 fusion proteins. The GST and GFP are cloned next to the N-terminus of EHD1. (b) Representative gel for liposome cosedimentation assay of the wild type and GST-EHD1. The supernatant (S) and pellet (P) for reactions of protein and liposomes containing designated PS content were run on an SDS-PAGE gel and stained with Coomassie. From left to right, each gel shows S and P fraction for increasing PS content on the liposomes. Note the presence of GST-EHD1 in the supernatant at highest PS concentration. (c) Quantitation of the enrichment of EHD1 in the pellet with increasing PS content. Bound fraction for gels in figure (b) is plotted against increasing PS content on liposomes. Data represents mean \pm SD for 3 independent experiments. (d) The binding plot shows similar membrane binding trends for GST-EHD1 and EHD1 ($\Delta 2-9$). (e) Comparison of stimulated ATPase activity of wild type and GST-EHD1. Note the difference in stimulated ATPase activity between WT and GST-EHD1 with PC, 20 and 40-PS liposomes. Data represents mean \pm SD for 2 and 4 independent experiments for GST and WT-EHD1 respectively. (f-g) Effect of addition of GST-EHD1 and GFP-EHD1 on 40-PS SMrT templates, in the presence of ATP, at 37°C. Note the absence of striations upon addition of GST (f) or GFP-EHD1 (g). (h-i) Binding of GST and GFP-EHD1 in the presence of ATP on 40-PS SMrT templates at RT. Scale Bar, 5 μm

4.3 Discussion

We have established the regions in EHD1 which are required for EHD1 membrane binding, assembly, and fission. Among EHD paralogs in mammals, the EHD2 structure is solved and outlines the regions required for membrane binding, although these studies have limited information regarding the significance of these sites in the context of protein function.

We have addressed whether the membrane binding regions are conserved among EHD1-2 and also extended their role in the context of the protein function. To understand whether the helical loop is required for membrane binding and function, we made mutations and categorized their importance in EHD1 function. We first concentrated on the role of membrane binding loop present in the helical domain. The helical loop is predominated by the presence of hydrophobic and positively charged residue, and both of the types of residues are thought to be important for EHD2 function (Daumke et al., 2007; Shah et al., 2014).

To distinguish between the roles of hydrophobic and charge-based interaction in EHD1 function, we made F322A and K328A mutants in EHD1 and characterized their binding, ATPase and fission activity. K328A showed membrane binding similar to WT EHD1, however, showed a difference in ATPase activity than wild type. We found that although the binding of K328A was quite indistinguishable from WT, stimulated ATPase activity of the mutant displayed concomitant increase with increasing membrane binding. WT EHD1 showed saturation of stimulated ATPase activity around 40 mol% PS and showed no further increase in ATPase activity with increased membrane binding at higher membrane charge. K328A stimulated ATPase activity, on the contrary, showed a linear increase and eventually showed ~2 fold higher ATPase activity than wild type at higher PS content. In literature, charge reversal mutation K328D in EHD2 manifests reduced binding to liposomes as well as cytosolic localization in cells (Daumke et al., 2007). EHD1-K328A, on the other hand, shows no defect in liposome binding, and presumably, EHD1-K328A mutant would not have a drastic effect on localization and function of EHD in cells (see below). We conclude that EHD1-K328 does not play an important role in membrane binding.

We next tested the effect of F322 on EHD1 function. Liposome cosedimentation assay indicated that phenylalanine to alanine mutant (F322A), unlike K328A, significantly affected EHD1 binding and showed almost no binding at 40-PS liposomes. Increasing the PS content only led to the partial rescue of membrane binding as the binding only reached to 50% of total protein even at the highest PS-content. Consistent with the absence of significant membrane

binding, ATPase activity of F322A mutant showed no stimulation with 40-PS liposomes, but higher PS content liposomes increased stimulated ATPase activity by two-fold when compared to wild type. This observation seemed counter intuitive as we saw that mutant protein showed 20-50 % mean bound protein fraction which is considerably lesser than wild type and even with a defect in binding, protein shows stimulation of ATPase activity either similar or higher than wild type.

While testing the ability of F322A mutant to catalyze fission on 40 and 80 PS SMrT templates we found that F322A showed no striations or fission on 40-PS SMrT templates. This observation is consistent with low binding and no ATPase activity with 40-PS liposomes. However increasing PS content to 80 on SMrT templates, partially rescued the fission ability of F322A and showed 1 cut.sec⁻¹ cumulative fission rate. This is lower than wild type fission rate on 40-PS SMrT templates and significantly lesser than WT fission rate on 80-PS SMrT templates. This extremely slow fission rate at 80-PS SMrT templates despite the 2 fold higher ATPase activity F322A highlights the importance of F322 in EHD1 membrane binding. Even though the mutant has incredibly high ATPase activity, it cannot compensate for the protein density reflecting that both protein density and stimulated ATPase activity for EHD1 mediated membrane fission.

Our results provide evidence that membrane binding loop in middle helical domain is conserved between EHD1 and 2. Moreover, hydrophobic interactions play a far more significant role in EHD1 recruitment to the membranes than electrostatic interaction. Recently, the structure of N-terminally truncated EHD4 in ATP_γS bound form (activated conformation) indicated that helical domain rotates by 50° which leads to separation and reorientation of the helical loop in the dimer. In the closed conformation (EHD2-AMP-PNP) F322 is present at the tip of the helical loop however in the activated conformation F322 reorients to the side of membrane binding loop. This reorientation exposes additional residues which interact with the membrane (Melo et al., 2017). As we have tested EHD1-F322A on SMrT templates in the presence of ATP, EHD1 presumably binds membrane in the activated conformation, and severe defect in membrane binding in F322A under these conditions indicates that F322 is primarily involved in EHD1 membrane binding.

Additionally, we have established that N-terminus region is required for EHD1 membrane binding and fission and that deletion of corresponding N-terminus residues which interact with the membrane in EHD2 also have a significant role in EHD1 function. EHD1(Δ2-

9) mutant displayed a severe defect in membrane binding, but this defect was less pronounced than what we observed for F322A. F322A showed virtually no binding to 40-PS liposomes, but EHD1(Δ 2-9) showed significantly higher binding under identical experimental conditions reflecting the predominance of the helical region in EHD1 membrane binding.

When compared to wild type, overall binding of EHD1(Δ 2-9) was significantly lesser as it showed ~50% bound fraction at the highest PS content. Similar to F322A, EHD1(Δ 2-9) binding defect could not be rescued by providing a maximal charge. EHD1 2-9 region contains 3 hydrophobic residues 2F, 4W, and 5V along with a lysine at 7th position. It is possible that the hydrophobic residues are required for additional anchoring/interaction to the membrane and in their absence, EHD1 cannot effectively associate with membranes leading to reduced binding. Alternatively, the binding defect could be due to defect in self-assembly on the membranes. EHD1(Δ 2-9) shows virtually linear membrane binding response to increasing PS content, reflecting the possible loss of cooperativity in membrane binding.

Stimulated ATPase activity of EHD1(Δ 2-9) was either equivalent or ~2 fold higher than wild type under identical conditions. F322A also showed this behavior. This is a counter-intuitive observation where loss of membrane binding of a mutant displays greater stimulation ATPase activity of than wild type.

EHD1(Δ 2-9) displayed interesting phenotype on SMrT templates. EHD1(Δ 2-9) addition to 40-PS SMrT templates led to a striated appearance on SMrT templates however to our surprise we did not observe fission events. EHD1(Δ 2-9)'s inability to catalyze membrane fission was quite striking, leading us to further investigate the difference between WT-EHD1 and EHD1(Δ 2-9) EHD1. To study the underlying reason behind EHD1(Δ 2-9) inability to catalyze fission we followed protein assembly induced membrane deformation by WT-EHD1 and EHD1(Δ 2-9) on 40-PS SMrT templates by estimating COV at various time points.

EHD1 mediated deformation led to a sharp change in COV values (~5 fold increase) in a very short time indicating the extensive membrane deformation capability of EHD1. EHD1(Δ 2-9) on the contrary was quite defective in catalyzing deformation to similar scales and led to a very shallow rise in COV over time. It could only show ~3 fold increase COV values even after a very long incubation. This reflected that the EHD1(Δ 2-9) is considerably defective in membrane deformation despite showing similar membrane binding to wild type. As we have shown earlier that ATP bound EHD1 forms scaffolds on SMrT templates (Chapter 2), which in turn deform the membrane, we suspect that the inability of EHD1(Δ 2-9) to deform

membrane lies at the assembly step. And as fission requires opposing bilayers to come in close proximity (~5 nm, width of the bilayer) (Kozlovsky and Kozlov, 2003; Kozlovsky et al., 2002) and constriction of the tube to a critical dimension; inability of EHD1(Δ 2-9) to assemble and deform to similar extent as wild type could be the primary reason of its inability to catalyse fission. Previous studies have indicated that N-terminal residues (2-9) bind hydrophobic pocket in G-domain and bridges interaction of unstructured KPF_{xxx}NPF loop to the hydrophobic pocket and keeps the protein in autoinhibited form (Shah et al., 2014). Recent studies indicate that this conformation is auto-inhibited conformation and ATP binding (ATP _{γ} S) to EHD leads to the formation of the active conformation where NPF loop interacts with G-domain leading to the formation of new protein-protein interaction surface which including the helical domain (Melo et al., 2017). We have tested the effect of (Δ 2-9) in the presence of ATP, indicating that EHD1 is in activated conformation and all the defects we see are shown by the protein in the activated conformation.

Comparison of all the membrane binding mutants brings out several unique characteristics of EHD1;

- a) A defect in membrane binding and no stimulated ATPase activity at 40-PS for F322A mutant indicate that the helical loop is the predominant membrane binding region EHD1 and EHD1(Δ 2-9) plays an accessory role in EHD1 membrane recruitment.
- b) Hydrophobic interaction in the helical loop predominates over electrostatic interaction in EHD1 binding.
- c) Differences in binding response of wild type and EHD1(Δ 2-9) to liposomes of increasing PS content (sigmoidal vs. a shallow binding curve) indicates that 2-9 region is required for EHD1 assembly on the membranes. This observation is also supported by a sharp and extensive membrane deformation on SMrT templates by EHD1 and a relatively shallow deformation response by EHD1(Δ 2-9). As the membrane deformation curve also an indirect reflection of self-assembly property of the protein, we hypothesize that 2-9 residues in EHD1 are involved in self-assembly, although at this point it's not clear whether the effect is created by providing second membrane binding site, affecting protein self-assembly or by a combination of both.
- d) We observed a striking phenomenon where EHD1 membrane binding mutants showed stimulation of ATPase activity higher than wild type even though the bound fraction of mutants is significantly lower than wild type protein. It is not very clear why do we see

this phenomenon, but it could be possible that membrane binding is required for stimulation of ATPase activity, but both activities do not go hand in hand. In fact higher ATPase activity of mutants at 80 or 100-PS liposomes indicate that 40-50 % bound fraction is enough to show maximal stimulation of ATPase activity and higher binding of wild type, in fact, comes in the way of stimulation of ATPase activity.

The defect seen for the N terminus mutant of EHD1 led us to investigate the effect of attaching a large protein (such as GFP or GST) at the N-terminus. Previously, N-terminus GFP and GST fused-EHD1 was utilized to understand localization and reconstitution of EHD1 function. We found that GST-EHD1 construct showed a defect in membrane binding and behaved quite similar to EHD1(Δ 2-9). However, estimation of ATPase activity of fusion protein indicated that the construct had a high basal ATPase activity which is similar to stimulated ATPase activity of wild type protein and was unresponsive to membrane binding i.e. GST-EHD1 is incapable of showing membrane binding dependent stimulation of ATPase activity. GST-EHD1 addition to 40-PS SMrT templates did not show any striation or fission. This observation was also true for GFP-EHD1 ruling out the possibility of protein specific effect on EHD1 function. The absence of the striated appearance of membrane tube and uniform distribution of protein on SMrT templates indicated that N-terminus GFP/GST fusion proteins are incapable of showing protein assembly responsible for catalyzing membrane deformation. This could be due to the steric effect of bulky protein on the function of N-terminus of EHD1. Based on our observation we propose that N-terminus is required for EHD1 membrane deformation and the addition of a large protein group negatively affects this ability and generates a protein which is unable to catalyze membrane deformation or fission. This observation also raises the question whether localization GFP-EHD is the true reflection of endogenous EHD protein.

Chapter-5

**Mechanism of EHD1
mediated membrane fission.**

5.1 Introduction.

5.1.1 Protein catalysts for membrane fission.

Membrane fission is an essential step for the vesicular transport and is intrinsically a thermodynamically unfavorable process. Biological membranes are held in a bilayer configuration by a strong hydrophobic effect, and any deformations which induce tilt in the either of the monolayers is energetically unfavorable (Kozlovsky and Kozlov, 2003). The biologically relevant pathway of membrane fission necessitates the process to occur in a non-leaky manner to prevent leakage of its content in the cytosol. The non-leaky fission is proposed to occur via a hemifusion intermediate which allows sequential fusion of monolayers, fusion of proximal monolayers followed by the lipid re-arrangement and fusion of distal monolayers of two bilayers when placed at a very close distance (Frolov et al., 2015; Kozlovsky and Kozlov, 2003; Schmid and Frolov, 2011) (Fig. 5-1-1). However, electrostatic repulsion between the lipids and stripping of the hydration shell around individual bilayers, pose an energetic barrier in bringing bilayers close to each other. To counter this thermodynamic barrier, cells have evolved protein machinery to catalyze hemifission intermediate formation and subsequently fission (Chernomordik and Kozlov, 2003; Frolov et al., 2015; Kozlovsky and Kozlov, 2003).

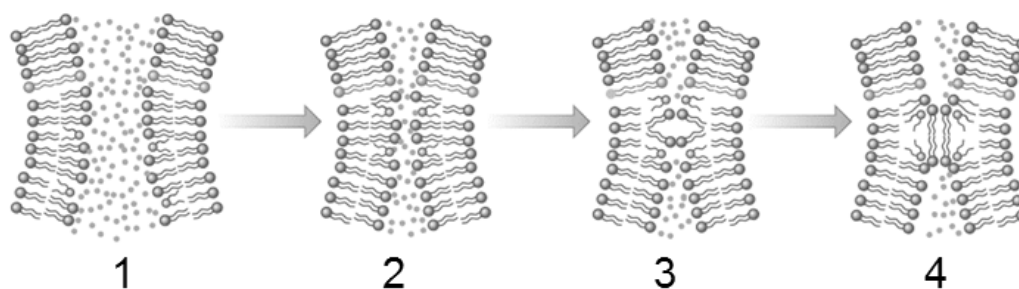


Figure 5-1-1. Membrane fission via a non-leaky, hemifusion intermediate. Membrane bud formation generates a neck like intermediate. 1, represents the vertical cross-section of the neck. 2-3, opposing bilayers are brought closer against the electrostatic repulsion between lipid head group and hydration forces. As bilayers come at the distance of a single bilayer (~4 nm) (3), lipids in the inner leaflet of opposing bilayers rearrange and form the hemifission intermediate. 4, hemifission intermediate. Adapted from (Schmid and Frolov, 2011)

5.1.2 Dynamin, a self-sufficient membrane fission catalyst.

Dynamin, a large multi-domain GTPase catalyzes membrane fission of clathrin-coated pits at the plasma membrane and *trans*-Golgi network (Schmid and Frolov, 2011). Dynamin is

the best studied and the only molecule which has been shown to catalyze membrane fission in a biochemically defined *in vitro* setup and also has been the only source of insight into protein-mediated membrane fission. Dynamin shows GTP-independent binding and tubulation of membranes (Danino et al., 2004; Pucadyil and Schmid, 2008; Sweitzer and Hinshaw, 1998) and by self-assembly, it can constrict tubular membrane templates (Bashkirov et al., 2008; Dar et al., 2015). Reconstitution of dynamin mediated fission using conductance measurements has provided valuable evidence that dynamin-mediated fission progresses via hemifission intermediate (Bashkirov et al., 2008). However, conductance measurements being average measurements lack spatial resolution. Using a microscopy based supported membrane tubes (SMrT) developed in our lab, we observe that dynamin in the absence of GTP, binds to PtdIns (4,5)P₂ containing SMrT templates, organizes itself in the form of a distinct scaffold and constricts the underlying tube to the dimension of 11.9 nm (radius, r). This scaffold upon GTP hydrolysis further constricts the underlying tube to reach a radius of 7.3 nm followed by the fission of the tube. Accounting for the bilayer thickness (~5 nm), dynamin scaffold upon GTP hydrolysis constricts the membrane tube to inner radius 2.3 nm (Dar et al., 2015); a distance conducive to catalyze form hemifission intermediate (Dar et al., 2015). Taken together, these results indicate that dynamin upon assembly constricts the membrane tube but requires GTP hydrolysis to bring membrane close enough to promote the formation of hemifission intermediate (Dar et al., 2015).

5.1.3 Understanding mechanism of EHD1 mediated fission.

To better understand how EHD1 catalyses membrane fission we broke down the reaction into; the effect of EHD1 assembly and the subsequent effect of ATP hydrolysis, on the underlying membrane tube. Comparison of such reaction intermediates to dynamin catalysed fission gives insights into the mechanism of EHD1 mediated membrane fission.

5.2. Results.

5.2.1 EHD1 assembly leads to expansion of tube dimension.

Comparison of EHD1 and dynamin assembly conditions on SMrT templates showed that, dynamin assembles and constricts SMrT templates independent of nucleotide (Dar et al., 2015), EHD1 on the other hand, requires ATP binding to assemble and deform the membranes (chapter-3). To compare the effect of the assembly of dynamin and EHD1 on the SMrT template, we performed EHD1 and dynamin assembly on 40 mol% PS SMrT templates. Dynamin was incubated with SMrT templates in the absence of nucleotide, and EHD1

assembly was performed in the presence of ATP γ S. Dynamin and EHD1 both deformed membrane tubes in similar timescales and led to the formation of alternative high and low-intensity regions on membrane tube upon assembly (Fig. 5-2-1 a). COV analysis of the membrane deformation before and after assembly indicated that both EHD1 and dynamin deform membrane to a similar extent (Fig. 5-2-1 b). Further analysis of the kinetics of the membrane deformation using kymograph displayed peculiar differences between dynamin and EHD1 mediated membrane deformation. Dynamin-mediated membrane deformation started as a localized formation of a low tube fluorescence which progressively decreases in intensity leading to the formation of a constriction (Fig. 5-2-1 c; yellow arrowheads). On the contrary, kymograph of EHD1 mediated deformation displayed a localized rise in fluorescence intensity while the adjacent region underwent a decrease in intensity (Fig. 5-2-1 d; compare orange and yellow arrowheads). Since the fluorescence of diffraction limited object is proportional to net area (Dar et al., 2015; Pucadyil and Holkar, 2016), the increase and decrease in fluorescence intensity reflect increase and a decrease of tube radius, respectively.

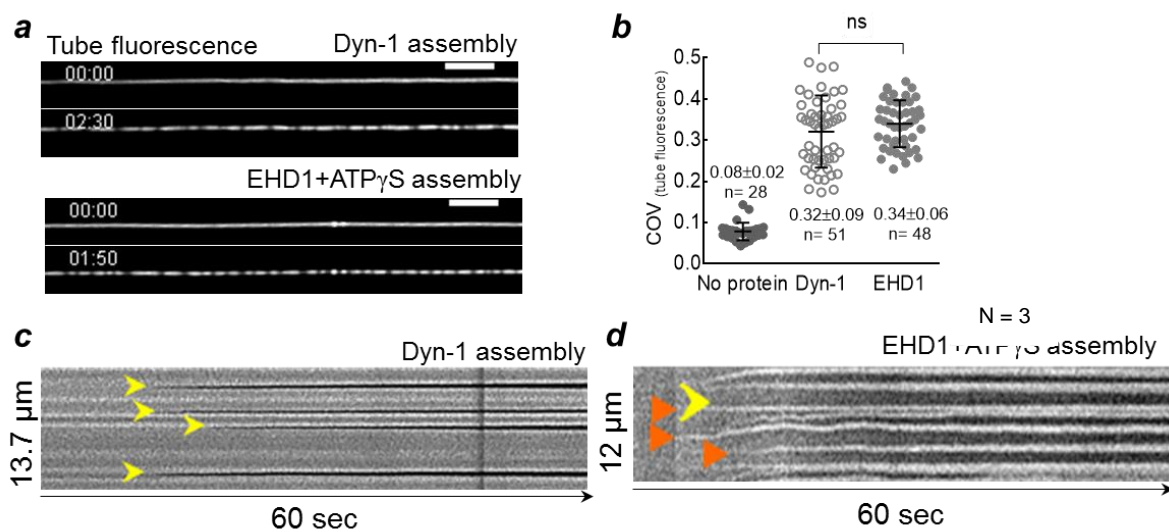


Figure 5-2-1. Dynamin and EHD1 deform the membrane to a similar extent. (a) Changes in tube fluorescence after Dynamin (Dyn-1) and EHD1 mediated membrane remodeling. Scale Bar, 5 μ m (b) Membrane deformation upon Dyn-1 and EHD1 assembly. (c-d) Representative kymograph of Dyn-1 (c) and EHD1 assembly (d). Yellow arrowhead in (c) and (d) indicate the decrease in tube intensity. Orange arrowheads in (d) indicate the emergence high-intensity region.

Dynamin scaffolds cause a decrease in tube radius (constriction) of the SMrT template (Dar et al., 2015), however, EHD1 assembly showed both increase and decrease of tube radius. To understand the origin of these changes to the localization of the protein, we analyzed the

localization of EHD1 scaffolds on membrane tube and compared it with dynamin localization. We utilized, extrinsically labeled fluorescent dynamin and EHD1.

EHD1 scaffolds showed co-localization to the increased tube radius (Fig. 5-2-2 a, a') which was opposite to the dynamin oligomer which localizes to constriction (Fig. 5-2-2 b, b'). Correlation of the protein to membrane intensity gave a positive correlation for EHD1 (Pearson's coefficient, $r = 0.78 \pm 0.16$; Fig. 5-2-2 c) and negative correlation for dynamin (Pearson's coefficient, $r = -0.58 \pm 0.17$). We next looked at the kinetics of membrane binding of EHD1. We have earlier shown that EHD1 binds uniformly to the membrane in the absence of ATP (chapter-3), whereas ATP-bound EHD1 distributes on the membrane in a punctate manner (chapter-3 and Fig. 5-2-2 d; BODIPY-EHD1+ATP, γ S). This punctae increase in intensity indicating growth of the EHD1 scaffold.

Together the kymograph of EHD1 assembly on the SMrT tube, localization of EHD1 scaffold to increased tube radius and the kinetics of ATP bound EHD1 on SMrT templates; indicate that assembly of ATP bound EHD1 leads to increase in tube radius (Fig. 5-2-2 d). We postulate that EHD1-assembly-induced increase in tube radius, leads to the formation of a membrane bulge like intermediate. This membrane bulge is a topologically inverted structure than what is observed for dynamin which, as shown earlier, constricts and thereby decreases the diameter of the tube.

5.2.2 EHD1-assembly-induced membrane bulge leads to constriction of the adjacent region.

To understand the consequence of the EHD1 assembly induced bulge formation, we looked at the changes in tube fluorescence of bulged and adjacent region and compared it to the tube fluorescence changes upon dynamin (dyn-1) assembly. To this end, we placed single pixel line along the time axis on the kymograph of change in tube fluorescence for the respective proteins, generated a line profile and plotted fluorescence changes against time course of the reaction. In the case of EHD1 assembly, bulged region underwent a gradual increase in fluorescence, while adjacent region displayed a concomitant decrease in tube fluorescence and formed a constriction like state. Dyn-1 assembly led to constriction formation irrespective of the changes in the tube fluorescence of the adjacent region (Fig. 5-2-2 e,

compare line profile of dynamin (dyn-1) and EHD1 assembly). This led us to conclude that EHD1 assembly causes both bulging and constriction of the tube.

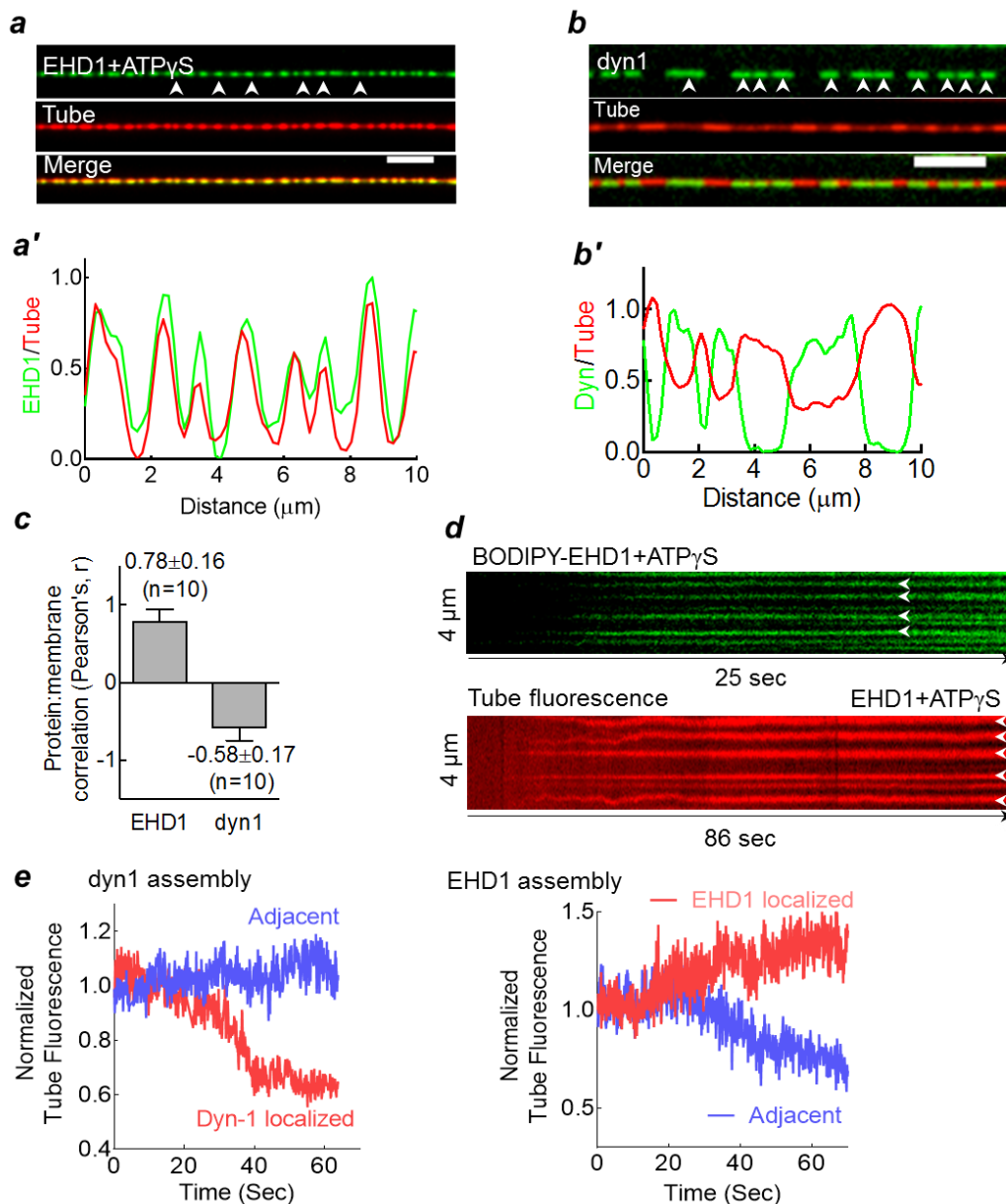


Figure 5-2-2. EHD1 assembly leads to the formation of bulge like intermediate. (a-b) EHD1 (a) and dyn-1 (b) localization on SMrT templates upon assembly. EHD1 scaffold co-localize with high-intensity regions on the membrane. (c) Pearson's correlation coefficient for EHD1 and dynamin localization to the membrane. (d) Representative kymograph of EHD1 assembly (in green) and tube fluorescence (Red) in the presence of ATP γ S. Note that EHD1 binds as punctae and grows in intensity. EHD1 assembly leads to bulge formation (white arrowheads). (e) Representative change in tube fluorescence upon Dyn-1 and EHD1 assembly. Note that in the case of Dyn-1, protein localized region undergoes constriction, while EHD1 assembly leads to increase in tube intensity. Also, an adjacent region in Dyn-1 assembly does not show changes, whereas, in the case of EHD1, adjacent region undergoes constriction. Scale Bar, 5 μ m. * Data in the b panel is generated by Srishti Dar and b and c panel are prepared by Thomas Pucadyil.

To confirm that EHD1 assembly induced bulge and constriction on SMrT templates are indeed the reflection of changes in tube dimension, we utilized GFP-encapsulated SMrT templates (Fig. 5-2-3 a) which have GFP asymmetrically tethered to the inner monolayer (see methods) and imaged the changes in GFP intensity upon EHD1 assembly. As GFP is only present in the lumen of a diffraction limited SMrT template, change in GFP fluorescence directly indicate changes in lumen dimensions. EHD1 assembly in the presence of ATP γ S led to clustering of GFP and change in GFP fluorescence mimicked membrane fluorescence changes upon assembly, reflecting that GFP fluorescence can report changes in tube topology seen with tube fluorescence reported with lipid fluorophore (Fig. 5-2-3 b). Kymograph of EHD1 assembly on GFP-encapsulated SMrT templates showed the appearance of both high and low GFP intensity on the tube (Fig. 5-2-3 c-d). These changes in SMrT template lumen dimension resembled changes in tube fluorescence, indicating the EHD1 assembly indeed causes bulging and constriction of the SMrT template.

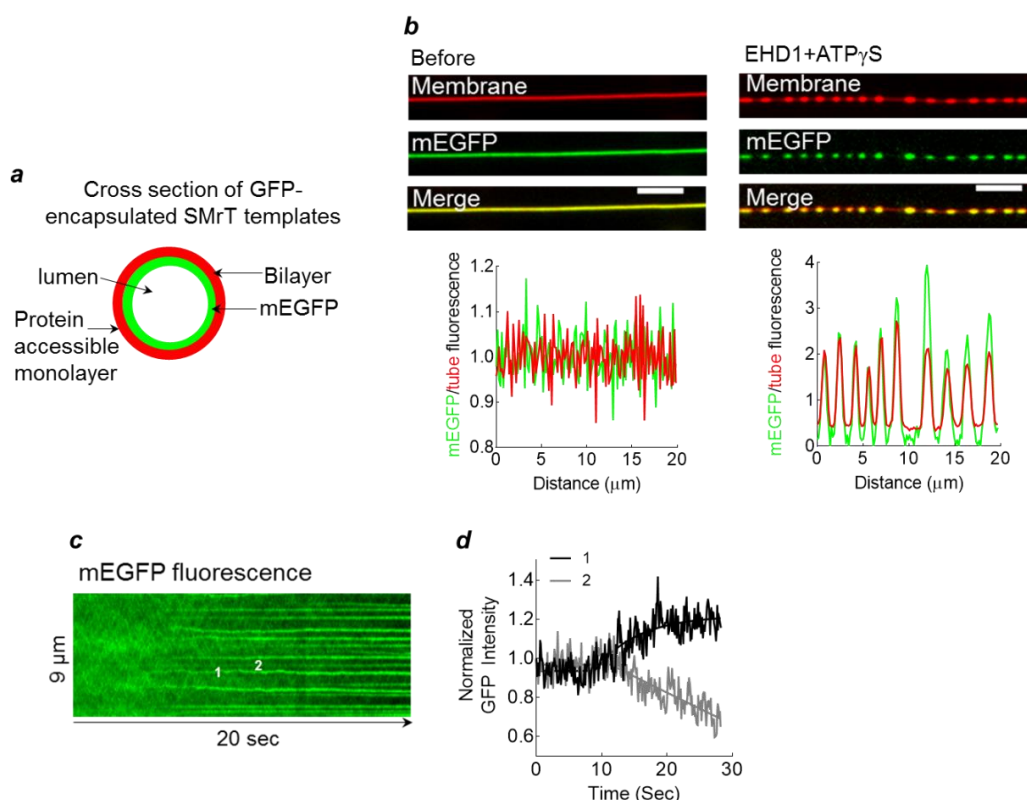


Figure 5-2-3. EHD1 assembly increases lumen dimension of SMrT template. (a) Organization of encapsulated GFP in SMrT template. (b) Localization of GFP fluorescence with tube fluorescence before and after EHD1 assembly. (c) Representative kymograph is displaying changes in GFP fluorescence upon EHD1 assembly. (d) Fluorescence trace of the marked region (1,2) in 'b.' (d) Localization of GFP fluorescence with tube fluorescence before and after EHD1 assembly. Scale Bar, 5 μm

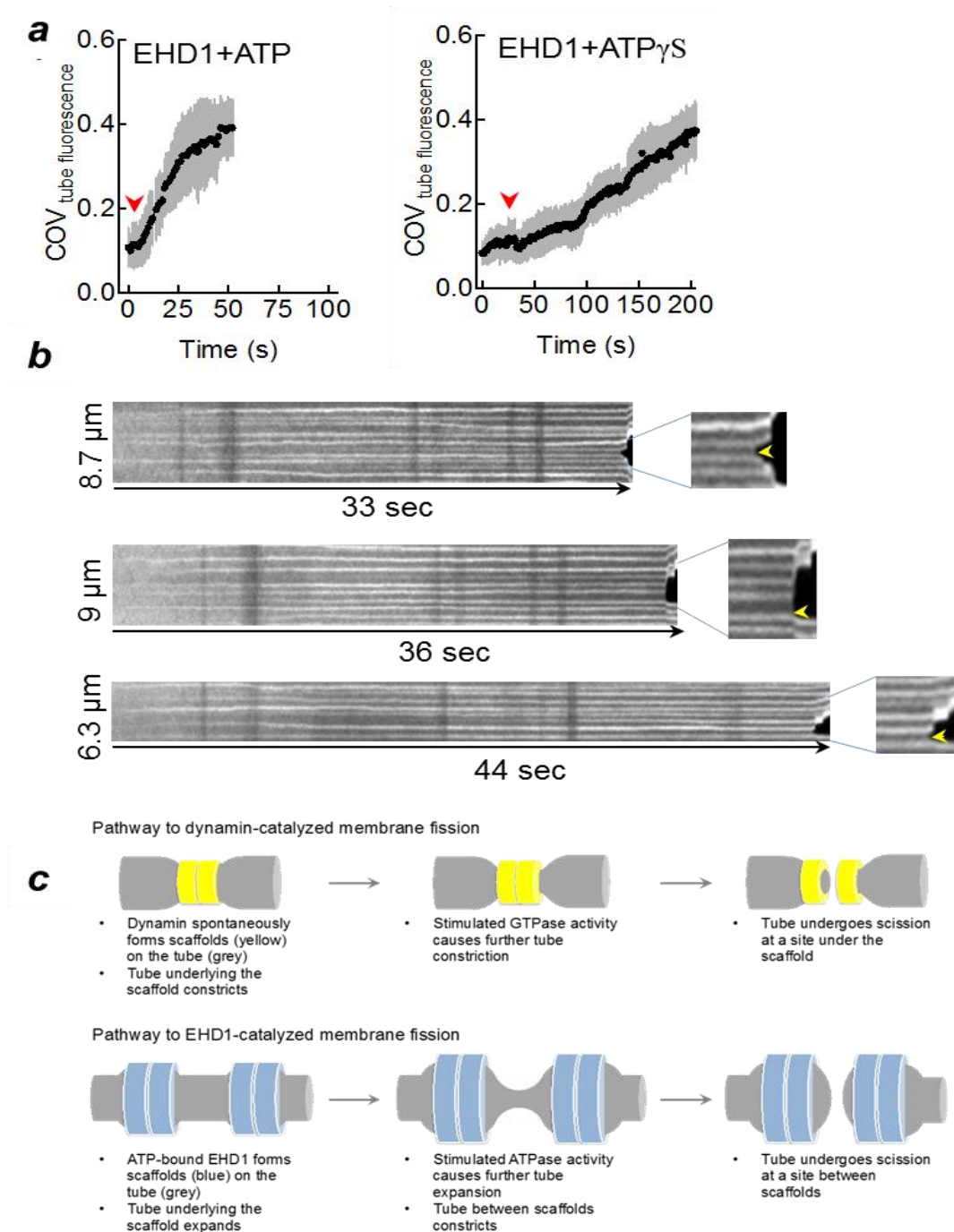


Figure 5-2-4. Pathway to EHD1 catalyzed membrane fission. (a) COV analysis of membrane deformation by EHD1 in the presence of ATP and ATP γ S (analyzed by Thomas Pucadyil). (b) 3 representative kymograph profiles of EHD1 mediated fission reaction. Yellow arrowhead in the inset shows the place of cut. (c) Alternate pathways to catalyze membrane fission. * Data in panel (a) and the model of dynamin and EHD1 catalyzed fission is generated by Thomas Pucadyil.

To gain insight into the role of bulge and constriction in membrane fission, we followed the fate of these regions in the presence of ATP. As we have shown earlier, EHD1 in the presence of ATP can catalyze membrane fission. Kymograph of the fission reaction indicated

that EHD1 form bulge and constriction both in the presence of ATP γ S and ATP and estimation of the extent of membrane deformation using COV indicated that EHD1 in the presence of ATP takes significantly lesser time (~ 50 s) to reach similar deformation than in the presence of ATP γ S (~200 s) (Fig. 5-2-4 a). Fission of tube appears to occur in the constricted region or at the boundary of bulge and constriction (Fig. 5-2-4 b).

5.3 Discussion

We show that EHD1 catalyzes constriction formation on SMrT templates via a novel pathway. Dynamin, which has been used to understand the mechanism of protein catalysed membrane fission, forms scaffold and constricts the membrane tube to form hemifission intermediate (Bashkirov et al., 2008; Danino et al., 2004; Dar et al., 2015; Shnyrova et al., 2013; Sweitzer and Hinshaw, 1998). GTP hydrolysis by the dynamin scaffold leads to the formation of hemifission intermediate which subsequently leads to fission (Dar et al., 2015).

Comparison of the dynamin and EHD1 assembly on SMrT templates show that although both the proteins cause the similar extent of membrane deformation, the mode of deformation appears to occur in a different manner. Dynamin assembly initiates a localized decrease in tube fluorescence and progressively constricts SMrT templates; tube fluorescence of the adjacent, dynamin lacking region is barely affected. EHD1 assembly, however, causes an increase in the tube fluorescence, reflecting the increase in the tube diameter. This way EHD1 assembly generates a topologically inverted membrane bulge like intermediate. Interestingly, bulge formation causes near simultaneous decrease in the fluorescence intensity in the adjacent region (Fig. 5-2-2 e; dynamin and EHD1 assembly) indicating that bulge formation is coupled to constriction of the adjacent region. EHD proteins exhibit closed and active conformation (Hoernke et al., 2017; Melo et al., 2017). In our assays, we have utilized ATP γ S to study EHD1 mediated membrane deformation, and we speculate that these changes on membrane tube upon EHD1 assembly occur due to oligomerization of the competent, active conformation.

EHD1 assembly induced membrane to bulge and constriction of the tube also correlate well with lumen dimension changes upon EHD1 assembly on GFP-encapsulated SMrT templates. EHD1 assembly led to the formation of alternative high and low GFP fluorescence, where the appearance of high intensity was coupled with low-intensity generation in the nearby region.

Based upon this observation, we propose that EHD1 assembly forms a bulge on the SMrT template and the constriction of the tube occurs due to membrane bulge formation. This leads us to propose that constriction formation in EHD1 mediated membrane deformation is the indirect effect of EHD1 assembly induced bulge formation. This kind of constriction formation is different from the dynamin-mediated constriction of membrane tube where dynamin assembly directly causes the constriction formation. We favour the hypothesis that EHD1 assembly constricts the underlying membrane as a consequence of formation of membrane bulges for following reasons; a) comparison of dyn-1 and EHD1 assembly indicates that in case of dynamin assembly, first sign of change in tube fluorescence starts as the decrease in the intensity, whereas first signs of change in fluorescence intensity in case of EHD1 assembly starts as the increase in tube fluorescence, b) during dynamin assembly, fluorescence of adjacent region does not change upon extended incubation of dynamin with SMrT templates, ruling out constriction dependent membrane expulsion which could lead to rise in intensity of the adjacent region, c) BODIPY EHD1 assembly (in the presence of ATP γ S) shows that EHD1 binds as punctae which grow in intensity indicating that co-localization of EHD1 with high membrane intensity is due to the EHD1 assembly, d) during EHD1 assembly, increase in the tube intensity either precedes or co-incides with decrease in tube intensity in the adjacent region.

We observed that EHD1 catalyzes fission in the presence of ATP and although we lack the spatial-resolution to precisely pinpoint the location of the cut, inspection of the kymograph of EHD1 fission reaction indicates that the fission of the tube appears to occur at the constricted region between adjacent membrane bulges. This could be possible as EHD1 assembly causes the bulging induced formation of constriction which in turn will generate extreme curvature gradient at the juncture of the two regions. This is also supported by the recent model where steep curvature gradient can catalyze membrane fission (Morlot et al., 2012).

We observed that EHD1 in the presence of ATP could cause deformation at the accelerated rate than EHD1 with ATP γ S. This discrepancy could occur due to ATP hydrolysis-dependent deformation of the membrane tube which in turn can accelerate the process of membrane deformation.

Based on these results we proposed that EHD1 catalyzes membrane fission via an alternate pathway where ATP-bound EHD1 binds membrane and oligomerizes. EHD1 oligomerization leads to expansion of tube diameter by forming a topologically inverted

membrane bulge like intermediate. As the result of bulge formation, adjacent membrane region undergoes constriction. Assembly of EHD1 leads to stimulation of ATPase activity which further increases the dimension of bulge, further constricting the adjacent membrane region and fission occur due to steep curvature gradient formed during this procedure (Fig. 5-2-4 c).

We propose the existence of alternate pathway to membrane fission. The existing model of fission indicates protein binding leads to constriction of the tube which then undergoes fission. We propose that the constriction can also be achieved by protein catalyzed expansion of membrane tube, which in turn leads to constriction of the adjacent region which over time leads to fission.

We have earlier seen that EHD1 mediated fission is affected by the initial tube radius. The tube dimension sensitivity of EHD1 mediated fission is most likely an intrinsic nature of the protein and is related to the extent of remodeling each oligomer can catalyze. EHD1 in ATP-bound form shows a punctate localization reflecting the oligomeric state of EHD1. These oligomers expand the underlying membrane which in turn results in the formation of constriction in the adjacent region. Existing mechanism of fission proposed that membrane fission occurs in the constricted region on the membrane; and the probability of fission in a constricted region is dependent on whether the constricted region reaches the dimension of a bilayer (~ 5 nm) to promote the formation of hemifission intermediate. In the EHD1 catalyzed fission mechanism, dimensions of the constriction would be defined by EHD1 scaffolding dependent membrane bulge formation on either side. As we see that EHD1 can induce similar extent of membrane deformation on thin and thick tubes, the inability to catalyze fission on thick tubes could be due to the physical limitation on the extent of tube expansion by EHD1 scaffold. Increasing protein concentration might not alter the outcome this trait as EHD1 can form a functional scaffold at lower (1 μ M) concentration, however it could expedite the rate of scaffold formation.

Mechanism of membrane fission by EHD1 is specific to EHD family and not a generalized feature of proteins involved in intracellular fission. Several dynamin family members are involved in fission and fusion at intracellular compartments. Dynamin-related protein1 (DRP1) is one of such protein proposed to catalyze fission of mitochondria. Cellular studies suggest that Drp1 scaffold binds mitochondria and constrict to catalyze fission (Friedman et al., 2011). This further strengthens the idea that mechanism of fission by EHD1 is not a generalized mechanism of intra-cellular fission catalysts.

6. References:

Altenbach, C., Greenhalgh, D. a, Khorana, H.G., and Hubbell, W.L. (1994). A collision gradient method to determine the immersion depth of nitroxides in lipid bilayers: application to spin-labeled mutants of bacteriorhodopsin. *Proc. Natl. Acad. Sci. U. S. A.* *91*, 1667–1671.

Altenbach, C., Froncisz, W., Hemker, R., McHaourab, H., and Hubbell, W.L. (2005). Accessibility of nitroxide side chains: absolute Heisenberg exchange rates from power saturation EPR. *Biophys. J.* *89*, 2103–2112.

Bashkirov, P. V, Akimov, S. a, Evseev, A.I., Schmid, S.L., Zimmerberg, J., and Frolov, V. a (2008). GTPase cycle of dynamin is coupled to membrane squeeze and release, leading to spontaneous fission. *Cell* *135*, 1276–1286.

Baykov, A.A., Evtushenko, O.A., and Avaeva, S.M. (1988). A malachite green procedure for orthophosphate determination and its use in alkaline phosphatase-based enzyme immunoassay. *Anal. Biochem.* *171*, 266–270.

Bhattacharyya, S., Rainey, M.A., Arya, P., Dutta, S., George, M., Storck, M.D., McComb, R.D., Muirhead, D., Todd, G.L., Gould, K., et al. (2016). Endocytic recycling protein EHD1 regulates primary cilia morphogenesis and SHH signaling during neural tube development. *Sci. Rep.* *6*, 20727.

Blume, J.J., Halbach, A., Behrendt, D., Paulsson, M., and Plomann, M. (2007). EHD proteins are associated with tubular and vesicular compartments and interact with specific phospholipids. *Exp. Cell Res.* *313*, 219–231.

Braun, A., Pinyol, R., Dahlhaus, R., Koch, D., Fonarev, P., Grant, B.D., Kessels, M.M., and Qualmann, B. (2005). EHD proteins associate with syndapin I and II and such interactions play a crucial role in endosomal recycling. *Mol. Biol. Cell* *16*, 3642–3658.

Cai, B., Katafiasz, D., Horejsi, V., and Naslavsky, N. (2011). Pre-sorting endosomal transport of the GPI-anchored protein, CD59, is regulated by EHD1. *Traffic* *12*, 102–120.

Cai, B., Caplan, S., and Naslavsky, N. (2012). cPLA2 α and EHD1 interact and regulate the vesiculation of cholesterol-rich, GPI-anchored, protein-containing endosomes. *Mol. Biol. Cell* *23*, 1874–1888.

Cai, B., Giridharan, S.S.P., Zhang, J., Saxena, S., Bahl, K., Schmidt, J.A., Sorgen, P.L., Guo, W., Naslavsky, N., and Caplan, S. (2013). Differential roles of C-terminal eps15 homology domain proteins as vesiculators and tubulators of recycling endosomes. *J. Biol. Chem.* *288*, 30172–30180.

Caplan, S., Naslavsky, N., Hartnell, L.M., Lodge, R., Polishchuk, R.S., Donaldson, J.G., and Bonifacio, J.S. (2002). A tubular EHD1-containing compartment involved in the recycling of major histocompatibility complex class I molecules to the plasma membrane. *EMBO J.* *21*, 2557–2567.

Chernomordik, L. V., and Kozlov, M.M. (2003). Protein-Lipid Interplay in Fusion and Fission of Biological Membranes*. *Annu. Rev. Biochem.* *72*, 175–207.

Chernomordik, L. V., and Kozlov, M.M. (2005). Membrane hemifusion: crossing a chasm in two leaps. *Cell* *123*, 375–382.

Chernomordik, L. V., Vogel, S.S., Sokoloff, A., Onaran, H.O., Leikina, E.A., and Zimmerberg, J. (1993). Lysolipids reversibly inhibit Ca²⁺-, GTP- and pH-dependent fusion of biological membranes. *FEBS Lett.* *318*, 71–76.

Cypher, L.R., Bielecki, T.A., Huang, L., An, W., Iseka, F., Tom, E., Storck, M.D., Hoppe, A.D., Band, V., and Band, H. (2016). CSF-1 receptor signalling is governed by pre-requisite EHD1 mediated receptor display on the macrophage cell surface. *Cell. Signal.* *28*, 1325–1335.

Danino, D., Moon, K.-H., and Hinshaw, J.E. (2004). Rapid constriction of lipid bilayers by the mechanochemical enzyme dynamin. *J. Struct. Biol.* *147*, 259–267.

Dar, S., Kamerkar, S.C., and Pucadyil, T.J. (2015). A high-throughput platform for real-time analysis of membrane fission reactions reveals dynamin function. *Nat. Cell Biol.* *17*, 1588–1596.

Daumke, O., Lundmark, R., Vallis, Y., Martens, S., Butler, P.J.G., and McMahon, H.T. (2007). Architectural and mechanistic insights into an EHD ATPase involved in membrane remodelling. *Nature* *449*, 923–927.

Demonbreun, A.R., Swanson, K.E., Rossi, A.E., Deveaux, H.K., Earley, J.U., Allen, M. V., Arya, P., Bhattacharyya, S., Band, H., Pytel, P., et al. (2015). Eps 15 homology domain (EHD)-1 remodels transverse tubules in skeletal muscle. *PLoS One* *10*, 1–17.

Doherty, K.R., Demonbreun, A.R., Wallace, G.Q., Cave, A., Posey, A.D., Heretis, K., Pytel, P., and McNally, E.M. (2008). The endocytic recycling protein EHD2 interacts with myoferlin to regulate myoblast fusion. *J. Biol. Chem.* *283*, 20252–20260.

Friedman, J.R., Lackner, L.L., West, M., DiBenedetto, J.R., Nunnari, J., and Voeltz, G.K. (2011). ER Tubules Mark Sites of Mitochondrial Division. *Science* (80-.). *334*, 358–362.

Frolov, V.A., Escalada, A., Akimov, S.A., and Shnyrova, A. V. (2015). Geometry of membrane fission. *Chem. Phys. Lipids* *185*, 129–140.

Fuller, N., and Rand, R.P. (2001). The influence of lysolipids on the spontaneous curvature and bending elasticity of phospholipid membranes. *Biophys. J.* *81*, 243–254.

Gagescu, R., Demaurex, N., Parton, R.G., Hunziker, W., Huber, L. a, and Gruenberg, J. (2000). The

recycling endosome of Madin-Darby canine kidney cells is a mildly acidic compartment rich in raft components. *Mol. Biol. Cell* *11*, 2775–2791.

Galperin, E., Benjamin, S., Rapaport, D., Rotem-Yehudar, R., Tolchinsky, S., and Horowitz, M. (2002). EHD3: A Protein That Resides in Recycling Tubular and Vesicular Membrane Structures and Interacts with EHD1. *Traffic* *3*, 575–589.

Giridharan, S.S.P., Cai, B., Vitale, N., Naslavsky, N., and Caplan, S. (2013). Cooperation of MICAL-L1, syndapin2, and phosphatidic acid in tubular recycling endosome biogenesis. *Mol. Biol. Cell* *24*, 1776–1790.

Grant, B.D., and Caplan, S. (2008). Mechanisms of EHD/RME-1 protein function in endocytic transport. *Traffic* *9*, 2043–2052.

Grant, B.D., and Donaldson, J.G. (2009). Pathways and mechanisms of endocytic recycling. *Nat. Rev. Mol. Cell Biol.* *10*, 597–608.

Grant, B., Zhang, Y., Paupard, M.C., Lin, S.X., Hall, D.H., and Hirsh, D. (2001). Evidence that RME-1, a conserved *C. elegans* EH-domain protein, functions in endocytic recycling. *Nat. Cell Biol.* *3*, 573–579.

Guilherme, A., Soriano, N.A., Furcinitti, P.S., and Czech, M.P. (2004). Role of EHD1 and EHBP1 in perinuclear sorting and insulin-regulated GLUT4 recycling in 3T3-L1 adipocytes. *J. Biol. Chem.* *279*, 40062–40075.

Hao, M., Lin, S.X., Karylowski, O.J., Stner, D.W., McGraw, T.E., and Maxfield, F.R. (2002). Vesicular and non-vesicular sterol transport in living cells: The endocytic recycling compartment is a major sterol storage organelle. *J. Biol. Chem.* *277*, 609–617.

Hoernke, M., Mohan, J., Larsson, E., Blomberg, J., Kahra, D., Westenhoff, S., Schwieger, C., and Lundmark, R. (2017). EHD2 restrains dynamics of caveolae by an ATP-dependent, membrane-bound, open conformation. *Proc. Natl. Acad. Sci.* 201614066.

Hopkins, C.R., Gibson, A., Shipman, M., Strickland, D.K., and Trowbridge, I.S. (1994). In migrating fibroblasts, recycling receptors are concentrated in narrow tubules in the pericentriolar area, and then routed to the plasma membrane of the leading lamella. *J. Cell Biol.* *125*, 1265–1274.

van IJzendoorn, S.C.D. (2006). Recycling endosomes. *J. Cell Sci.* *119*, 1679–1681.

Jahn, R., Lang, T., and Südhof, T.C. (2003). Membrane Fusion. *Cell* *112*, 519–533.

Jovic, M., Kieken, F., Naslavsky, N., Sorgen, P.L., and Caplan, S. (2009). Eps15 Homology Domain 1-associated Tubules Contain Phosphatidylinositol-4-Phosphate and Phosphatidylinositol-(4,5)-

Bisphosphate and Are Required for Efficient Recycling. *Mol. Biol. Cell* *20*, 2731–2743.

Jović, M., Naslavsky, N., Rapaport, D., Horowitz, M., and Caplan, S. (2007). EHD1 regulates beta1 integrin endosomal transport: effects on focal adhesions, cell spreading and migration. *J. Cell Sci.* *120*, 802–814.

Kalil, K., and Dent, E.W. (2005). Touch and go: Guidance cues signal to the growth cone cytoskeleton. *Curr. Opin. Neurobiol.* *15*, 521–526.

Kamiguchi, H., and Lemmon, V. (1997). Neural cell adhesion molecule L1: signaling pathways and growth cone motility. *J Neurosci Res* *49*, 1–8.

Klug, C.S., and Feix, J.B. (2008). Methods and Applications of Site-Directed Spin Labeling EPR Spectroscopy. *Methods Cell Biol.* *84*, 617–658.

Kobayashi, H., and Fukuda, M. (2013). Rab35 establishes the EHD1-association site by coordinating two distinct effectors during neurite outgrowth. *J Cell Sci* *126*, 2424–2435.

Kooijman, E.E., Chupin, V., Fuller, N.L., Kozlov, M.M., de Kruijff, B., Burger, K.N.J., and Rand, P.R. (2005). Spontaneous curvature of phosphatidic acid and lysophosphatidic acid. *Biochemistry* *44*, 2097–2102.

Kozlovsky, Y., and Kozlov, M.M. (2003). Membrane fission: model for intermediate structures. *Biophys. J.* *85*, 85–96.

Kozlovsky, Y., Chernomordik, L. V., and Kozlov, M.M. (2002). Lipid intermediates in membrane fusion: formation, structure, and decay of hemifusion diaphragm. *Biophys. J.* *83*, 2634–2651.

Kunding, A.H., Mortensen, M.W., Christensen, S.M., and Stamou, D. (2008). A Fluorescence-Based Technique to Construct Size Distributions from Single-Object Measurements: Application to the Extrusion of Lipid Vesicles. *Biophys. J.* *95*, 1176–1188.

Lasiecka, Z.M., Yap, C.C., Caplan, S., and Winckler, B. (2010). Neuronal early endosomes require EHD1 for L1/NgCAM trafficking. *J. Neurosci.* *30*, 16485–16497.

Lee, D.W., Zhao, X., Scarselletta, S., Schweinsberg, P.J., Eisenberg, E., Grant, B.D., and Greene, L.E. (2005). ATP binding regulates oligomerization and endosome association of RME-1 family proteins. *J. Biol. Chem.* *280*, 17213–17220.

Lee, S., Uchida, Y., Wang, J., Matsudaira, T., Nakagawa, T., Kishimoto, T., Mukai, K., Inaba, T., Kobayashi, T., Molday, R.S., et al. (2015). Transport through recycling endosomes requires EHD1 recruitment by a phosphatidylserine translocase. *EMBO J.* *34*, 669–688.

Lin, S.X., Grant, B., Hirsh, D., and Maxfield, F.R. (2001). Rme-1 regulates the distribution and function of the endocytic recycling compartment in mammalian cells. *Nat. Cell Biol.* 3, 567–572.

Lu, Q., Insinna, C., Ott, C., Stauffer, J., Pintado, P.A., Rahajeng, J., Baxa, U., Walia, V., Cuenca, A., Hwang, Y.-S., et al. (2015). Early steps in primary cilium assembly require EHD1/EHD3-dependent ciliary vesicle formation. *Nat. Cell Biol.* 17, 228–240.

Mate, S.E., Van Der Meulen, J.H., Arya, P., Bhattacharyya, S., Band, H., and Hoffman, E.P. (2012). Eps homology domain endosomal transport proteins differentially localize to the neuromuscular junction. *Skelet. Muscle* 2, 19.

Mattila, J.-P., Shnyrova, A. V, Sundborger, A.C., Hortelano, E.R., Fuhrmans, M., Neumann, S., Müller, M., Hinshaw, J.E., Schmid, S.L., and Frolov, V.A. (2015). A hemi-fission intermediate links two mechanistically distinct stages of membrane fission. *Nature* 524, 109–113.

Maxfield, F.R., and McGraw, T.E. (2004). Endocytic recycling. *Nat. Rev. Mol. Cell Biol.* 5, 121–132.

Meinecke, M., Boucrot, E., Camdere, G., Hon, W.-C., Mittal, R., and McMahon, H.T. (2013). Cooperative Recruitment of Dynamin and BIN/Amphiphysin/Rvs (BAR) Domain-containing Proteins Leads to GTP-dependent Membrane Scission. *J. Biol. Chem.* 288, 6651–6661.

Melo, A.A., Hegde, B.G., Shah, C., Larsson, E., Isas, J.M., Kunz, S., Lundmark, R., Langen, R., and Daumke, O. (2017). Structural insights into the activation mechanism of dynamin-like EHD ATPases. *Proc. Natl. Acad. Sci.* 2, 201614075.

Mintz, L., Galperin, E., Pasmanik-Chor, M., Tulzinsky, S., Bromberg, Y., Kozak, C.A., Joyner, A., Fein, A., and Horowitz, M. (1999). EHD1—An EH-Domain-Containing Protein with a Specific Expression Pattern. *Genomics* 59, 66–76.

Morlot, S., and Roux, A. (2013). Mechanics of Dynamin-Mediated Membrane Fission. *Annu. Rev. Biophys.* 42, 629–649.

Morlot, S., Galli, V., Klein, M., Chiaruttini, N., Manzi, J., Humbert, F., Dinis, L., Lenz, M., Cappello, G., and Roux, A. (2012). Membrane Shape at the Edge of the Dynamin Helix Sets Location and Duration of the Fission Reaction. *Cell* 151, 619–629.

Mukherjee, S., Zha, X., Tabas, I., and Maxfield, F.R. (1998). Cholesterol distribution in living cells: fluorescence imaging using dehydroergosterol as a fluorescent cholesterol analog. *Biophys. J.* 75, 1915–1925.

Munnik, T., and Wierchowicka, M. (2013). Lipid-Binding Analysis Using a Fat Blot Assay. In *Plant Lipid*

- Signaling Protocols, T. Munnik, and I. Heilmann, eds. (Totowa, NJ: Humana Press), pp. 253–259.
- Naslavsky, N. (2006). Interactions between EHD Proteins and Rab11-FIP2: A Role for EHD3 in Early Endosomal Transport. *Mol. Biol. Cell* *17*, 163–177.
- Naslavsky, N., Rahajeng, J., Rapaport, D., Horowitz, M., and Caplan, S. (2007). EHD1 regulates cholesterol homeostasis and lipid droplet storage. *Biochem. Biophys. Res. Commun.* *357*, 792–799.
- Páli, T., Bartucci, R., Horváth, L.I., and Marsh, D. (1992). Distance measurements using paramagnetic ion-induced relaxation in the saturation transfer electron spin resonance of spin-labeled biomolecules: Application to phospholipid bilayers and interdigitated gel phases. *Biophys. J.* *61*, 1595–1602.
- Pant, S., Sharma, M., Patel, K., Caplan, S., Carr, C.M., and Grant, B.D. (2009). AMPH-1/Amphiphysin/Bin1 functions with RME-1/Ehd1 in endocytic recycling. *Nat. Cell Biol.* *11*, 1399–1410.
- Park, M., Penick, E.C., Edwards, J.G., Kauer, J.A., and Ehlers, M.D. (2004). Recycling Endosomes Supply AMPA Receptors for LTP. *Science* (80-.). *305*, 1972–1975.
- Picciano, J. a, Ameen, N., Grant, B.D., and Bradbury, N. a (2003). Rme-1 regulates the recycling of the cystic fibrosis transmembrane conductance regulator. *Am. J. Physiol. Cell Physiol.* *285*, C1009–C1018.
- Posey, A.D., Pytel, P., Gardikiotes, K., Demonbreun, A.R., Rainey, M., George, M., Band, H., and McNally, E.M. (2011). Endocytic recycling proteins EHD1 and EHD2 interact with Fer-1-like-5 (Fer1L5) and mediate myoblast fusion. *J. Biol. Chem.* *286*, 7379–7388.
- Posey, A.D., Swanson, K.E., Alvarez, M.G., Krishnan, S., Earley, J.U., Band, H., Pytel, P., McNally, E.M., and Demonbreun, A.R. (2014). EHD1 mediates vesicle trafficking required for normal muscle growth and transverse tubule development. *Dev. Biol.* *387*, 179–190.
- Pucadyil, T.J., and Holkar, S.S. (2016). Comparative analysis of adaptor-mediated clathrin assembly reveals general principles for adaptor clustering. *Mol. Biol. Cell.*
- Pucadyil, T.J., and Schmid, S.L. (2008). Real-Time Visualization of Dynamin-Catalyzed Membrane Fission and Vesicle Release. *Cell* *135*, 1263–1275.
- Rainey, M.A., George, M., Ying, G., Akakura, R., Burgess, D.J., Siefker, E., Bargar, T., Doglio, L., Crawford, S.E., Todd, G.L., et al. (2010). The endocytic recycling regulator EHD1 is essential for spermatogenesis and male fertility in mice. *BMC Dev. Biol.* *10*, 37.
- Reinecke, J.B., Katafiasz, D., Naslavsky, N., and Caplan, S. (2015). Novel Functions for the Endocytic Regulatory Proteins MICAL-L1 and EHD1 in Mitosis. *Traffic* *16*, 48–67.

- Roux, A., Uyhazi, K., Frost, A., and De Camilli, P. (2006). GTP-dependent twisting of dynamin implicates constriction and tension in membrane fission. *Nature* *441*, 528–531.
- Schmid, S.L., and Frolov, V. a. (2011). Dynamin: Functional Design of a Membrane Fission Catalyst. *Annu. Rev. Cell Dev. Biol.* *27*, 79–105.
- Shah, C., Hegde, B.G., Morén, B., Behrmann, E., Mielke, T., Moenke, G., Spahn, C.M.T., Lundmark, R., Daumke, O., and Langen, R. (2014). Structural Insights into Membrane Interaction and Caveolar Targeting of Dynamin-like EHD2. *Structure* *22*, 409–420.
- Sharma, M., Naslavsky, N., and Caplan, S. (2008). A role for EHD4 in the regulation of early endosomal transport. *Traffic* *9*, 995–1018.
- Sharma, M., Panapakkam Giridharan, S.S., Rahajeng, J., Naslavsky, N., and Caplan, S. (2009a). MICAL-L1 Links EHD1 to Tubular Recycling Endosomes and Regulates Receptor Recycling. *Mol. Biol. Cell* *20*, 5181–5194.
- Sharma, M., Jovic, M., Kieken, F., Naslavsky, N., Sorgen, P., and Caplan, S. (2009b). A model for the role of EHD1-containing membrane tubules in endocytic recycling. *Commun. Integr. Biol.* *2*, 431–433.
- Shnyrova, A. V, Bashkirov, P. V, Akimov, S. a, Pucadyil, T.J., Zimmerberg, J., Schmid, S.L., and Frolov, V. a (2013). Geometric Catalysis of Membrane Fission Driven by Flexible Dynamin Rings. *Science* (80-.). *339*, 1433–1436.
- Sudhof, T.C., and Rothman, J.E. (2009). Membrane Fusion: Grappling with SNARE and SM Proteins. *Science* (80-.). *323*, 474–477.
- Sweitzer, S.M., and Hinshaw, J.E. (1998). Dynamin undergoes a GTP-dependent conformational change causing vesiculation. *Cell* *93*, 1021–1029.
- Taguchi, T. (2013). Emerging roles of recycling endosomes. *J. Biochem.* *153*, 505–510.
- Tanaka, E., and Sabry, J. (1995). Making the connection: Cytoskeletal rearrangements during growth cone guidance. *Cell* *83*, 171–176.
- Tanaka-Takiguchi, Y., Itoh, T., Tsujita, K., Yamada, S., Yanagisawa, M., Fujiwara, K., Yamamoto, A., Ichikawa, M., and Takiguchi, K. (2013). Physicochemical Analysis from Real-Time Imaging of Liposome Tubulation Reveals the Characteristics of Individual F-BAR Domain Proteins. *Langmuir* *29*, 328–336.
- Warnock, D.E., Hinshaw, J.E., and Schmid, S.L. (1996). Dynamin self-assembly stimulates its GTPase activity. *J. Biol. Chem.* *271*, 22310–22314.

Wu, C., Cui, Z., Liu, Y., Zhang, J., Ding, W., Wang, S., Bao, G., Xu, G., Sun, Y., and Chen, J. (2016). The importance of EHD1 in neurite outgrowth contributing to the functional recovery after spinal cord injury. *Int J Dev Neurosci* 52, 24–32.

Xie, S., Naslavsky, N., and Caplan, S. (2014). Diacylglycerol Kinase alpha Regulates Tubular Recycling Endosome Biogenesis and Major Histocompatibility Complex Class I Recycling. *J. Biol. Chem.* 289, 31914–31926.

Xie, S., Bahl, K., Reinecke, J.B., Hammond, G.R. V, Naslavsky, N., and Caplan, S. (2016). The endocytic recycling compartment maintains cargo segregation acquired upon exit from the sorting endosome. *Mol. Biol. Cell* 27, 108–126.

Yamashiro, D.J., Tycko, B., Fluss, S.R., and Maxfield, F.R. (1984). Segregation of transferrin to a mildly acidic (pH 6.5) para-golgi compartment in the recycling pathway. *Cell* 37, 789–800.

Yap, C.C.C., Lasiacka, Z.M., Caplan, S., and Winckler, B. (2010). Alterations of EHD1/EHD4 protein levels interfere with L1/NgCAM endocytosis in neurons and disrupt axonal targeting. *J. Neurosci.* 30, 6646–6657.

Yeung, T., Gilbert, G.E., Shi, J., Silvius, J., Kapus, A., and Grinstein, S. (2008). Membrane phosphatidylserine regulates surface charge and protein localization. *Science* 319, 210–213.